2007-07-18

Loading Rate Effects on Axial Pile Capacity in Clays

Michael Paul Garner
Brigham Young University - Provo

LOADING RATE EFFECTS ON AXIAL PILE CAPACITY IN CLAYS

by

Michael Paul Garner

A thesis submitted to the faculty of

Brigham Young University

in partial fulfillment of the requirements for the degree of

Master of Science

Department of Civil and Environmental Engineering

Brigham Young University

August 2007

BRIGHAM YOUNG UNIVERSITY

GRADUATE COMMITTEE APPROVAL

of a thesis submitted by

Michael Paul Garner

This thesis has been read by each member of the following graduate committee and by majority vote has been found to be satisfactory.

Date	Kyle M. Rollins, Chair
Date	Steven E. Benzley
Date	Travis M. Gerber

BRIGHAM YOUNG UNIVERSITY

As chair of the candidate's graduate committee, I have read the thesis of Michael Paul Garner in its final form and have found that (1) its format, citations, and bibliographical style are consistent and acceptable and fulfill university and department style requirements; (2) its illustrative materials including figures, tables, and charts are in place; and (3) the final manuscript is satisfactory to the graduate committee and is ready for submission to the university library.

Date

Kyle M. Rollins
Chair, Graduate Committee

Accepted for the Department

E. James Nelson
Graduate Coordinator

Accepted for the College

Alan R. Parkinson
Dean, Ira A. Fulton College of Engineering and Technology

ABSTRACT

LOADING RATE EFFECTS ON AXIAL PILE CAPACITY IN CLAYS

Michael Paul Garner

Department of Civil and Environmental Engineering

Master of Science

In order to design more efficient and reliable structures, axial load tests are performed on foundation piles. Traditionally, static tests with an average duration of approximately twenty-four hours have been performed on test piles to obtain their axial capacity. These static tests require multiple piles used as anchors in addition to the test pile. Static tests are both expensive and time consuming. An alternative to static testing is dynamic testing which requires sophisticated interpretation, can damage the pile and may not produce accurate results.

There is a relatively new testing method called the Statnamic Testing Method which tests foundation piles at a very fast rate, but still slower than with dynamic tests. As the rate at which load is applied to a test pile increases, the axial capacity also increases, particularly in clay. Research suggests that shear strength of soil typically

increases 10% per log cycle increase in strain rate. Strain rate effects can vary widely and may be influenced by many factors including plasticity index, structure, ageing, overconsolidation ratio, temperature, etc.

Statnamic testing was performed for this work. Nine static tests were performed on six different piles identical to the Statnamic test pile and driven through the same soil profile. The static tests had times to failure ranging from ten seconds to eighteen hours.

Failure load increased by 13.7% per log cycle increase in velocity. Statnamic tests need more careful analysis when performed in clay to avoid over predicting pile capacity. A factor of 0.55 should be applied to Statnamic capacity to predict static capacity.

ACKNOWLEDGMENTS

I would like to thank Dr. Kyle M. Rollins for all of his help and for his patience with me. Funding for this study was provided by the Utah Department of Transportation under contract 03-9144, and this support is gratefully acknowledged. The conclusions and opinions expressed in this document do not necessarily reflect those of the Utah DOT. I also thank Dr. A. Gray Mullins, Michael Stokes and Danny Winters for assistance with the Statnamic testing and analysis. My wife Marissa deserves my biggest thanks for her encouragement and support as well as patience. Now I will have much more time to spend with her. Lastly I want to thank my parents, my Uncle Richard and my father-in-law for encouraging me to stay in school.

TABLE OF CONTENTS

LIST OF TABLES

LIST OF FIGURES

1 Introduction

In order to build more economic and reliable structures, tests on foundation piles are often necessary. When pile capacity is tested, the rate at which load is applied is important to consider because it can significantly affect the measured capacity. Originally, ASTM standards for axial pile load tests required load to be applied over a period of 16 to 20 hours with the slow maintained load (SML) test. About 30 years ago, a modified procedure, known as the quick maintained load (QML) test method, permitted load to be applied in one to five hours. In the last 10 years, the Statnamic load test, which applies load in 0.1 to 0.2 seconds, has been used for axial load testing. The Statnamic method can apply loads of up to 45 MN (5000 tons) without a reaction frame which greatly reduces the cost of load testing for large capacity piles. Unfortunately, concerns have developed regarding procedures for obtaining the static capacity from this rapidly applied load.

Engineers have known for years that the rate at which soils, especially clays, are loaded affects their ultimate strength. This increase in strength is due to the viscosity of the soil itself and the water in the soil and is in addition to the damping resistance developed during dynamic loading. The fact that strength increases with increased rate of loading has been well documented, beginning with the research of Casagrande and Wilson (1951). The real challenge is to quantify this increase in

strength and to accurately identify the factors which affect it. If this can be done, then axial capacity from a test conducted at any rate of loading could be converted to a standard loading rate and meaningful comparisons between different testing rates can be obtained.

A more recend test method, the Statnamic test, which will be discussed at length, later in this study, typically applies load in about 0.1 seconds. The Statnamic test is thought to provide an accurate estimate of static capacity of piles in sandy soils. However, when Statnamic testing of piles is performed in stiff, overconsolidated clays, the capacity of the piles may tend to be over-predicted by as much as 30% (Brown, 1994). This increase in predicted capacity appears to be due to an increase in the shear strength of clay as strain rate increases. A better understanding of strain rate effects on clays will help engineers to design foundations with accurate, predicted capacities.

1.1 Objectives and Scope of Work

The objectives of this study are:

1. To verify that the rate at which clay is loaded affects its shear strength and therefore the apparent capacity of a pile which is driven into clay.
2. To identify the factors that may affect the magnitude of the loading rate effects
3. Determine correction factors which could be used to account for loading rate for axial load testing.

To achieve these objectives, a detailed search of prior published literature was undertaken and is presented in chapter 2. In addition, a series of axial load tests were performed on five full scale test piles. These test piles are essentially identical and were driven into the same soil profile which includes soil traditionally thought to be affected by the rate at which load is applied. The axial capacity of these piles was evaluated, each at a different rate of load, using hydraulic actuators and a Statnamic device. Failure load was reached at times ranging from 0.1 second to 18 hours. Based on interpretation of the failure loads and measured shear strengths for each test, an evaluation of the effect of loading rate on axial pile capacity is made. Finally, adjustment factors to account for the influence of loading rate are developed.

2 Literature Review

This literature review first reviews the findings of previous studies regarding loading rate effects on clays. Next some background on pile load testing including Statnamic load testing is presented.

As the rate of load application increases (or the strain rate increases), the undrained strength, s_u of clay also increases, due to viscous properties of clay (Briaud and Garland, 1985; Leroueil and Marques, 1996). This is an important phenomenon that must be addressed in any pile test where capacity is derived from clays. Clays have consistently been shown to exhibit significant "rate effects", while with sand this phenomenon is less pronounced as displayed by Hyde et al. (1998). Factors other than grain size may also influence the effect of load rate phenomena. Leroueil and Marques (1996) found that due to viscosity in clays, s_u increases by about 10% per log cycle increase in load rate but decreases about 10% for each 12^0 C increase in temperature. Other factors that influence rate effects include, but are not limited to: plasticity index, overconsolidation ratio (O.C.R.), soil structure, water content and aging. Though all of these factors have been shown to affect strain rate phenomenon, little research has been done to quantify their effects.

2.1.1 Theory on Rate Effects

Researchers agree that viscosity in the soil is the reason for an increase in strength at higher rates of strain.

Briaud and Garland (1985)

Briaud and Garland (1985) explained the physical reasons for rate-dependent properties of clays. They attribute rate dependent properties to three elements: pore water, particle contacts and water/soil skeleton interaction.

Water in pores is more viscous than clay particles. Water is a Newtonian fluid so by doubling the shearing rate of water the shear strength will also double. Therefore, the higher the water content of the clay, the higher the viscosity of the clay.

Viscosity is also a factor in the particle contacts of the clay. These contacts consist of a mineral particle and its adsorbed water layer penetrating into the adsorbed water layer of another mineral particle. The viscosity of the adsorbed water layer is greater than that of the free water in pores. Therefore, if the overlap of adsorbed water layers becomes greater, then the viscosity of the clay will be greater. The overlap of layers is greater in overconsolidated clays because they are forced closer together. Higher viscosity can also be seen if the adsorbed layers are thicker, such as with clays having high plasticity indexes.

Shear strength due to water/soil skeleton interaction varies with the rate of shear in the soil. The path of least resistance is found when the rate of shear is slow. With faster rates, the soil skeleton does not have time to deform and find the path of least resistance. Shear strength goes up with increased rate of strain. With higher rates of strain, pore pressures become more negative or less positive. Pore pressure

becoming more negative or less positive increases the shear strength of the soil. Permeability therefore affects the strain rate effects because with lower permeability, pore pressure does not dissipate when soil is sheared quickly, but it will dissipate if load is applied slowly enough.

Briaud and Garland (1985) also presented a mathematical model of shear capacity of soil which is given by the equation below.

$$\frac{S_{u1}}{S_{u2}} = \left(\frac{t_2}{t_1}\right)^n \quad \textbf{(2.1)}$$

where:

S_{u1} = Undrained shear strength measured with time to failure t_1
S_{u2} = Undrained shear strength measured with time to failure t_2
n = Viscous exponent

$$n = 0.44\left(\frac{S_{u(ref)}}{p_a}\right)^{-0.22} \quad \textbf{(2.2)}$$

where:

$S_{u(ref)}$ = Reference shear strength (time to failure = 1 hour)
p_a = Atmospheric pressure

$$n = 0.028 + 0.00060w \quad \textbf{(2.3)}$$

where:

w = Water content (%)

$$n = 0.035 + 0.00066PI \quad \textbf{(2.4)}$$

where:

PI = Plasticity index

$$n = 0.036 + 0.046LI \quad \textbf{(2.5)}$$

where:

LI = Liquidity index

Briaud and Garland (1985) recommend that n be taken as the most conservative value from Equation 2.2 to 2.5. The viscous exponent, n however, would preferably be obtained by performing two undrained shear tests and calculating it directly, using Equation 2.1.

Briaud and Garland (1985) also presented data showing that n increases with increasing O.C.R. but gave no mathematical correlation between the two variables.

Kutter and Sathialingam (1992)

Kutter and Sathialingam (1992) proposed a mathematical model based on the elastic-viscoplasticity theory of Perzyna (1966). This article is relevant because in the course of explaining their model, they also explained a great deal about elastic-viscoplacticity theory. Their model uses the hypothesis that plastic strains require time to occur. Since plastic strains show more viscous effects than do elastic strains, the model assumes elastic strains are rate-independent. In this model, all strain rate effects are dictated by a single parameter, the coefficient of secondary compression, C_α.

The coefficient of secondary compression, C_α remains constant for normally consolidated soils, but is low in the early stages of secondary compression and rises in later stages for overconsolidated soils. At high strain rates, normally consolidated clay may behave like overconsolidated clay (such as exhibiting dilatancy) and overconsolidated clay may act like normally consolidated clay (including contractive tendencies) at low strain rates. This is consistent with findings of other researchers as discussed in section 2.1.3.

2.1.2 Results of Previous Published Tests on Shear Strength Rate Effects

Most clays show an increase in undrained shear strength, s_u with increased rate of strain. Data points were taken from many published s_u tests on different clays. In order to quantify the increase in strength, the s_u values of many soils were normalized by dividing these values by each respective s_u loaded at 1% strain per hour. These data points are compiled in Figure 2.1, which is a semi-log graph. Kulhawy and Mayne (1990) produced a similar graph with the same resulting relationship of parameters. Many of the data in Figure 2.1 were used in their graph as well.

Figure 2.1 is shown with two best fit lines. Equation 2.6 is the best equation of the power best fit line which is curved on the graph. The R^2 value is 0.79. Equation 2.7 is the log best fit line and has an R^2 value of 0.77. There is some scatter in the graph, but the trend is obvious. Simply stated, Equation 2.7 shows that s_u of clay increases by 9% with every tenfold increase in strain rate. This is consistent with findings of previous researchers who have shown the increase in s_u to be linear with increasing rate of strain on a semi-log graph.

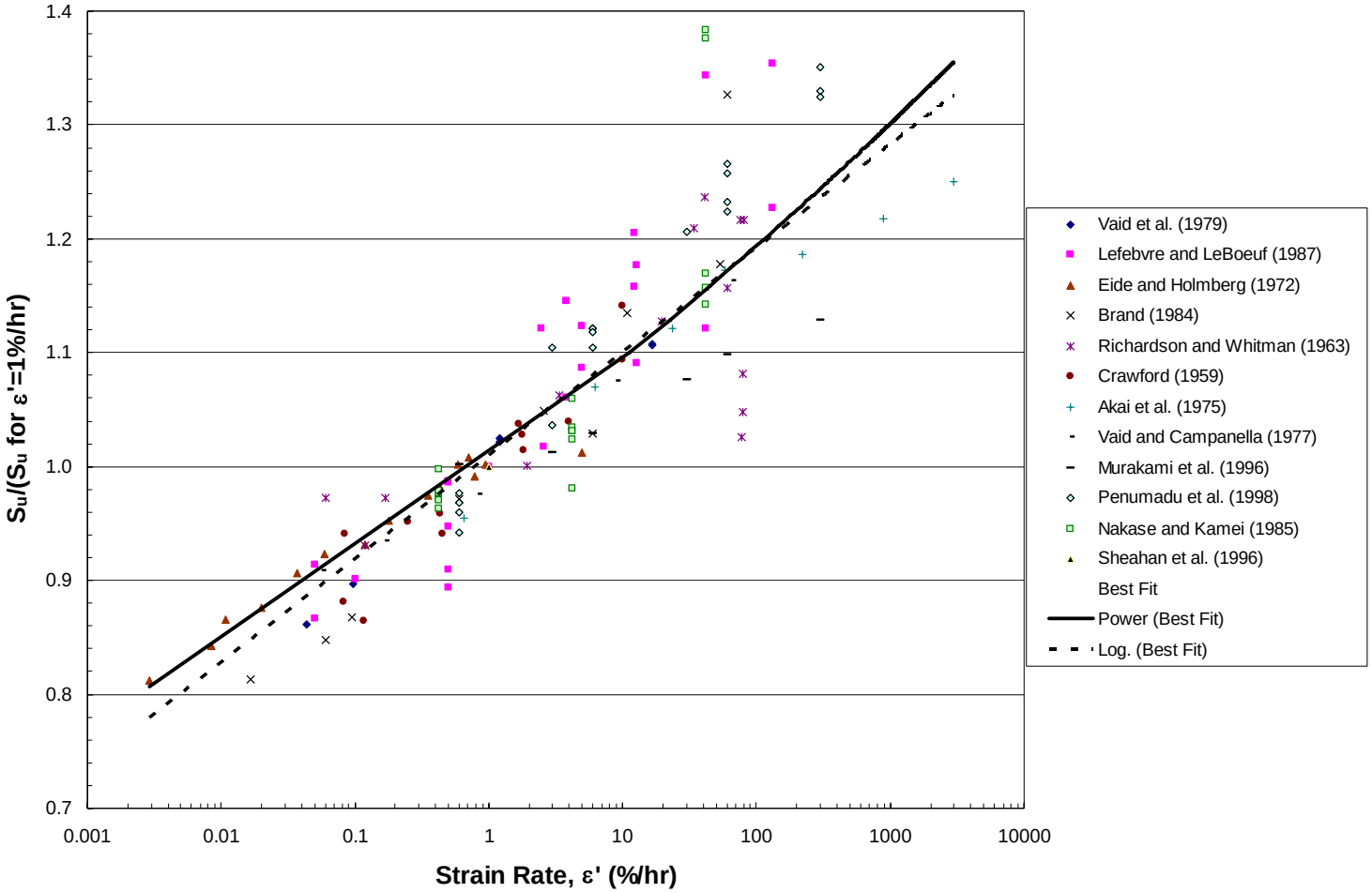

Figure 2.1 Effect of Strain Rate on Undrained Shear Strength

Equation 2.7 supports the idea that the increase in shear strength with increasing rate of strain is not linear. It also supports the idea of a threshold strain rate which is explained in section 2.1.3. Equation 2.6 has a slightly higher R^2 value than that of Equation 2.7 which gives it more reliability.

$$\frac{s_u}{s_u at \frac{1\%}{hr}} = 1.005 \times \varepsilon'^{0.0375} \quad \textbf{(2.6)}$$

$$\frac{s_u}{s_u at \frac{1\%}{hr}} = 0.091 \times \log(\varepsilon') + 1.01 \quad \textbf{(2.7)}$$

The scatter in the available data from various researchers may be due to any of several factors. There may be leakage into or out of the test specimen. Water may be redistributed within the test specimen. A wide range of soil types has been used in testing, including cemented clays and recompacted clays. Mode of shearing, range of strain rates and varying O.C.R. may also affect results of tests (Sheahan et al., 1996).

Equation 2.8 accounts for the non-linear nature of rate effects. This equation has been used by many researchers and is presented by Hyde et al. (1998). Researchers suggest that $k = 1$ or $k = 1 - \alpha(10^{-6})\beta$, where $\beta = 0.2$ and $\alpha = 1$ for clays and $\alpha = 0.1$ for sands (Hyde et al.,1998). This model holds true for high rates of strain, but may not be applicable for slower tests. Although previous researchers

suggest that α equal 1, Hyde et al. (1998) suggest that the value might be much higher and that it might change dynamic shear resistance by an order of magnitude.

$$\tau_d = \tau_s \left(k + \alpha \left(\frac{\Delta v}{v_0} \right)^{\beta} \right) \quad \textbf{(2.8)}$$

where

τ_d = Dynamic shear resistance
τ_s = Static shear resistance
Δ_v = Relative velocity of pile and soil
v_0 = Reference velocity (1 m/s)

Hyde et al. (1998) analyzed the data of several researchers and found considerable scatter. They concluded that from previous research, no clear guidance can be found concerning the relationship between shear strength and velocity. They also concluded that this relationship will depend on factors which include the following: clay type, in-situ effective stress, strength, stress history, aging and sampling factors.

Penumadu et al. (1998) studied the self-boring pressuremeter test, SBPT. The reason for their research was that the SBPT is a convenient in-situ test, but it tends to predict higher s_u values than laboratory triaxial tests. They conducted SBPT tests with strain rates between 0.01 and 5%/min. These tests showed about 15% increase in undrained shear strength for every tenfold increase in strain rate.

Penumadu and Chameau (1997) studied stress-controlled pressuremeter tests and found that local creep and consolidation occur during each holding interval of a

stress-controlled test. Local consolidation increases the undrained shear strength. Creep throughout each test produces greater deformation which results in a decrease in measured undrained shear strength. Penumadu and Chameau (1997) also stated that strain rate effects are dependent on mode of shearing and that strain rate effects for extension tests are higher than for compression tests.

2.1.3 Influence of O.C.R. on Strain Rate Effects

As was stated above, one factor which might affect the magnitude of rate effects in clay is O.C.R. Sheahan et al. (1996) conducted tests on unstructured clays which showed s_u increasing by 9.5% every log cycle of strain rate increase at a stain rate range of 5-50% per hour for soil with O.C.R. ranging from 1 to 8. Their tests also showed that from 0.05-5% strain per hour, the increase is 6.5%/log cycle for normally consolidated soil, 4.5% for O.C.R. = 2 and nearly no increase for O.C.R. = 8. These findings seem to suggest that not only does strain rate effect s_u, but also that the rate effect is not linear. At lower strain rates, O.C. soils showed no rate effect and N.C. soils showed less rate effect than at higher rates. Other researchers have also shown that the amount of rate effect increases with increased rate (Richardson and Whitman, 1963; Berre and Bjerrum, 1973 and Vaid and Campanella, 1977). In section 2.1.1 the fact that pore pressure becomes more negative or less positive with a quickly applied shear stress was stated. This phenomenon is especially true in soils that are overconsolidated (Hajduk et al., 1998).

Rate effects may be reduced or nonexistent at lower strain rates for both O.C. and N.C. clays. Some researchers have identified a “threshold strain rate” at and

below which s_u is constant (showing no rate effects). Sheahan et al. (1996) and previous researchers have shown that this threshold strain rate increases with increasing O.C.R. (Berre and Bjerrum, 1973, and Vaid and Campanella, 1977). This explains why there was no rate effect on clays with an O.C.R. of 8 at strain rates of 0.05 to 5%/hour in tests by Sheahan et al. (1996).

Penumadu et al. (1998) analyzed undrained shear tests of several other researchers. Like Sheahan et al. (1996) they also saw a threshold strain rate phenomenon which they called “upper yield”. They concluded that this “upper yield” occurs at a strain rate of approximately 0.01%/min. and increased with increasing O.C.R.

Katti et al. (2003) analyzed the tests of Sheahan et al. (1996) and came to some interesting conclusions. They made a plot of normal stress versus deviatoric stress space which they refer to as the effective stress path. For normally consolidated clay, with increasing strain rate, the stress path moves to the right. This move shows that in faster tests, the excess pore pressure is lower than with slower tests. At higher strain rates, the stress paths are similar to stress paths of clays with higher O.C.R. Katti et al. (2003) proposed an equation which models the apparent increase in O.C.R. with an increase in strain rate. This model is summarized by Equation 2.9.

$$O.C.R. = e^{[C_1 \ln(\varepsilon'/\varepsilon'_0)+C_2+D_1]/D_2} \quad \textbf{(2.9)}$$

where:

ε’ = Strain rate
ε'_0 = Reference strain rate
C_1 = Material parameter that reflects change in shear induced excess pore water pressure as result of change in strain rate
C_2 = Material parameter—normalized shear induced excess pore water pressure at peak stress at reference strain rate
D_1 = Material parameter—normalized shear induced excess pore water pressure at peak stress for normally consolidated clay at reference strain rate
D_2 = Material parameter that reflects change in normalized shear induced excess pore water pressure at peak stress as result of change in O.C.R. at reference strain rate

2.1.4 Influence of Plasticity Index on Strain Rate Effects

Because of the increased shear strength shown by in-situ vane shear tests, Bjerrum (1973) proposed a correction factor, μ which should be multiplied by in-situ vane shear test shear strength to obtain actual shear strength. This correction factor is based on plasticity index and ranges from 1 (for a PI of zero) and between 0.5 and 0.6 (for a PI of 120).

Hanzawa and Tanaka (1992) analyzed undrained shear strength tests with a wide range of PI values. Their research suggests that PI does not influence the rate effect of clays.

2.2 Pile Capacity in Clay

It has been shown above that the shear strength of soil increases as the rate of load or strain rate is increased. Since piles in clay derive their capacity from shear resistance, their capacity follows a similar trend as the shear strength of the soil they

are driven into. Shear resistance of piles has been modeled by some researchers. Smith (1960) proposed the model outlined by Equation 2.10.

$$R_t = R_s(1 + Jv) \quad \textbf{(2.10)}$$

where:

R_t = Total resistance
R_s = Static resistance
v = Velocity of pile
J = Damping coefficient

This model may be inadequate since the increase in strength with velocity is linear; the increase in strain rate has been shown to be non-linear.

Briaud and Garland (1985) proposed a model that takes into account the non-linear nature of rate effects. This model is introduced in Equation 2.1 with shear capacity of soil being shown to vary with different times to failure. Briaud and Garland (1985) and Briaud et al. (2000) also applied this same model to the capacity of piles. They substituted the undrained shear strength variables in Equation 2.1 with ultimate pile capacity. Briaud et al. (2000) specifically referenced Statnamic tests which were analyzed by this equation with good success.

In a different approach Hyde et al. (1998) applied Equation 2.8 to pile capacity.

2.2.1 Failure Load Determination

When axial load tests are performed, reference frames are built around, but do not touch, the pile. Linear voltage displacement transformers (LVDTs) or string

potentiometers are placed between the test pile and the reference frame which does not move. In this manner, the movement of the pile relative to the soil around it (or the absolute movement) can be obtained. This deflection is graphed versus the load applied to the pile.

2.2.1.1 Davisson Failure Method

According to Coduto (2001), Davisson's method of failure load determination has become the standard method of failure load determination for static and Statnamic load tests. When this method is used a Davisson line is drawn on the Load versus Deflection plot. This line crosses the y-axis at 4mm + B/120. The Davisson line has a slope of D/EA. The slope of the line is the compression of the pile without any side friction. The failure load is the value where the Davisson line crosses the Load versus Deflection curve (Coduto, 2001).

$$Deflection = 4mm + \frac{B}{120} + \frac{PD}{EA} \tag{2.11}$$

where:

B = Foundation Diameter
P = Load
D = Foundation Depth
A = Foundation Cross-Section Area
E = Foundation Modulus of Elasticity

2.2.2 Static Load Testing Method

Currently, the standard test for axial capacity of foundation piles is a static test which applies a vertical load directly to the pile head, usually in a series of increasing

load increments. For many years, the standard static test was the slow maintained load test (SML) which loads a pile to failure in 16 to 20 hours. Today, quick maintained load tests (QML) which load the pile to failure in one to five hours are also used. Static load tests are loaded slowly enough that any dynamic effects are negligible and therefore not accounted for. Commonly the reaction is provided by reaction piles or ground anchors which must be installed prior to the test. Sometimes, weights are placed directly onto the test pile, which is of course the ideal scenario since no interaction with reaction piles and the test pile is possible (Poulos, 1998); however, cost and safety concerns increase as the failure load increases. Static tests are the most commonly used method for obtaining pile capacity because they apply a load which is similar to the loads applied by structures which piles are meant to support. During static tests, the entire test pile is in compression. The force in the pile decreases with depth and this decrease in force represents the static resistance of the pile. The entire pile moves in the same direction with nearly the same velocity which equals the rate of loading (Middendorp et al., 1992).

Static tests, being direct tests, are the most precise way to determine axial load capacity of piles, but they do have some disadvantages. A major problem with static tests is that they are very expensive, and require a large amount of time to set up because of the load frames which are usually required. Because of high cost, and time required to perform static load tests, testing methods which determine load capacity indirectly are continually sought.

2.2.3 Dynamic Load Testing Method

An alternative to static load testing is dynamic load testing by means of a drop hammer or pile driving hammer. Dynamic load testing does not require a load frame or reaction piles to be constructed, just a pile driving hammer which is typically already located on site. Therefore, in many cases, dynamic load tests can be an efficient and cost effective alternative to static load tests.

The duration of the impact load provided by the pile hammer is very short compared to the time it takes for the resulting stress wave to travel down the length of the pile to the bottom. Because of the relatively slow propagation of stress waves, the entire pile does not experience compression at the same time. In fact, portions of the pile are in tension as other portions are in compression. The result is that some portions of the test pile may be moving upward while others are moving downward. Therefore, effects of the stress wave propagation need to be considered whenever static capacity is derived from a dynamic load test (Coduto, 2001).

Middendorp et al. (1992) explain some disadvantages of dynamic load tests compared with static load tests. These disadvantages include the following:

- Tension waves produced by stress wave phenomena can damage a pile.
- Damage to the pile can also result from eccentric loading.
- Highly educated engineers are required to analyze the results.
- Large drop-masses become difficult to lift and guide when dropped for high capacity piles.

2.2.4 Statnamic Load Testing Method

The Statnamic testing method is a relatively new way to test pile capacity. The method was developed by Berminghammer Corp of Canada and TNO Building and Construction Research of the Netherlands (Brown, 1994). The Statnamic test supplies loads to the test pile in a unique way. A reaction mass is placed on top of the pile and then is accelerated upward by the combustion of a fast burning, solid fuel. As the force of the burning fuel accelerates the reaction mass, an equal and opposite force pushes the test pile downward.

Before a test takes place, the reaction mass is lowered until it is resting on the test pile. At the bottom of the reaction mass is a cylinder which acts as a combustion chamber. A piston is part of the assembly placed on top of the pile. The piston is inserted inside the cylinder to create a combustion chamber similar to the combustion chamber of an internal combustion engine. A schematic of this mechanism is shown in Figure 2.2.

The Statnamic testing method has many potential advantages over static or dynamic testing methods. As its name suggests, it has characteristics of both static and dynamic tests. The duration of a Statnamic test is on the order of ten times longer than that for a dynamic load test. With load applied over a longer period of time, stress waves do not develop as with the dynamic load tests. With the Statnamic load test, the entire test pile moves in the same direction, much like piles tested under static loads (Middendorp et al., 1992; Brown, 1994). This fact makes the Statnamic test easier to analyze than dynamic load tests. Nevertheless, it is clear that the Statnamic test is in fact a dynamic event and as such, dynamic effects need to be accounted for

(Middendorp et al., 1992; Goble et al., 1995). No sudden impact is associated with the Statnamic test. Therefore, with a Statnamic test, damage to the test pile which is common to dynamic tests is almost eliminated (Abe et al., 1998).

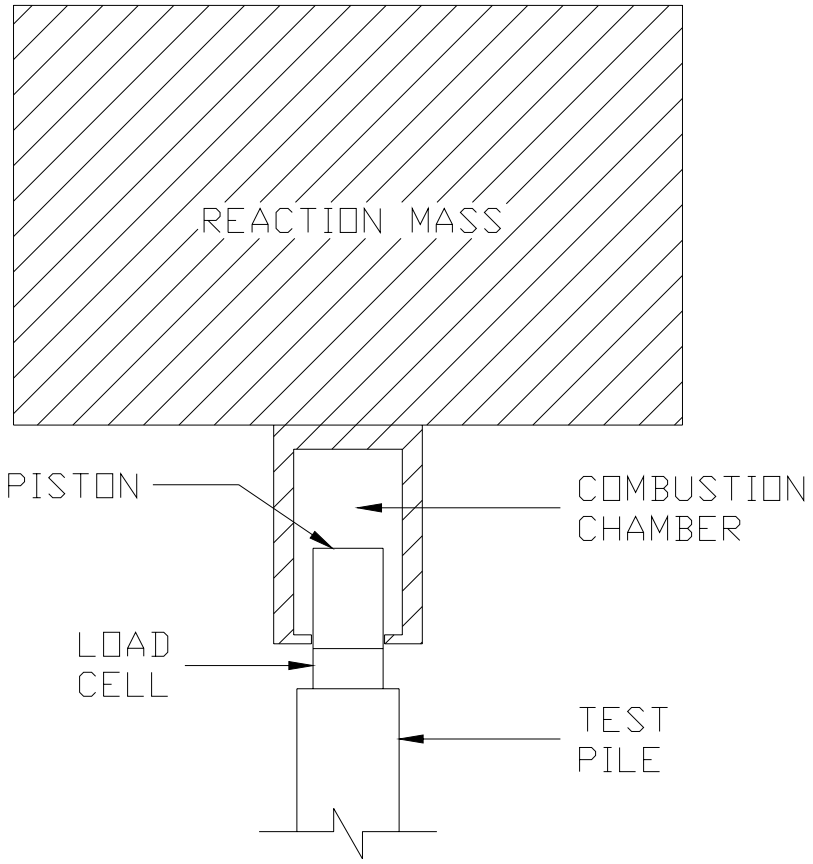

Figure 2.2 Schematic of the Statnamic Device

2.2.4.1 Unloading Point Method

The Statnamic testing method is useful if it can accurately predict the static capacity of a pile. It does however have dynamic components associated with it, due to the nature of the rate at which load is applied, therefore some kind of analysis

method is required to predict static capacity. An analysis method which is useful in many applications is referred to as the "Unloading Point Method" and was introduced by Middendorp et al. (1992). This analysis method has become the accepted standard method for obtaining predicted static capacity of foundation piles from Statnamic test data.

The UP method models the pile as a rigid body. This assumption is a valid one because during a Statnamic test, the entire pile is moving in the same direction with nearly the same velocity. Longer piles cannot be modeled as a rigid body since stress waves develop and the entire pile may not be moving in the same direction. A short pile will deflect nearly as much at the toe as it does at the top and stress waves will not develop. Middendorp and Bielefeld (1995) describe a wave number, N_w. This wave number is used to determine if the UP method is applicable to any given Statnamic test. N_w is calculated using Equation 2.12.

$$N_w = \frac{D}{L} = \frac{cT}{L} \qquad \textbf{(2.12)}$$

where:

D = Wave Length
L = Length of Pile
c = Wave Speed (Typical values: 4000 m/s for concrete, 5000 m/s for steel.)
T = Time of test

Middendorp and Bielefeld (1995) showed that the Unloading Point Method accurately uses Statnamic data to predict axial capacity for piles with an N_w value greater than 12. Several other analysis methods have been proposed for application to

longer piles and some of them are outlined by Mullins et al. (2002). Only an explanation of the method proposed by Middendorp et al. (1992) will be given here, since it applies to all Statnamic load tests analyzed in this work.

The Unloading Point Method by Middendorp et al. (1992) is briefly explained below.

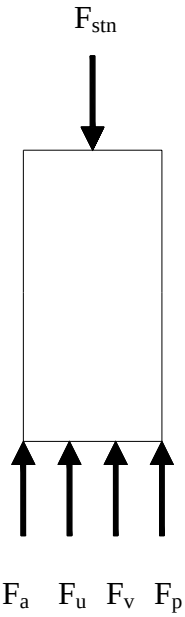

Figure 2.3 Free-Body Diagram of Statnamic Test Pile

The forces applied to the pile are as follows:

1. F_{stn}, the Statnamic load which is measured directly by the load cell.
2. F_a = ma = mass times acceleration. The mass is the known mass of the pile. Some soil may adhere to the sides of the pile and could be included in this mass calculation. The acceleration is obtained directly by

accelerometers (mounted on top of the pile) and its direction may be up or down.

3. F_u, the static or corrected load. This is the load value after damping and inertial forces are subtracted.
4. F_v, the damping force = Cv = damping factor times velocity. The damping factor is a calculated value which equals force / velocity and the method for calculating it is explained below. The velocity is obtained by integrating the accelerometer data.
5. F_p = Water pore pressure resistance. Currently, this value is taken out of equations when using the UP method. For simplicity, it is assumed to be accounted for as part of the damping. Hence:

$$F_u(t) = F_{stn}(t) - F_a(t) - F_v(t) \quad \textbf{(2.13)}$$

It should be noted that this method lumps end bearing and side friction together.

- Segment 1: The reaction mass is placed on the test pile. A small static load along with a small displacement can be seen.
- Segment 2: The launch of the reaction mass and the initial portion of the test is elastic.
- Segment 3: The velocity and inertia increase at a greater rate. Full Statnamic load is reached at the end of this area at (t_4).

- Segment 4: The Statnamic load decreases but, because of inertia the pile continues to deflect until it reaches its maximum deflection at the end of this area. Static capacity is fully mobilized in this area. Because of zero velocity at the end of this area, damping is zero and Equation 2.13 is reduced to Equation 2.14.

$$F_u(t_{u\max}) = F_{stn}(t) - F_a(t) \quad \textbf{(2.14)}$$

- Segment 5: Pile is unloaded fully, and a permanent offset results if full static capacity was mobilized.

The damping coefficient C_4 can be calculated by rearranging Equation 2.14. The result is Equation 2.15.

$$C_4 = \frac{F_{stn}(t_4) - F_u(t_{u\max}) - ma(t_4)}{v(t_4)} \quad \textbf{(2.15)}$$

where:

$F_{stn}(t_4)$ = maximum Statnamic load (t_4 is defined by the point at which the maximum Statnamic load occurs)
$F_u(t_{umax})$ = static load at maximum displacement as computed by Equation 2.14
$ma(t_4)$ = mass of the pile x acceleration at maximum Statnamic load
$v(t_4)$ = velocity at maximum Statnamic load

With the value C_4 from Equation 2.15, Equation 2.13 can be rewritten as Equation 2.16.

$$F_u(t) = F_{stn}(t) - C_4 v(t) - ma(t) \qquad \textbf{(2.16)}$$

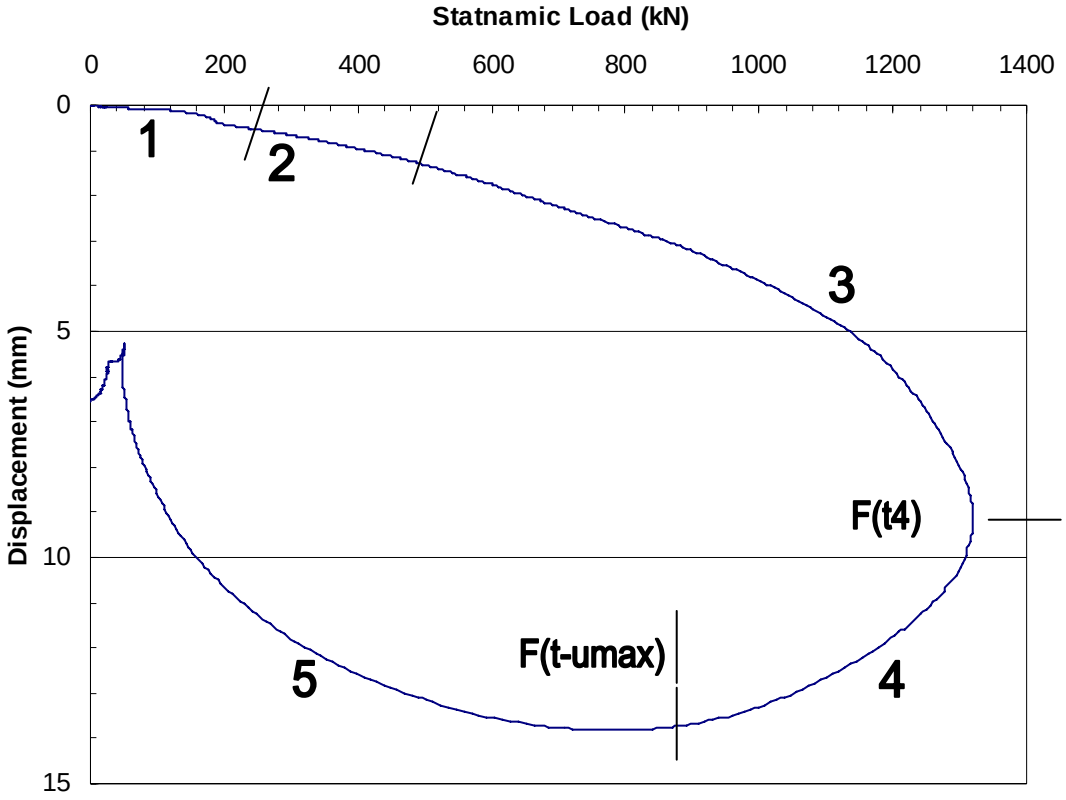

Figure 2.4 Typical Statnamic Load Versus Displacement Curve

Figure 2.4 illustrates five important parts of a typical Statnamic load test. Equation 2.16 can be used to calculate the static soil resistance at any value, t.

The Unloading Point method has been proven useful by finite element analysis conducted by several engineers (Middendorp et al., 1992; Nishimura and Matsumoto, 1995). It has provided results similar to those obtained by actual static load tests (Middendorp et al., 1992; Brown, 1994; Nishimura and Matsumoto, 1995). Given the velocity of test piles during Statnamic tests, Equation 2.8 suggests that the increase in shear resistance for a Statnamic test should be around 100%. Hyde et al. (1998) also

point out that α could be higher than one and could make dynamic shear resistance increase by an order of magnitude. Work still needs to be done in order to use the Statnamic test to accurately predict static capacity of deep foundations in clays.

2.2.4.2 Shortcomings of the Unloading Point Method

The most obvious shortcoming of the Statnamic load method is that it is a dynamic test and therefore will never have the precision of the static test when deriving static capacity. Goble et al. (1995) point out that the mass of the pile could be considerably increased by soil adhered to the pile. The mass of soil moving with the pile cannot be determined. If adhered soil increases the mass considerably, then the inertial component of the Statnamic load will be underestimated and in turn the static capacity will be overestimated.

Damping effects, particularly in clay, are not well understood. Pore pressure resistance could be a large contributor to the Statnamic resistance especially in clayey soils. The pore pressure resistance is assumed to be taken into account as a part of the damping, but this is a crude model (Middendorp et al., 1992). According to Brown (1994), the Unloading Point method may over predict static capacity in stiff, overconsolidated clays by 25 to 30%. Dynamic shear resistance in clays versus rate of shearing is nonlinear (Hyde et al., 1998; Goble et al., 1995). The Unloading Point method does not account for this phenomenon. Nishimura and Matsumoto (1995) state that the Unloading Point method tends to overestimate the damping factor, C. This overestimation tends to underestimate pile head stiffness at the beginning of the test.

The Unloading Point method is only useful when applied to relatively short piles. With longer piles the rigid body assumption is not valid (Goble et al., 1995). Goble et al. (1995) argued that the unloading phase of a Statnamic test is short enough to generate stress waves and therefore large tension stresses. This would then, violate the assumption that a pile loaded with a Statnamic device can be modeled as a rigid body as the Unloading Point method does. However, there is evidence that shows large tension stresses do not develop during unloading (Goble et al., 1995).

2.2.4.3 Factors to Accurately Predict Static Capacity

Mullins et al. (2002) developed adjustment factors to account for "rate increase" of Statnamic load tests in different soil types. They are: 0.96 for rock, 0.91 for sand, 0.69 for silt and 0.65 for clay. Statnamic failure load is multiplied by the appropriate factor to obtain the corrected static test load.

3 Geotechnical Investigation of Test Site

Geotechnical investigations were performed previously at the test site to characterize an area of approximately 800 square meters. Most of the in-situ and laboratory tests of subsurface soils were performed between March 1999 and March 2001. The results of these tests are presented by Cole (2003) who used the same test site and test piles 11 through 25 which were used in this study as well. All of the data in chapter 3 are from Cole (2003), including charts and tables which are used here with permission.

3.1 Test Site Overview

The field testing was performed on property owned by the Utah Department of Transportation, UDOT. The test site is located at South Temple and I-15 in Salt Lake City, Utah. The topography of the site is quite flat at approximately 1289 meters above sea level. Prior to the installation of the test piles, 1.1 m of surface soils were removed from the test site. The resulting surface is referred to as the ground surface in this thesis. Figure 3.1 is a map of the site which shows locations of various tests and sample locations.

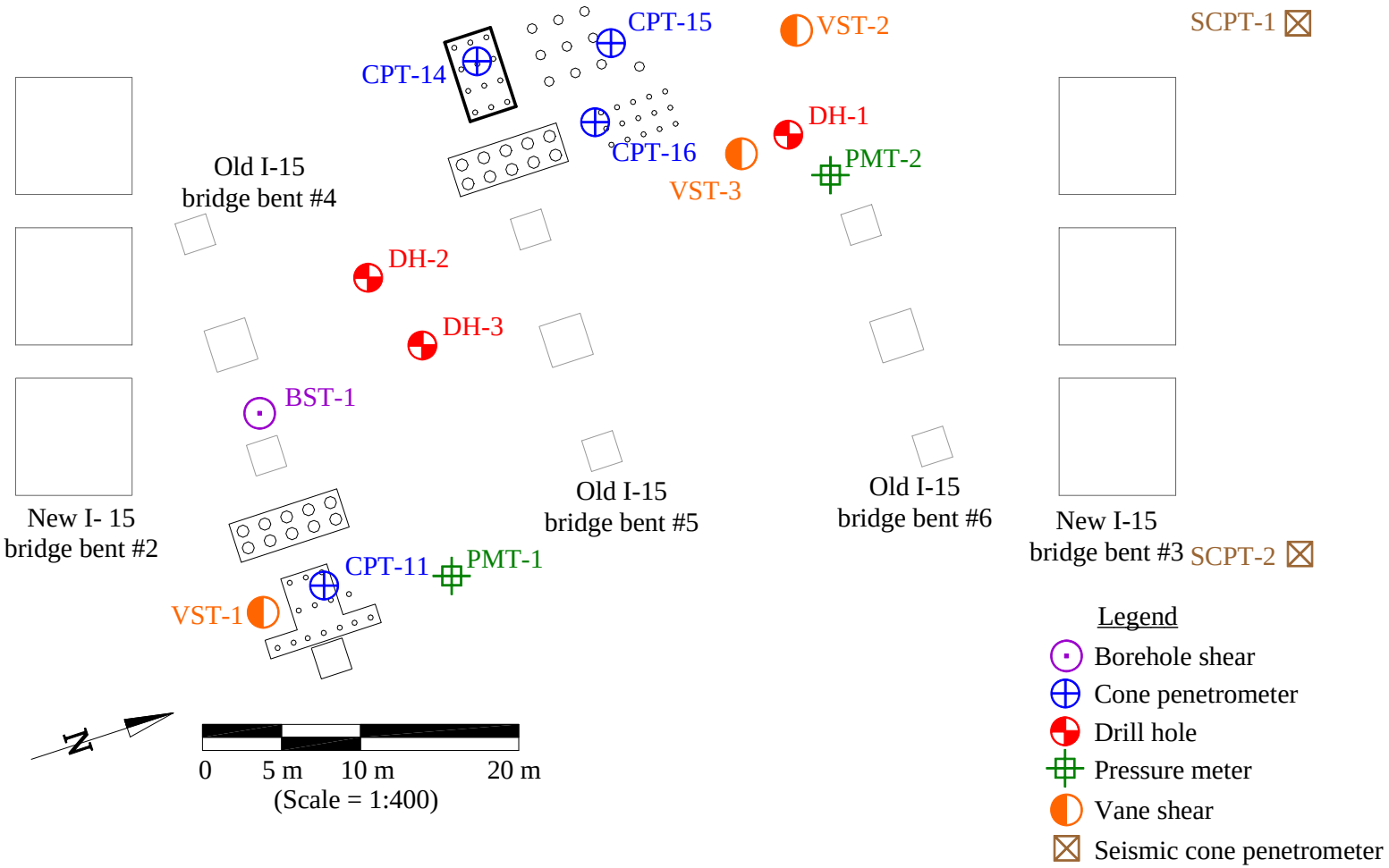

Figure 3.1 Site Map and Test Locations (Cole, 2003)

3.2 Soil Profile and Properties

Soil test boring were performed by RB&G Engineering and the soil samples were obtained in general accordance with ASTM D 1586 and D1587. A 152 mm hollow stem auger with a plug at the end was used to drill the test holes. The locations of these drill holes are mapped by Figure 3.1. For cohesive soils, relatively undisturbed samples were taken with 76.2 mm diameter Shelby tubes and for cohesionless soils, disturbed samples were taken with a 50.8 mm outside diameter split-spoon sampler. The geotechnical investigation showed that the subsurface is relatively consistent laterally within the investigated area. Table 3.1 gives a description of the soil profile in this area.

Table 3.1 General Soil Description (Cole, 2003)

Depth Below Ground Surface (m)	General Soil Description
0 – 1.0	Brown to dark brown fat clay, moist.
1.0 – 2.8	Olive lean clay with silty sand seams, wet.
2.8 – 3.4	Brown to dark brown silty sand, wet
3.4 – 4.0	Gray to olive lean clay with silty sand seams, wet.
4.0 – 5.0	Brown to gray silty sand, wet
5.0 – 9.6	Gray to green-gray sensitive lean clay, wet.
9.6 - 11	Dark brown to black lean clay with silt and silty sand layers, wet.

3.2.1 Laboratory Testing

Laboratory testing was done at the soils laboratory at Brigham Young University. Index properties obtained from the laboratory testing are presented in Table 3.2 and in graphical form in Figure 3.2.

In the upper 5 meters, the natural moisture content, w_n was less than the liquid limit, which indicates that the soil is overconsolidated. However, the natural moisture content is greater than the LL below 6 meters which generally means that the soil is normally consolidated and could also be sensitive in some cases.

3.2.1.1 Consolidation

Relatively undisturbed samples from drill hole DH-1 were tested in general conformance to ASTM D 2435. The results are shown in Table 3.3. Below approximately 6.5 meters, the soils are normally consolidated. Above 6.5 meters, the soil appears to be overconsolidated with OCR increasing as depth decreases. This is likely due to desiccation from the fluctuation of the ground water level.

3.2.1.2 Shear Strength Properties

In the laboratory, miniature vane shear tests (MVST) and unconfined compression tests (UC) were performed to obtain shear strength values. The results of these tests are shown in Table 3.5 in tabular form and in graphical form in Figure 3.2 (c).

Table 3.2 Index Properties from Drill Holes (Cole, 2003)

Drill Hole	Depth below excavated ground (m)	Natural moisture content[a] (%)	Material finer than 0.075 mm [b] (%)	Moist / saturated unit weight [c] (kN/m^3)	Liquid limit, LL [d] (%)	Plastic limit, PL [d] (%)	Plasticity index, PI [e] (%)	Liqudity index, LI [f] (%)	USCS Symbol [g]
DH-3	0.08	32.4	-	-	63	20	43	0.3	CH
DH-3	0.1	32.4	-	-	47	20	27	0.5	CH
DH-1	0.2	29	90.2	19.8	49	27	22	0.1	CL
DH-2	0.2	34.4	-	-	61	38	23	-	MH
DH-3	0.4	30.1	-	-	57	19	37	0.3	CH
DH-3	0.4	30.1	-	-	46	19	27	0.4	CH
DH-3	0.5	36.9	-	-	37	26	11	1	ML
DH-3	0.7	43.8	-	-	45	19	25	1	CL
DH-3	1	25.1	-	-	29	16	13	0.7	CL
DH-3	1.1	27.9	-	-	35	20	15	0.5	CL
DH-3	1.3	28.2	-	-	23	17	5	2	CL-ML
DH-3	1.4	20.9	-	-	NP[h]	NP[h]	NP[h]	NP[h]	SM
DH-3	1.6	29.4	-	-	37	18	20	0.6	CL
DH-1	1.7	62.8	51	18.6	NP[h]	NP[h]	NP[h]	-	ML
DH-3	1.7	32.8	-	-	31	15	16	1.1	CL
DH-2	1.8	35	-	-	31	18	13	1.3	CL
DH-1	1.9	27.3	79.7	19.6	33	21	12	0.05	CL
DH-1	2.5	28.6	90.2	19.1	38	23	15	0.3	CL

Table 3.2 Index Properties from Drill Holes (Cole, 2003) (Continued)

Drill Hole	Depth below excavated ground (m)	Natural moisture content[a] (%)	Material finer than 0.075 mm [b] (%)	Moist / saturated unit weight [c] (kN/m^3)	Liquid limit, LL [d] (%)	Plastic limit, PL [d] (%)	Plasticity index, PI [e] (%)	Liqudity index, LI [f] (%)	USCS Symbol [g]
DH-2	2.7	28	-	-	35	21	13	0.5	CL
DH-1	3.6	28.8	97.4	19.9	36	22	14	0.5	CL
DH-1	4.4	32.9	32.7	-	NP[h]	NP[h]	NP[h]	NP[h]	SM
DH-2	4.5	23.7	-	-	NP[h]	NP[h]	NP[h]	NP[h]	SM
DH-1	5.4	45	99.4	18.3	60	30	30	0.5	CH
DH-1	6.3	54.1	96.7	17.6	52	28	24	1.1	CH
DH-2	8.2	66	-	-	46	27	19	2.1	CL
DH-1	8.9	62.2	99.7	15.8	59	29	30	1.1	CH
DH-1	10.3	53.1	97.4	17.7	63	27	36	0.7	CH

[a] ASTM D 2216

[b] ASTM D 422 and D 1140

[c] Determined from consolidation and unconfined compression data

[d] ASTM D 4318

[e] PI = LL - PL

[f] $LI = (w_n – PL)/(LL – PL)$

[g] ASTM D 2487

[h] LL or Pl could not be determined, reported as non-plastic (NP)

Table 3.3 Consolidation Test Parameters (Cole, 2003)

Depth below excavated ground (m)	Initial void ratio, e_0	Pre-consolidation pressure, s'_{pc} (kPa)	Overconsolid-ation ratio, OCR	Compression Index, Cc [a]	Recompression index, Cr [b]
0.2	0.79	144	30.0	0.185	0.03
1.9	0.73	72	3.9	0.2	0.025
2.5	0.81	96	4.1	0.12	0.025
3.6	1.52	72	2.1	0.19	0.025
5.4	1.68	81	1.7	0.57	0.06
6.3	1.36	86	1.5	0.42	0.04
8.9	1.78	96	1.3	0.535	0.04
10.3	1.52	105	1.2	0.62	0.05

[a] Strain compression index, $C'_c = C_c/(1+e_0)$

[b] Strain recompression index, $C'_r = C_r/(1+e_0)$

Table 3.4 Laboratory Shear Testing Results (Cole, 2003)

Depth below excavated ground (m)	Unconfined shear strength (kPa)	Laboratory miniature vane shear strength (kPa)	Strain at 50% the ultimate soil resistance
0.2	101	-	0.03
0.5	-	69	
1.5	-	43	
1.9	25	-	0.01
2.6	-	45	
3.6	22	-	0.013
3.7	-	60	
5.4	28	-	0.05
5.6	-	43	
6.3	23	-	0.03
6.6	-	29	
8.8	-	31	
10.3	28	-	0.018

3.2.2 In-Situ Testing

3.2.2.1 Cone Penetration Testing (CPT)

Cone penetration testing was performed by Cone-Tec Inc. The location of each sounding can be found in Figure 3.1. The data acquired by the cone penetration testing includes: cone tip resistance, q_c; sleeve friction, f_s; and pore water pressure, u. CPT data are presented in Figure 3.3. The results at all four CPT locations are very consistent, indicating that the soil profile in the test area is consistent laterally.

CPT results were used to estimate the undrained shear strength, s_u of the fine grained, cohesive layers using Equation 3.1.

$$s_u = \frac{q_c - \sigma_v}{N_k} \quad \textbf{(3.1)}$$

where:

σ_v = Total overburden stress
q_c = Cone tip resistance
N_k = Bearing capacity factor for electric cone, 15 used here

The resulting s_u values are presented in Table 3.3 (c). Three layers can be readily distinguished in the s_u profile. From the ground surface to 1.0 m, s_u averages 66 kPa; from 1.5 to 4.0 m, s_u averages 108 kPa and from 5 to 10 m, s_u has an average of 31 kPa.

3.2.2.2 Standard Penetration Testing (SPT)

Standard penetration tests, SPT were conducted in the cohesionless, silty sand layers. A 65 kg automatic trip hammer was used to advance the sampler. The number of blows (blow-count), N required to drive the sampler 0.3 m is recorded in

(a). Based on previous energy measurements, 80% of the theoretical free-fall energy is actually applied by the hammer. Equation 3.2 was used to normalize the blow count to 60% energy and correct for effective overburden stress, producing $(N_1)_{60}$. Results are posted in Figure 3.2(a).

$$(N_1)_{60} = N\left(\frac{p_a}{\sigma'_v}\right)^{\frac{1}{2}}\left(\frac{E_{applied}}{60\%}\right) \quad \textbf{(3.2)}$$

where:

N = Blow count (blows/3 m)
p_a = Atmospheric pressure
$E_{applied}$ = Energy applied to drill rod (80%)
σ'_v = Effective overburden stress

The relative density, Dr was estimated from SPT data, using Equation 3.3. Relative density results are posted in Figure 3.4 and agree well with relative density values attained by CPT testing.

$$D_r = \sqrt{\frac{(N_1)_{60}}{40}} \quad \textbf{(3.3)}$$

3.2.2.3 Shear Wave Velocity Testing

Cone-Tec, Inc. performed shear wave velocity tests. Locations of these tests (labeled SCPT-1 and SCPT-2) are mapped in Figure 3.1. Resulting shear wave velocity, V_s values are presented in Figure 3.4(e). V_s was used to estimate maximum shear modulus, G_{max} and elastic modulus, E_{max}.

$$G_{\max} = \rho V_s^{\,2} \tag{3.4}$$

$$E_{\max} = 2(1+\nu)G_{\max} \tag{3.5}$$

where:

ρ = Mass density of the soil
ν = Poisson's ratio (estimated based on soils type)

Table 3.5 Results from Seismic Cone Testing (Cole, 2003)

Depth below excavated ground (m)	Average V_s (m/s)	Poisson's ratio, ν (estimated)	Maximum shear modulus, G_{max} (MPa)	Maximum modulus of elasticity, E_{max} (kPa)
0.0 - 1.0	134	0.25	31	78
1.0 - 4.0	178	0.25	55	137
4.0 - 6.0	185	0.25	59	148
6.0 - 10.0	128	0.25	28	71
10.0 - 12.0	157	0.25	43	107

3.2.2.4 Field Vane Shear Testing

Peak undrained shear strength, s_{up} and remoulded undrained shear strength, s_{ur} were obtained by field vane shear testing, FVST. A vane with a torque arm length of 0.305 m and a tapered vane diameter of 63.5 mm was used. Vane shear values were multiplied by a correction factor, μ from Bjerrum (1973). Results are presented versus depth in Figure 3.4.

3.2.3 Soil Profile

A composite soil profile with soil and strength properties is provided in Figure 3.5 which summarizes the result from the field and laboratory testing.

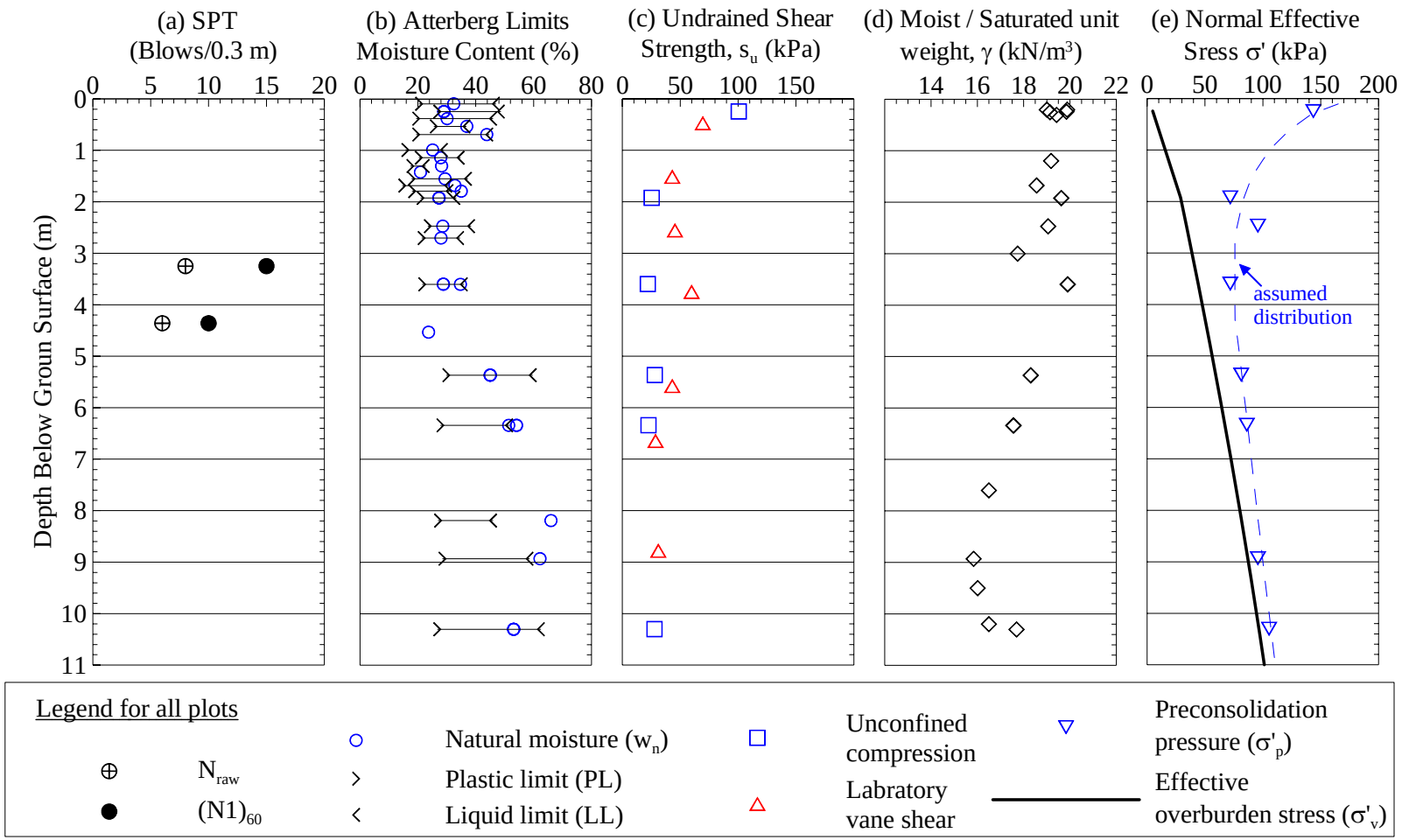

Figure 3.2 Summary of Test Results with Depth (Cole, 2003)

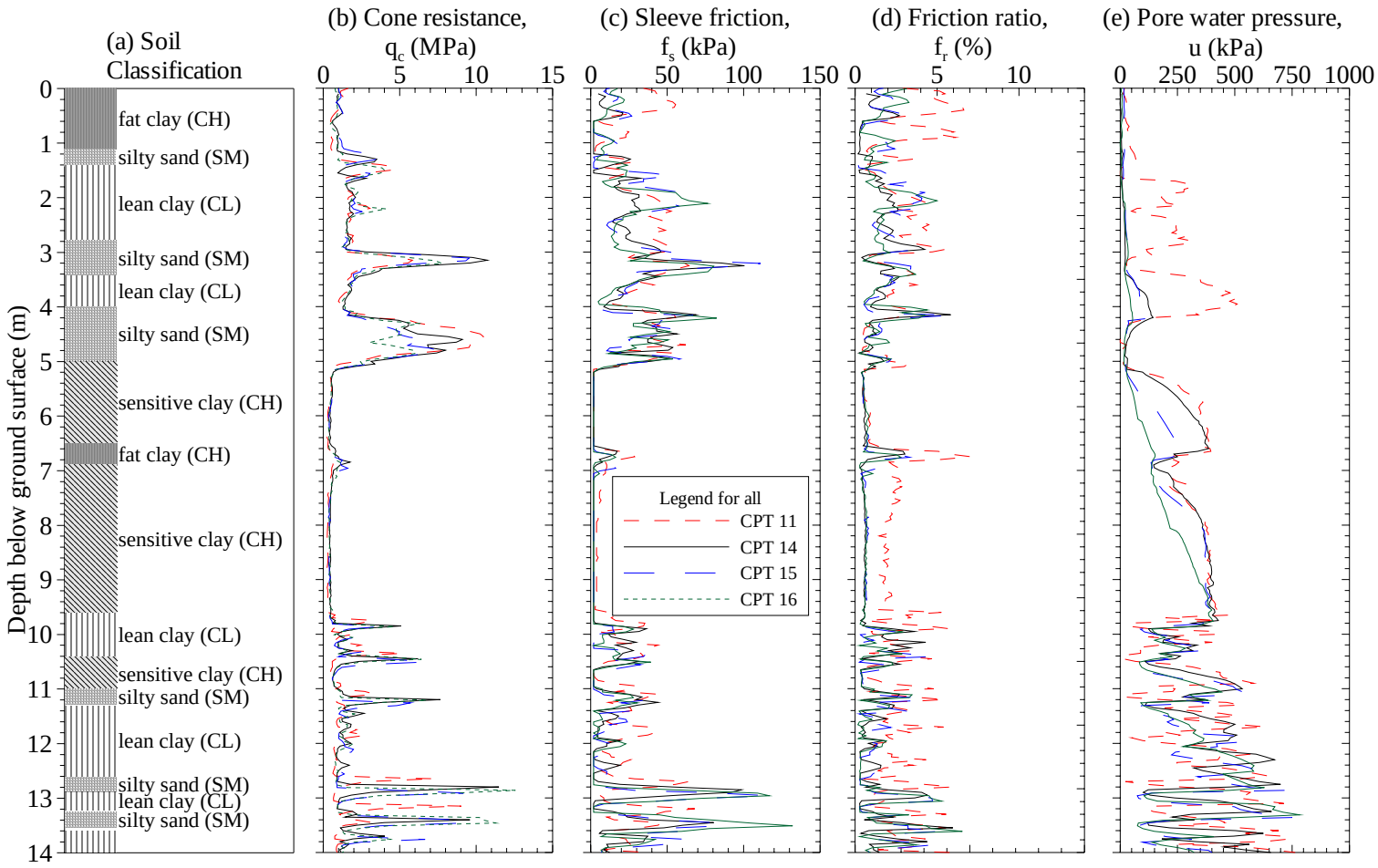

Figure 3.3 Summary of Classification and CPT Results (Cole, 2003)

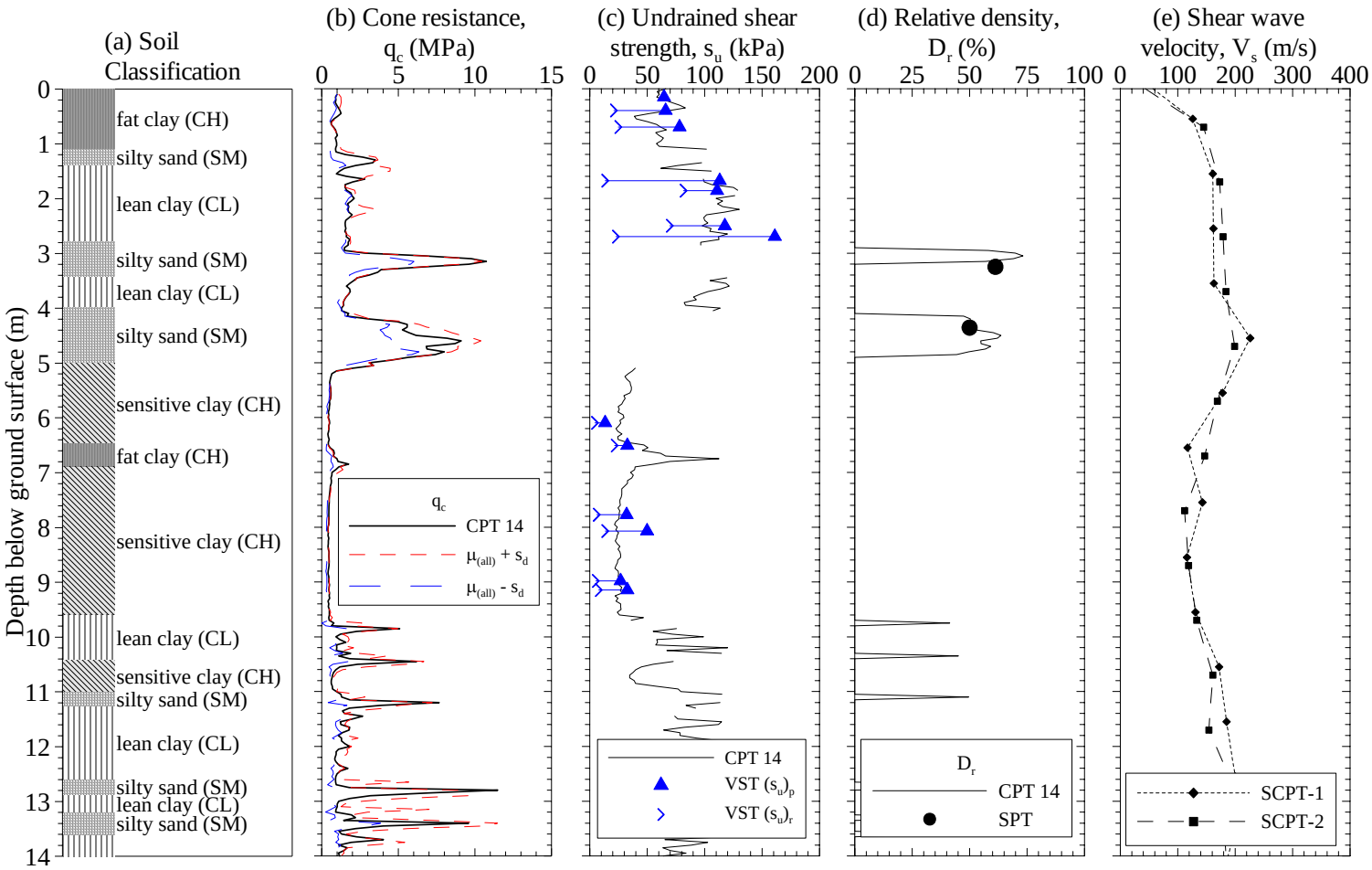

Figure 3.4 Soil Profile Showing q_c and Estimates of s_u, D_r V_s (Cole, 2003)

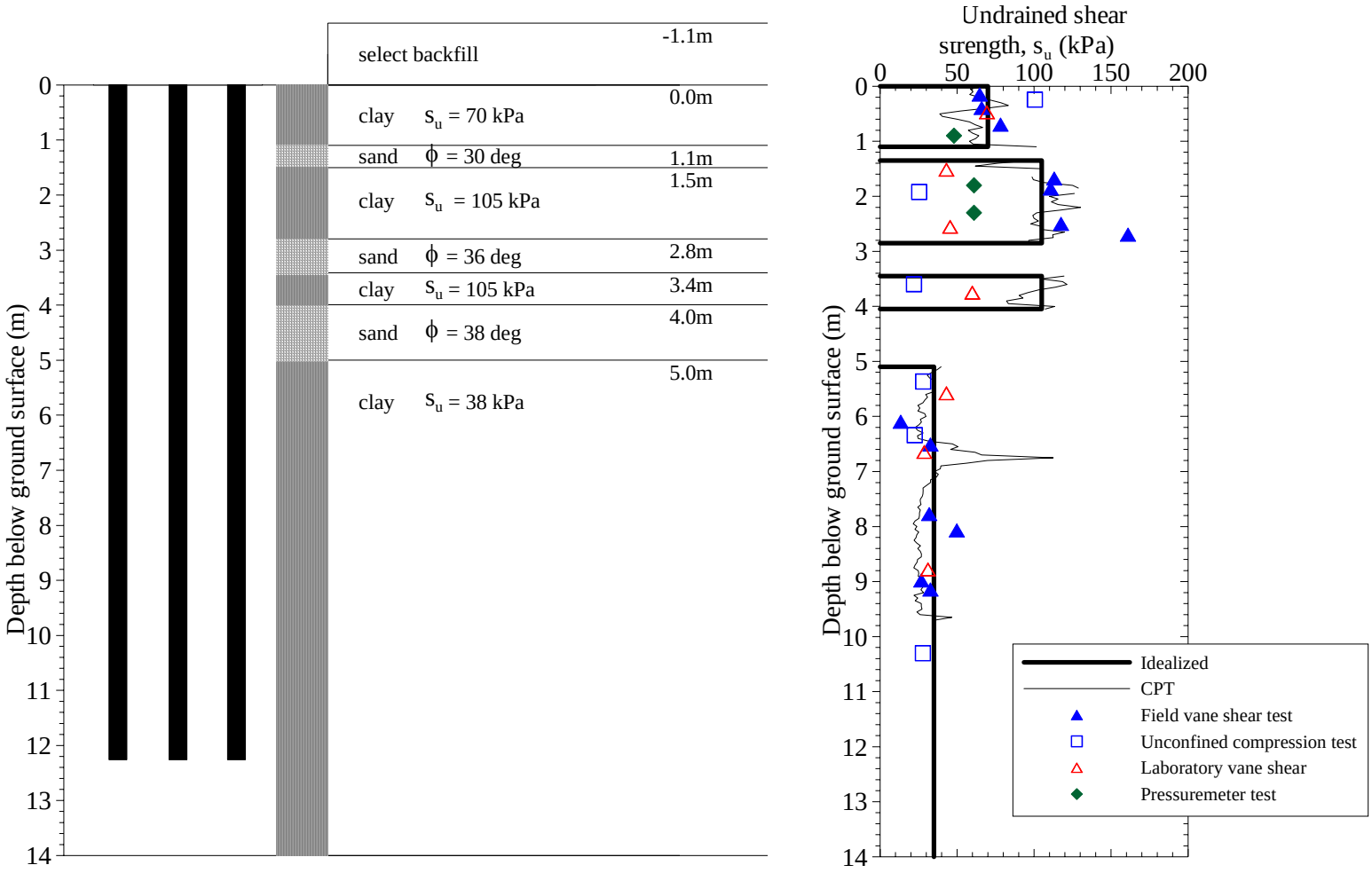

Figure 3.5 Idealized Soil Profile and Strength Properties (Cole, 2003)

4 Field Testing

At the test site, several test piles were loaded, each with a different rate of load application. Figure 4.1 provides an overall map of the test site. Tests using an actuator were conducted on piles in the 15 pile group while the Statnamic test was performed on a single pile about 50 m southwest of the 15 pile group.

Nine tests were performed at different rates of loading on six test piles. A summary showing the number of the test pile, the loading rates that were applied, the date of the test and the means for applying the load is provided in Table 4.1. The tests are subsequently referred to according to their respective times to failure or the duration of the test if the failure load was not reached based on the Davisson failure criteria. The first set of static load tests were performed in November of 2002. These tests include the 18 hour, 48 minute, 2 minute and 10 second tests conducted on test piles 24, 21, 18 and 15, respectively. The 54 minute, 3 minute and 25 second tests were performed in August of 2004 on test pile 14. Finally, supplemental tests were conducted at rates of 2 minutes and 20 seconds on test piles 18 and 15, respectively. To differentiate between these three sets of static tests, they will be referenced according to the year in which they were performed, “2002 Static Load Tests”, “2004 Static Load Tests” and “2006 Static Load Test”, respectively.

Table 4.1 Summary of Tests, Load Duration and Application Method

Test Pile	Loading Duration	Date Conducted	Load Application Method
24	18 hour (1080 min.)	Nov. 2002	MTS 110 kip Actuator
21	48 min.	Nov. 2002	MTS 110 kip Actuator
18	2 minutes 2 minutes	Nov. 2002 Aug. 2006	MTS 110 kip Actuator 400 kip Hydraulic Jack
15	10 second (0.17 min.) 26 sec. (0.43 min.)	Nov. 2002 Aug. 2006	MTS 110 kip Actuator 400 kip Hydraulic Jack
14	54 minutes 3 minutes 25 second (0.05 min.)	Aug. 2004 Aug. 2004 Aug. 2004	300 kip Hydraulic Jack 300 kip Hydraulic Jack 300 kip Hydraulic Jack
26	0.1 second (0.0017 min.)	Aug. 2004	Statnamic Device

4.1 Test Pile Characteristics and Construction

Each of the test piles consisted of a steel pipe with an inside diameter of 12 inches (304.8 mm) and an outside diameter of 12.75 inches (323.9 mm). The pipe piles conformed to ASTM A252 Grade 2 specifications. Based on tests conducted by Geneva Steel, the average yield strength was 404.5 MPa (58.7 ksi) and the tensile strength was 584.1 MPa (84.7 ksi). The test piles were driven to a depth of approximately 40 ft (12.2 m) using a hydraulic hammer. A steel plate was welded flush at the toe to close the end of each pile prior to driving. When the test piles were originally driven in August of 1999, strain gage pairs were attached to the outside faces along the length of the pile and the gages were protected with angle irons which

were welded to the sides of the pile. However, by the time of the testing program in 2002, the gages were no longer functioning.

To provide strain data along the length of the test piles for the next set of tests, an instrumented pipe was inserted inside the 12 inch test piles. Centered inside each test pile was a 152 mm (6 inch) ID schedule 40 steel pipe with a wall thickness of 7.11 mm (0.28 inch) (see Figure 4.2 for a drawing of the test pile cross-section). Strain gages were attached to the outside of the inner pipe along two opposing lines along the pipe's length. These inner pipes were installed in two shorter sections which could be more easily handled and transported to the field site after being instrumented at the university lab. Because of headroom limitations it was also necessary to install the inner pipes in two segments. Therefore, one section was lowered into the pile with approximately one foot of length remaining outside the top of the pile. Then the top section of the inner pipe was raised up and welded to the lower section and both were lowered together to their final position at the base of the outer steel pipe pile. A small steel collar was used as a coupler to aid in the attachment of the two pipe sections. It was necessary to keep the inner pipe centered in the of the pile, so spacers were made of small pieces of rebar and welded to the inner pipe to keep it centered.

Once the inner pipe was in place, a cementitious grout was placed inside the large and small pipes to connect them together so that the two pipes along with the grout would act as a single unit. In the 2002 test piles the grout was pumped through a pvc pipe to prevent the grout from free-falling and trapping air in the grout. The 2004 test piles had grout poured directly from a concrete truck into the pile.

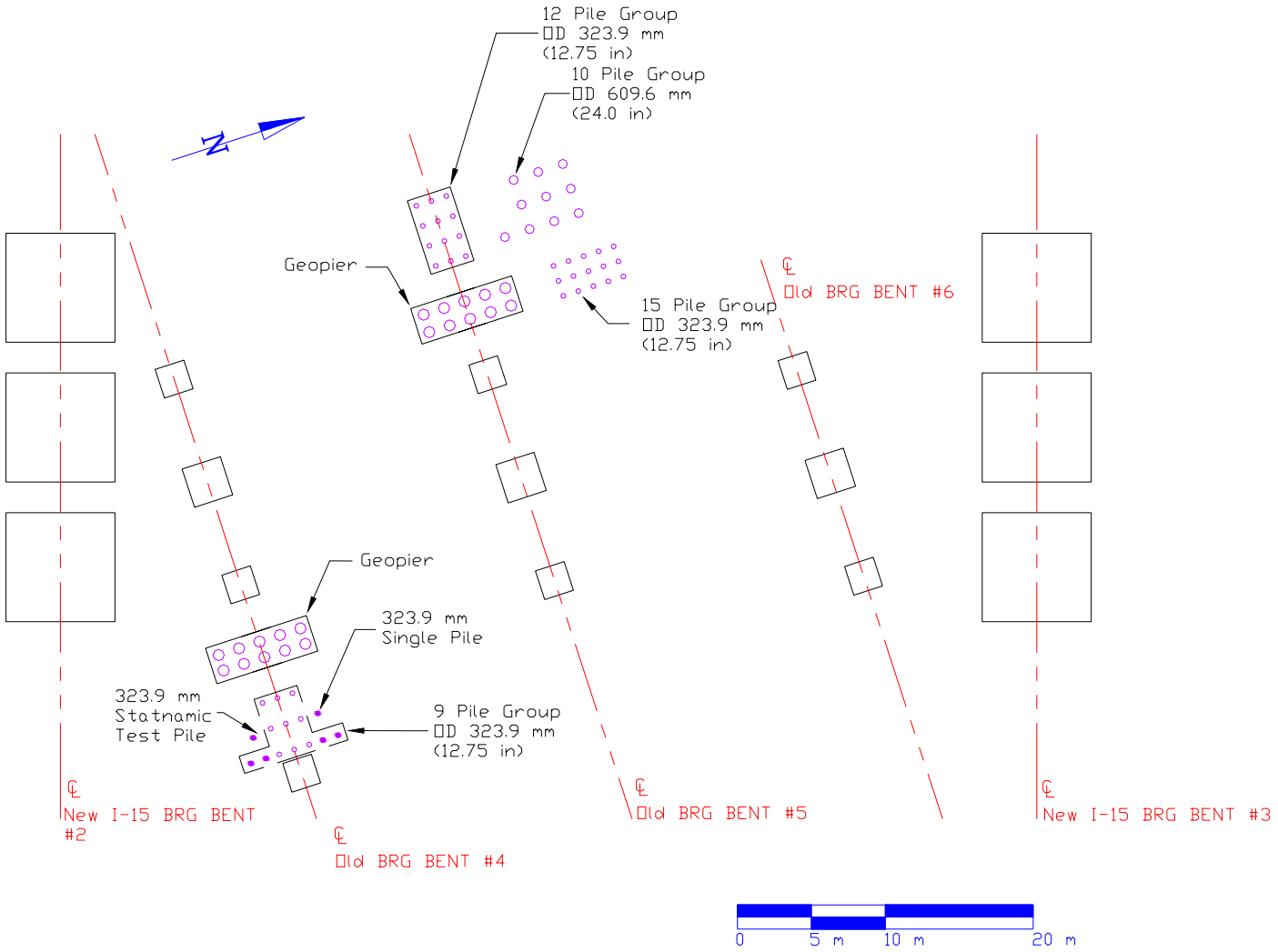

Figure 4.1 Map of Test Site (I-15 and S. Temple in Salt Lake City, Utah)

The grout had a compressive strength of approximately 3.3 ksi and an elastic modulus of approximately 3,320 ksi. Two angle irons were welded on opposing sides of the inner pipe along the length of it, in order to protect the strain gages and their wires. A cross section of the test piles is presented in Figure 4.2 below. The cross sections of all the test piles were similar. Some test piles had angle irons on the outside of the outer pile similar to those on the inner pile.

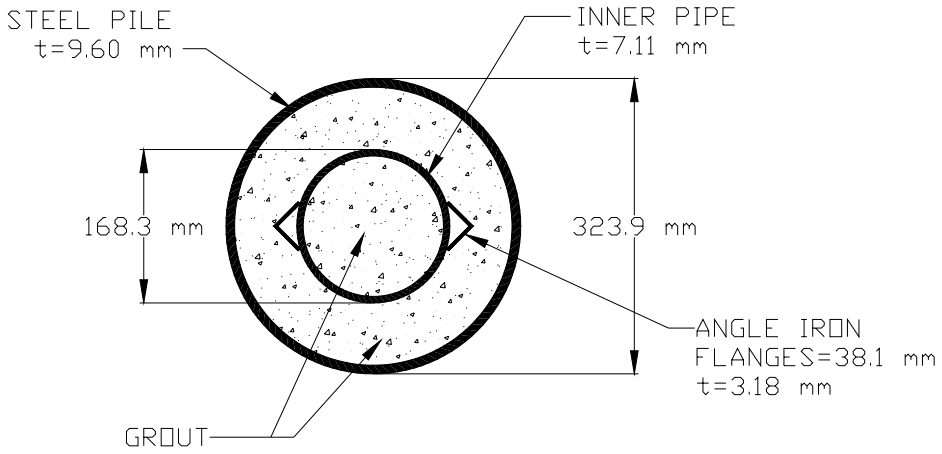

Figure 4.2 Cross Section of Test Pile

After the grout was placed and cured, the steel and grout were ground flat and parallel to the ground. A steel plate was then welded to the top of the pile. The steel plate acted as a surface to react against and transfer load evenly to the entire pile cross-section.

4.2 Static Load Tests

4.2.1 Description of Test Layout

Figure 4.3 is a map of the portion of the test site where the static load tests were performed. The test piles in the 15 pile group were spaced at approximately 1.07 m (3.5 ft) on centers. The map includes numbers which are assigned to each pile. The individual piles will be referred to by the numbers assigned here and the test pile numbers shown in Table 4.1 refer to the number shown in Figure 4.3.

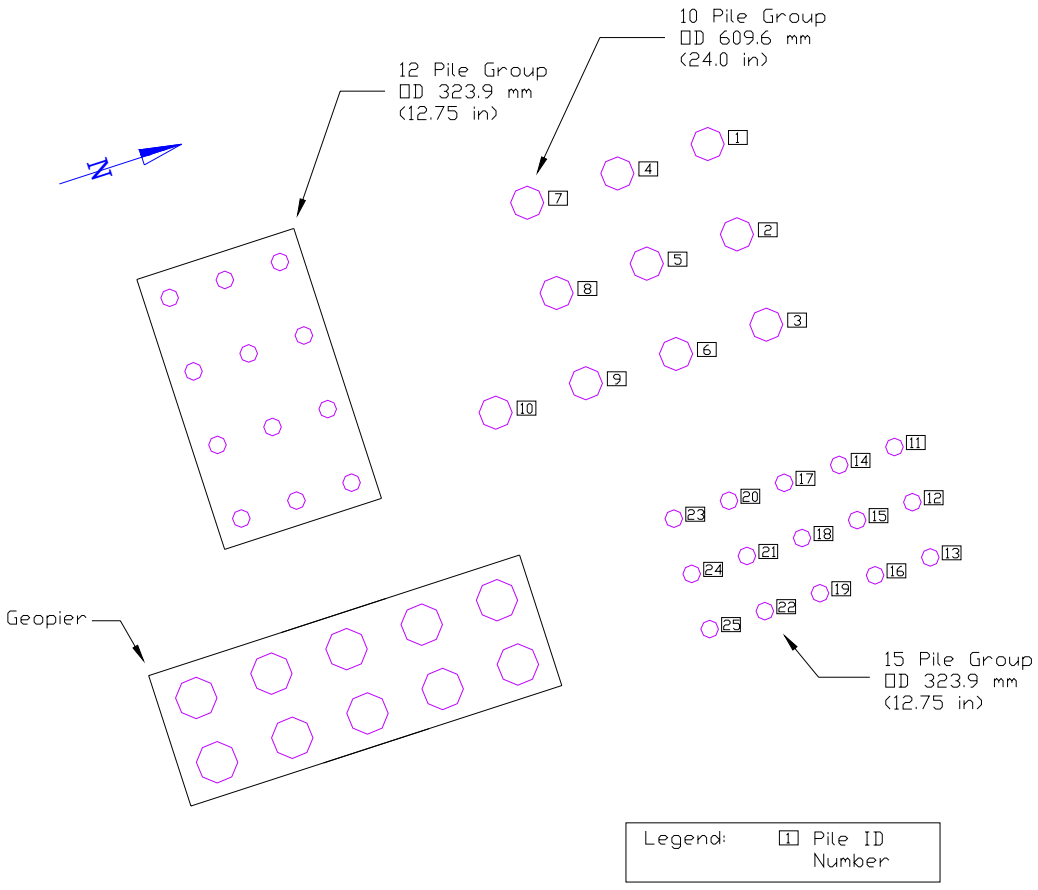

Figure 4.3 Pile Identification

For each of the static load tests, a steel reaction frame was built above the pile to be tested. The reaction frame was attached to at least two separate, previously-driven reaction piles which surrounded the test pile. A hydraulic jack was then placed between the reaction frame and the test pile. The jack was extended while it was held in place by the reaction frame. Therefore, when the jack was extended it loaded the test pile and displaced it downward.

Three different test frames were built. The first test frame was constructed for the 2002 static load tests. This frame was designed so that load tests could be performed on test piles 15, 18, 21 and 24. As shown in Figure 4.4, the main reaction beam was lined up over these four test pile so that the same beam could serve as a reaction. A 488 kN (110 kip) MTS actuator was centered over each test and reacted against the main reaction beam. The reaction beam was in turn held in place by four tie-rods attached to each of four reaction piles (piles 11, 13, 23, and 25 in Figure 4.4) as shown in Figure 4.4. The tie-rods were bolted to a 25 mm thick plate which was welded to each reaction pile. In addition, the reaction beam was supported on each end by a pipe section to hold the beam at the proper elevation above the test piles so the actuator could fit between the test pile and the reaction beam. The MTS actuator was powered by a 30 gallon per minute hydraulic pump which received electric power from a mobile generator. The MTS actuator and pump system made it possible to control the rate of loading during the field testing. A photograph of the load frame and actuator system during the 2002 load test is provided in Figure 4.5

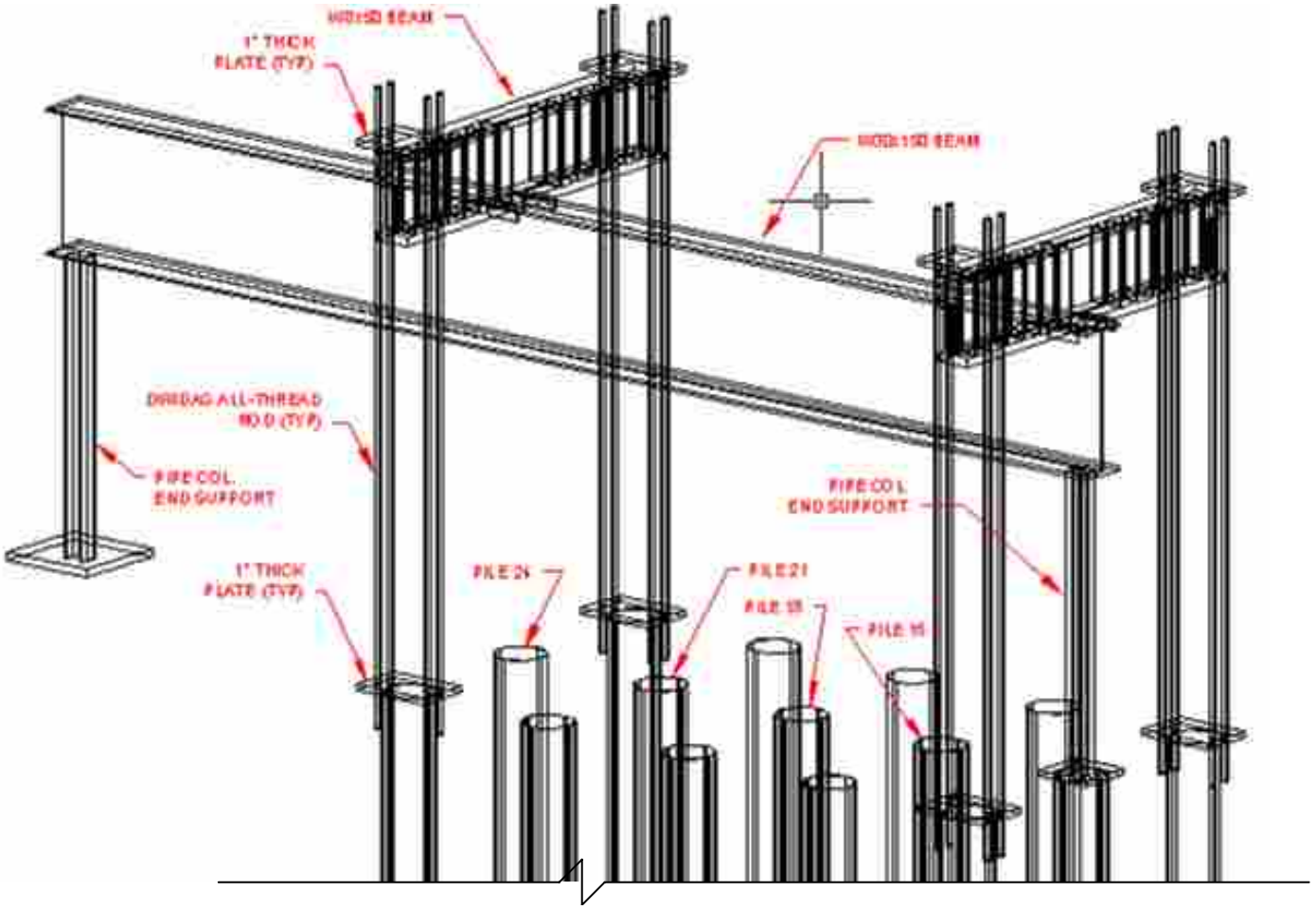

Figure 4.4 Static Load Test Frame (2002 Static Load Tests)

Figure 4.5 Static Load Test Frame (2002 Static Load Tests)

Figure 4.6 Static Load Test Frame (2004 Static Load Tests)

A photograph of the frame for the 2004 static load tests is shown in Figure 4.6. Figure 4.6 shows a deep I-beam which is the member of the reaction frame directly reacted against by the loading jack. This beam was anchored to one 600 mm diameter pile in the foreground (pile number 3) and a smaller cross beam was anchored to two piles (pile numbers 16 and 19) in the background to provide a reaction for the other end of the I-beam. The deep beam and the smaller beam were welded together to attach the deep beam to piles 16 and 19. Steel tubing was welded to surrounding piles and to the deep beam to brace the frame laterally. The test pile in this photograph is the 54 minute test pile (pile number 14) and is located directly beneath the deep beam in the picture.

Two swivel plates were used during each static test; one between the jack and the reaction frame, and the other between the jack and the test pile. These swivel plates prevent eccentric load or moment from being applied to the test pile. They were used to ensure that the force from the jack was applied to the test piles as a purely axial load.

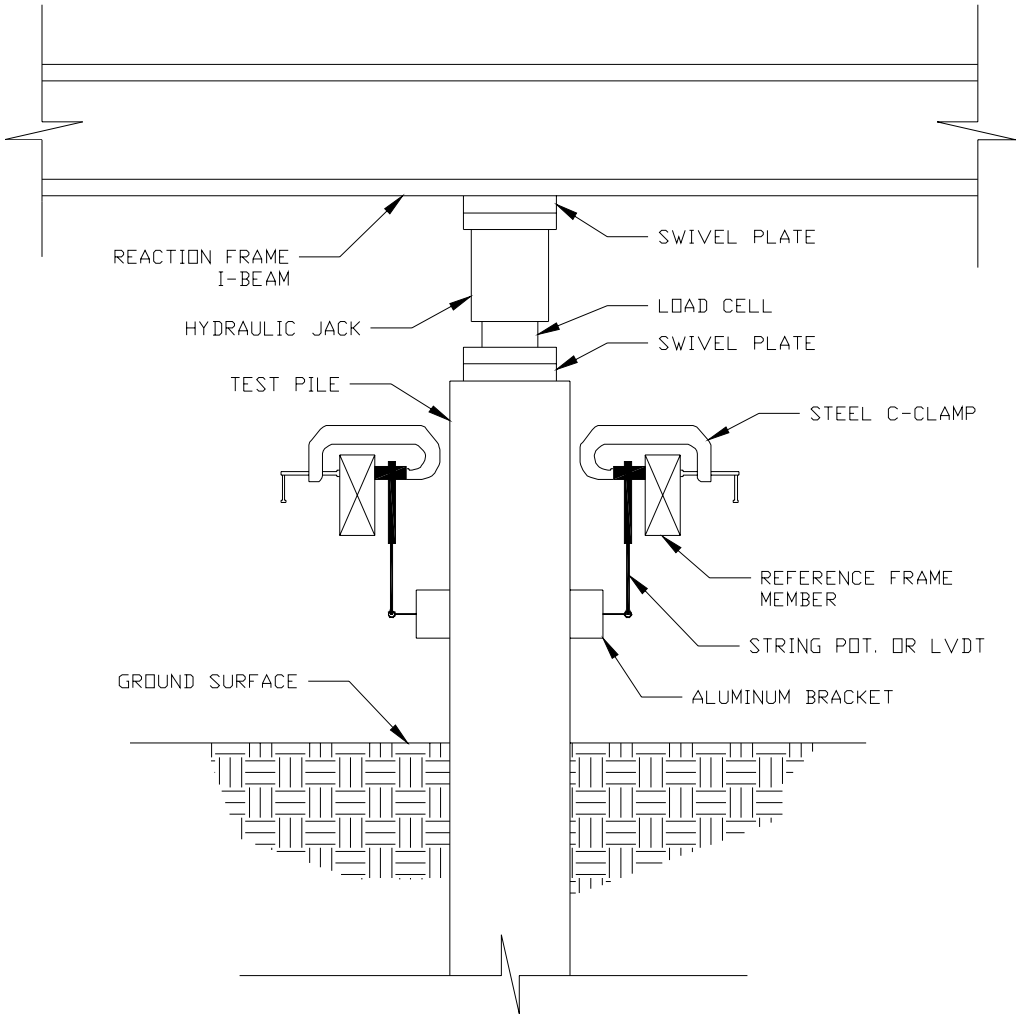

Figure 4.7 Elevation View of Static Load Test

The configuration of the equipment used in the 2004 and 2006 static load tests is shown in Figure 4.7.

4.2.2 Instrumentation

During the static tests, there were typically three types of instrumentation used to collect test data: a load cell, strain gages, and string potentiometers.

4.2.2.1 Load Cell

A resistance type strain gage load cell was used to determine the applied load during the tests. The load cell was calibrated in the BYU structural laboratory prior to the testing. The load cell was placed between the test pile and the load frame as shown in Figure 4.7 to monitor the full axial load which was applied to the pile.

4.2.2.2 Strain Gages

Strain gages were located at various depths along each test pile. Details on their precise locations for each pile are provided in section 4.2.8. Two strain gages were used at each indicated depth. The gages were placed on opposing sides of the pile. When test data were collected, the average of the two strain gage values at each depth was generally used to reduce any possible variations errors due to misalignment of the applied load or discrepancies in the measured strain. The two strain values should be equal if no bending occurs and thus strain and therefore stress are uniform for any given depth across the pile.

4.2.2.3 String Potentiometers

Three string potentiometers were used for each test to measure the vertical deflection at the top of the pile. They were placed at equal spacing around the circumference of the pile. An independent reference frame of wood was built around each test pile. The supports for this frame were located at least 3 pile diameters away from the edge of the test pile to keep them from moving during the test. The reference frame did not move, so when string potentiometers are attached to the reference frame and the test pile, the relative movement between them indicates the absolute deflection of the pile.

The string potentiometers were attached to the reference frame using clamps. A small aluminum bracket for each string potentiometer was attached to the pile with epoxy. The location and attachment of the string potentiometers is shown in Figure 4.7. The displacement of the pile head was based on the average of the string potentiometer data.

4.2.2.4 Data Acquisition System

Data from instrumentation were gathered using an Optim Megadac data acquisition system. One channel was used for each instrument. Manual deflection readings were also taken of the load and deflection of the 18 hour, 54 minute and 48 minute tests.

4.2.3 2002 Static Load Test Procedure

For each of the static load tests, the hydraulic actuator which was placed between the test pile and the load frame was extended. The extension of the jack

resulted in a force which displaced the test pile downward. The rate of loading was selected so that the time to failure would change by a factor of about 20 for each test.

4.2.3.1 18 Hour Test

For this test, loads were applied to test pile 24 with nine equal increments of approximately 50 kN in order to simulate a slow maintained load (SML) test. The load increments were selected so that each load would be approximately 25% of the design load or about 12.5 % of the expected ultimate load. Each load increment was held constant for a minimum of 2 hours and until the deflection rate was less than 0.001 in/min. After which the next load increment was applied. The test was terminated when the displacement was essentially continuous while the ultimate load was maintained. Plots of load and deflection versus time are provided in Figure 4.8.

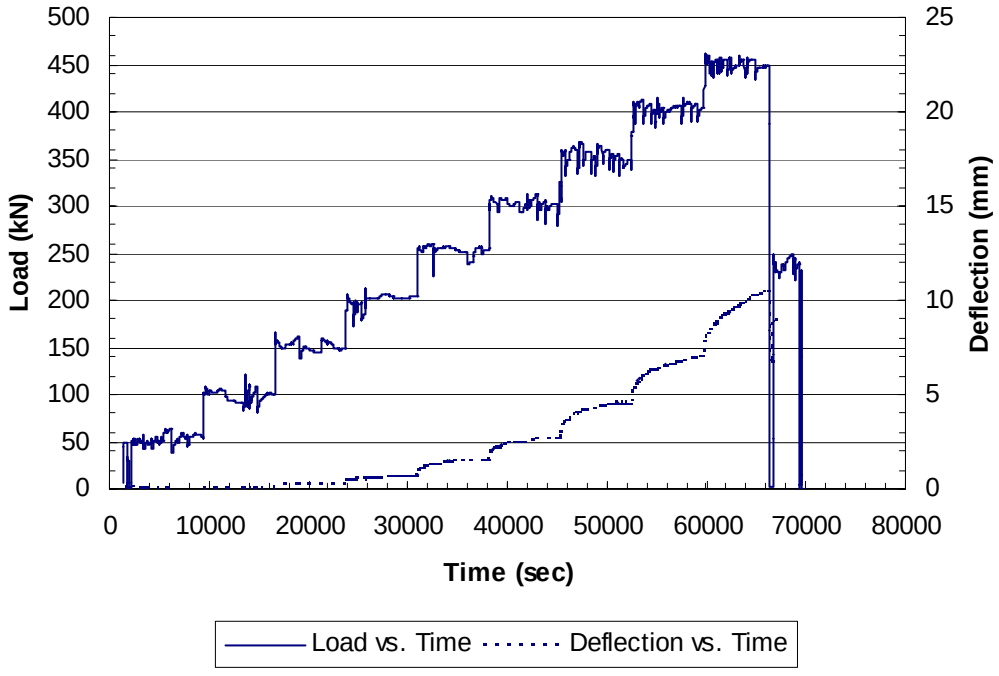

Figure 4.8 Load and Deflection Versus Time (18 Hour Test)

4.2.3.2 48 Minute Test

The 48 minute load test was performed on test pile 21 with nine load increments of approximately 50 kN. Each load increment was held constant for a period of about 5 minutes to simulate a quick maintained load (QML) test. Plots of load and displacement versus time for the test are provided in Figure 4.9. The data acquisition apparently failed to record the last increment of the load test.

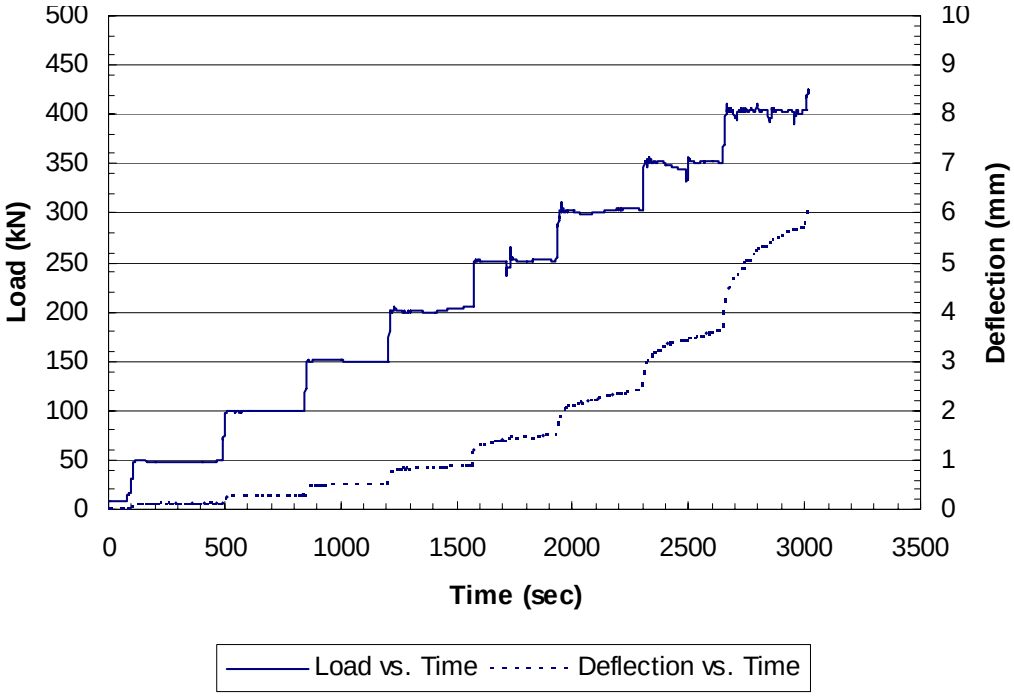

Figure 4.9 Load and Deflection Versus Time (48 Minute Test)

4.2.3.3 2 Minute Test

For this test the load was applied to test pile 18 uniformly and continuously at a rate such that the maximum capacity of the actuator (110 kips) would be reached

after approximately 2 minutes. Plots of load and displacement versus time for this test are provided in Figure 4.10.

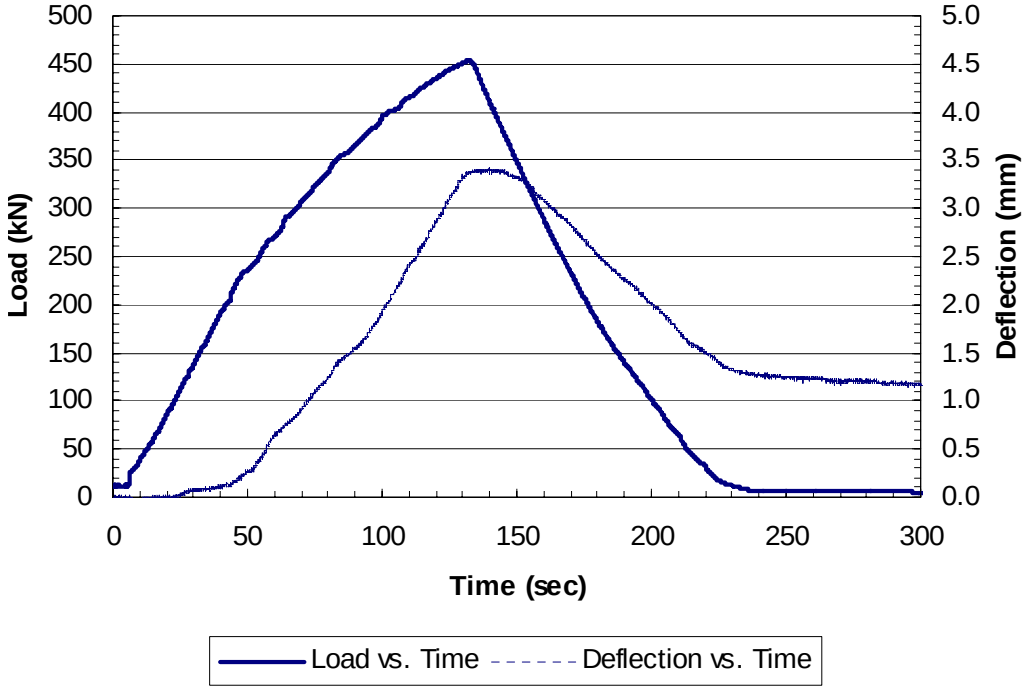

Figure 4.10 Load and Deflection Versus Time (2 Minute Test)

4.2.3.4 10 Second Test

Load was applied to test pile 15 at a rate designed to reach the maximum load capacity of the actuator in a few seconds. Plots of load and deflection versus time for this test are provided in Figure 4.11. Unfortunately, the control system malfunctioned and would not allow the load to exceed about 400 kN which was approximately 80 percent of the maximum actuator capacity. Three additional attempts were made to

reach the maximum capacity but in each case it was not possible to exceed the limit of approximately 400 kN.

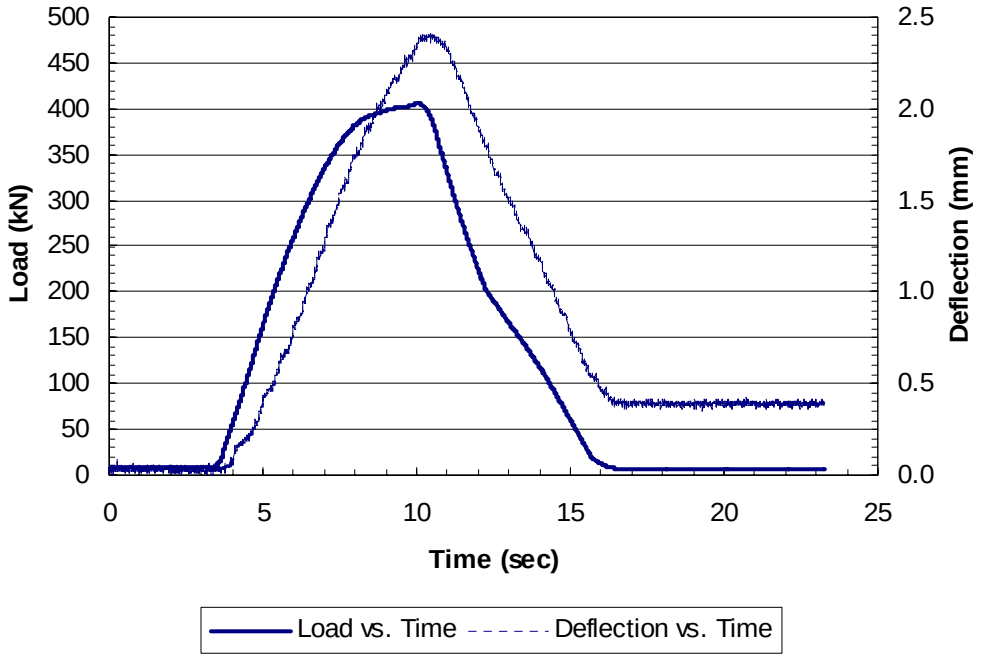

Figure 4.11 Load and Deflection Versus Time (10 Second Test)

4.2.4 2004 Static Load Test Procedure

The QML load test which resulted in failure in about 48 minutes in 2002 was repeated on a new pile in 2004. The test was repeated for two reasons. First, the strain gauge leads for the original test pile were cut during installation. After repeated efforts to determine which lead went to which strain gage were unsuccessful, the need for a new test became clear. Secondly, as will be shown subsequently, the load-deflection curve for the 48 minute test was almost identical to that for the 18 hour test despite the fact that it would be expected to be about 10% greater based on the

increase rate of loading. Therefore, it was desirable to repeat the test to see if this result would be repeated or if the average pile capacity from the two tests would provide a better estimate of the pile capacity at this rate of loading considering the variability in soil properties that might be expected in natural soil deposits. All of the 2004 static load tests were performed on the same test pile, pile 14. After a 54 minute test was performed, a 3 minute test was performed followed by a 25 second test. Because these tests were to be performed after previous pile load tests to failure, the shear strength of the soil surrounding the pile may have decreased from a peak level to a residual value. Nevertheless, the tests were relatively easy to perform and were thought to provide some estimate of the lower bound increase in pile capacity due to variations in loading rate.

4.2.4.1 54 Minute Test

Prior to the test, the capacity of the pile was estimated to be 620 kN. In order to produce failure at a time of about one hour, the load was increased by 53 kN every five minutes. However, due to the lack of control on the pump, the first load increment overshot the desired load increment and was increased to 106 kN. From there on, load increased by 53 kN every five minutes. Each load step was held constant manually, by engaging and stopping the hydraulic pump which fed the jack. Plots of load and displacement versus time for this test are provided in Figure 4.12. The test was terminated when the pile deflected faster than the jack could be extended so that the load did not increase and displacement did not stabilize under the applied load.

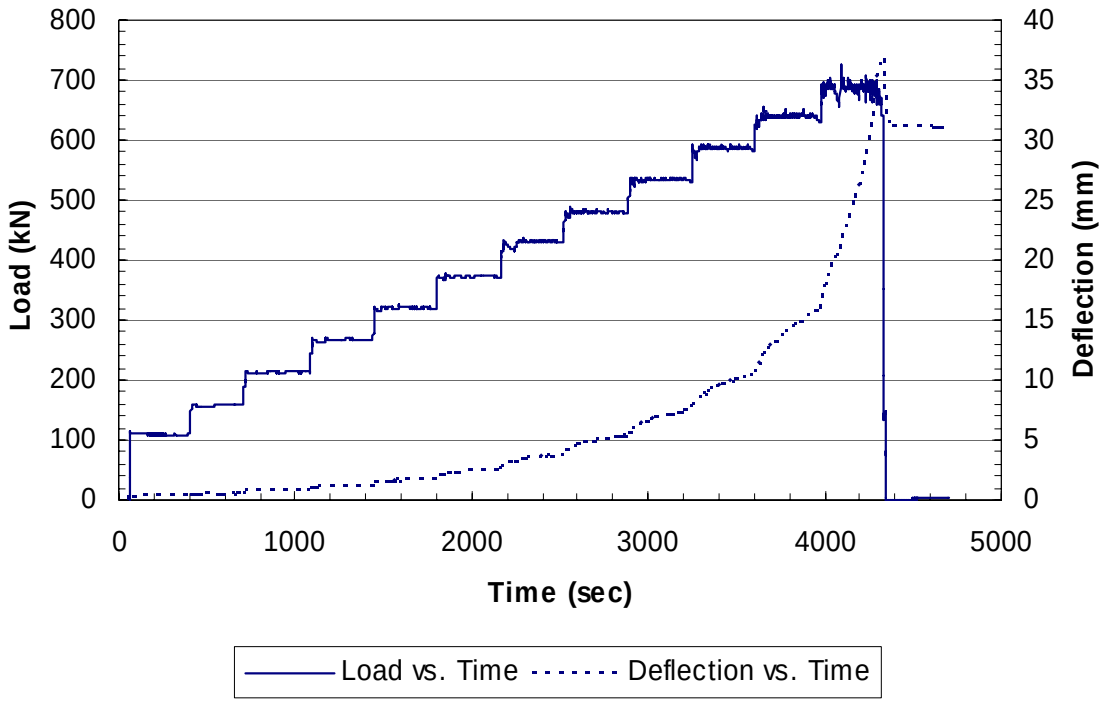

Figure 4.12 Load and Deflection Versus Time (54 Minute Test)

4.2.4.2 3 Minute Test

The 3 minute test was performed just minutes after the 54 minute test on pile 14. Since the pile capacity when loaded at 54 minutes was already known, it was hypothesized that the pile would reach failure at a load slightly higher than 544 kN if loaded to failure in 3 minutes even if the load was applied shortly after the 54 minute test was completed. Load was increased by approximately 106 kN every 30 seconds. Data gathered during the 3 minute test is presented in Figure 4.13. Load was applied to the test pile in increments of approximately 110 kN to model a continuously increasing load.

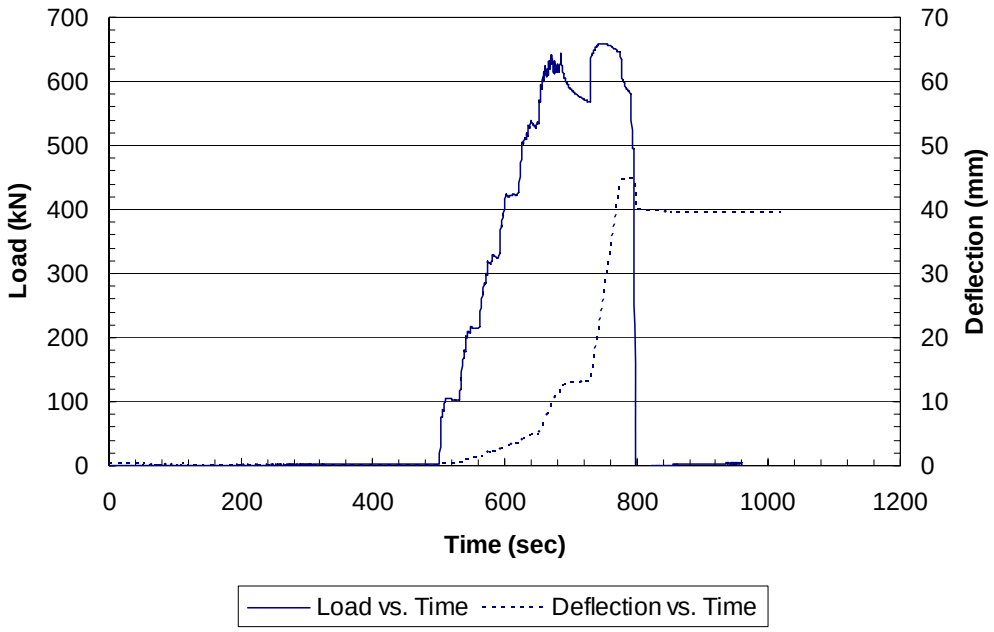

Figure 4.13 Load and Deflection Versus Time (3 Minute Test)

4.2.4.3 25 Second Test

The pump was turned on to fail the pile as quickly as possible with the loading apparatus being used. Failure load was reached in approximately 25 seconds. Data acquired during this test are shown in Figure 4.14

4.2.5 2002 Load Versus Deflection Curves and Failure Load Determination

Load versus deflection curves were developed for each static test. From these curves, a failure load was established using Davisson's method of failure determination in order to compare the different tests in a standard way. Davisson's method is outlined in section 2.2.1.1.

The pile head load versus deflection (settlement) curve for the 18 hour test is plotted in Figure 4.15. The Davisson line is also plotted and the failure load by the Davisson criteria for the 18 hour test is 451 kN.

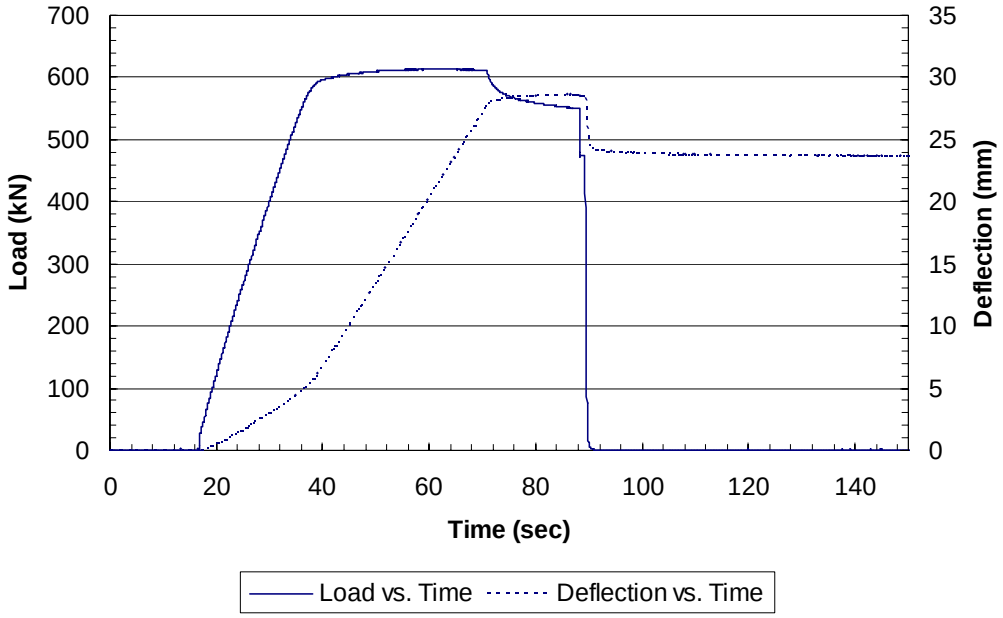

Figure 4.14 Load and Deflection Versus Time (25 Second Test)

The pile head load versus deflection curve for the 48 minute test is plotted in Figure 4.16. Each point on the curve represents the maximum deflection at the end of each load increment. The Davisson slope is also plotted in Figure 4.15 and it may be seen that the load-deflection curve did not reach failure according to the Davisson Method. Therefore, an attempt was made to project the probable failure point of this test. A polynomial trend line of the existing data points was generated and can be seen in Equation 4.1. The equation for pile head load P in kN is given by the Equation 4.1.

$$P = 2.1E\text{-}10\delta^4 - 6.5E\text{-}8\delta^3 + 1.9E\text{-}5\delta^2 + 0.0013\delta + 0.011 \quad (4.1)$$

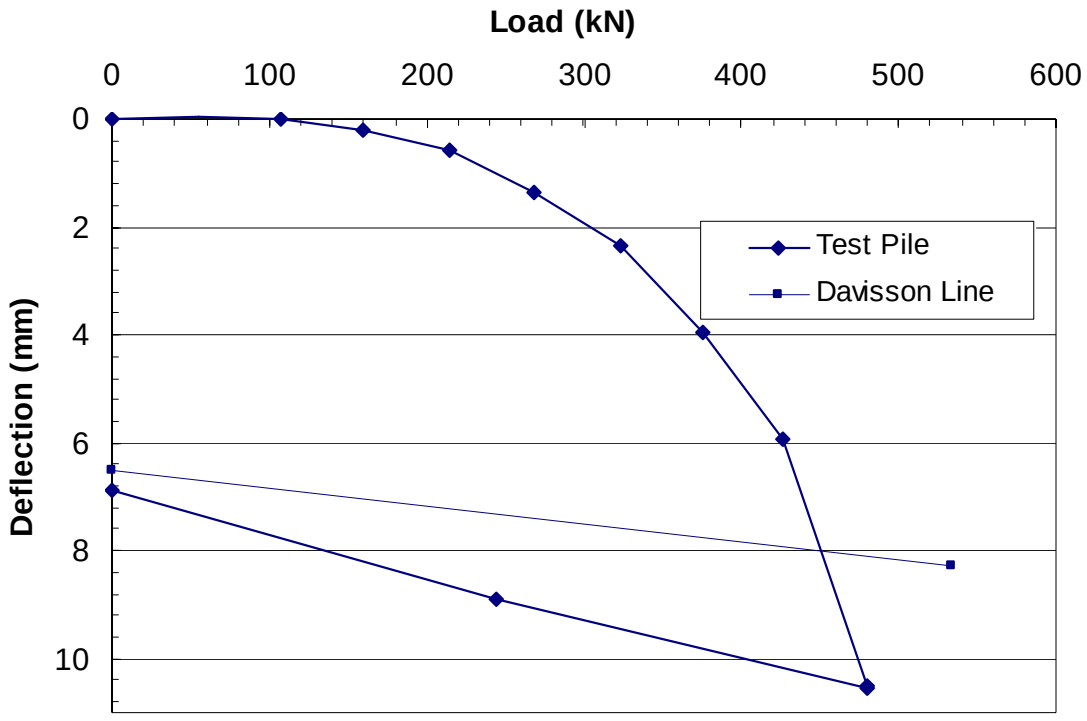

Figure 4.15 Load Versus Deflection (18 Hour Test)

where δ is the pile head deflection in mm. This equation has a value for the coefficient of determination, R^2 is 0.9997. This value, being essentially one, shows that the equation closely models the data points. Using Equation 4.1 and setting it equal to the equation for the Davisson line, the intersection defining the failure value was calculated to be 471 kN.

Pile head load versus deflection curves for the 2 minute tests conducted in 2002 are plotted in Figure 4.17. The Davisson failure line is also plotted in each figure and it is clear that the load-deflection curves do not cross the Davisson line defining failure during the 2002 tests.

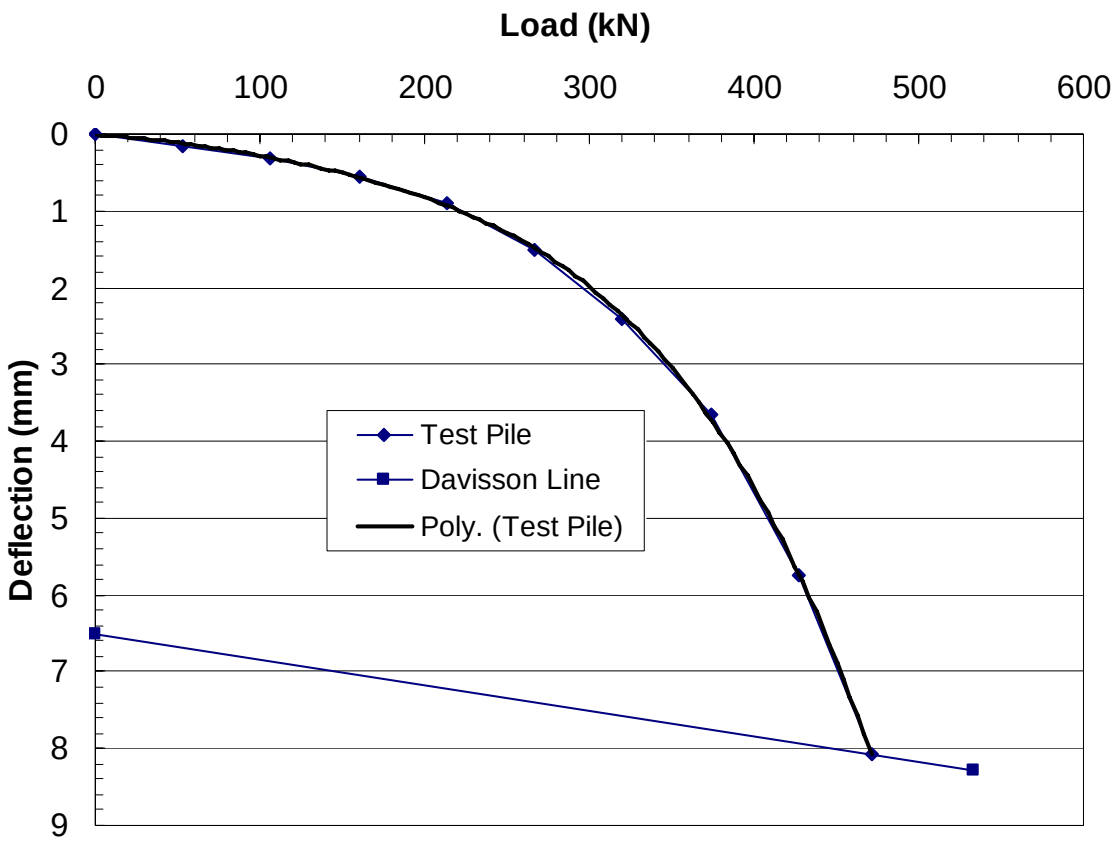

Figure 4.16 Load Versus Deflection With Estimated Failure (48 Minute Test)

As indicated previously, three additional 2 minute tests were performed in 2002 in an effort to obtain the full capacity (490 kN) of the actuator. However, with the increased pile capacity produced with the higher rate of the loading the failure load exceeded the maximum capacity which could be produced by the MTS actuator. Therefore, as discussed previously, the load test was repeated in 2006 on the same test pile to define the failure load. The pile head load versus deflection curve for the test in 2006 is also plotted in Figure 4.17 and the initial pile head deflection was set equal to the final deflection from the 2002 tests. The failure load defined by the intersection with the Davisson line was found to be 651 kN.

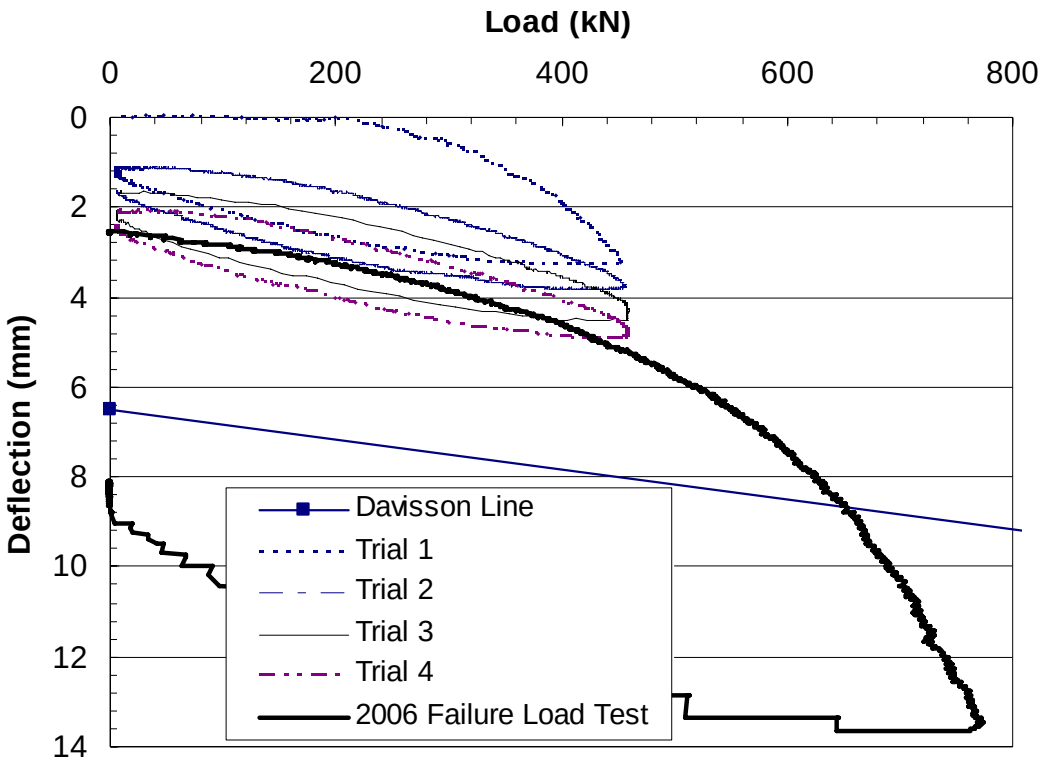

Figure 4.17 Load Versus Deflection (2 Minute Test)

Pile head load versus deflection curves for the 10 second tests conducted in 2002 are plotted in Figure 4.18. Once again the load-deflection curve does not cross the Davisson line defining failure because the pile capacity greatly exceeds the capacity of the MTS actuator. It is also difficult to extrapolate the measured curve to obtain a failure load in this case. Therefore, the test was repeated in 2006 with a larger actuator so that the failure load could be defined. As indicated previously, a total of nine 10 second tests were performed in 2002 in an effort to obtain the full capacity (490 kN) of the actuator. The failure load was test was performed in 2006 and actually had a duration of 26 seconds. The failure load per the Davisson method was 700 kN.

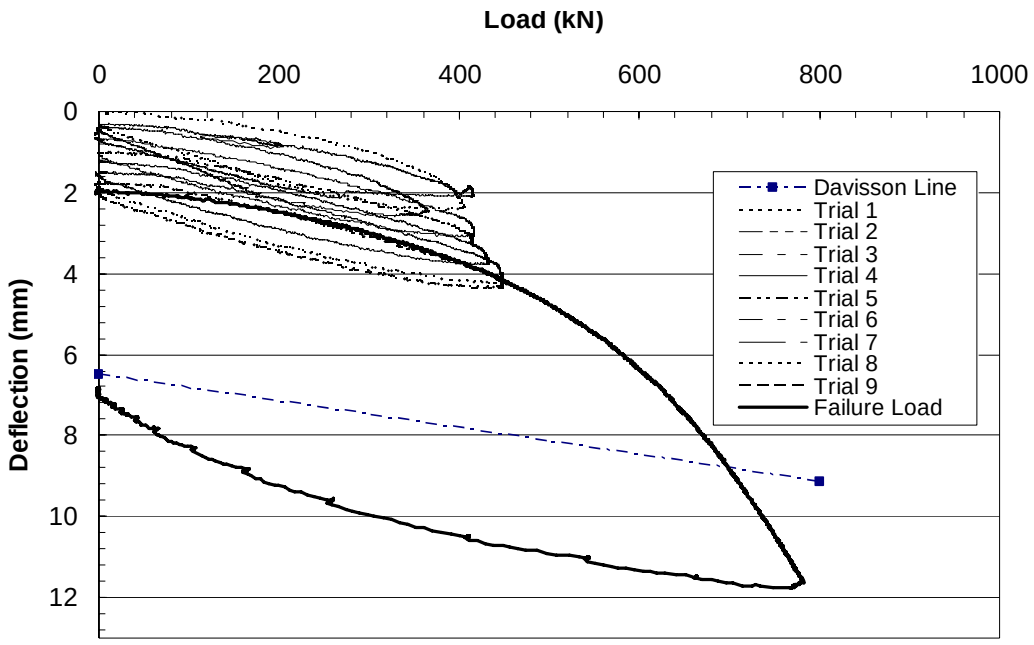

Figure 4.18 Load Versus Deflection (10 Second Test)

4.2.6 2004 Load Versus Deflection Curves and Failure Load Determination

Pile head load versus deflection curves for the three pile load tests conducted on test pile 14 are presented in Figure 4.19, Figure 4.20 and Figure 4.21. The Davisson method was also used to determine the failure load for the 2004 static load tests. The interpreted failure loads for the 54 minute test, 3 minute test and 25 second tests were determined to be 544 kN, 570 kN, and 600 kN, respectively.

The 54 minute test was the first axial load test performed on this pile, and therefore the failure load can be compared with load tests of different failure times.

Though the 3 minute and 25 second tests were performed on a test pile which was already loaded to failure, they still showed failure loads that increased in magnitude with decreasing time to failure.

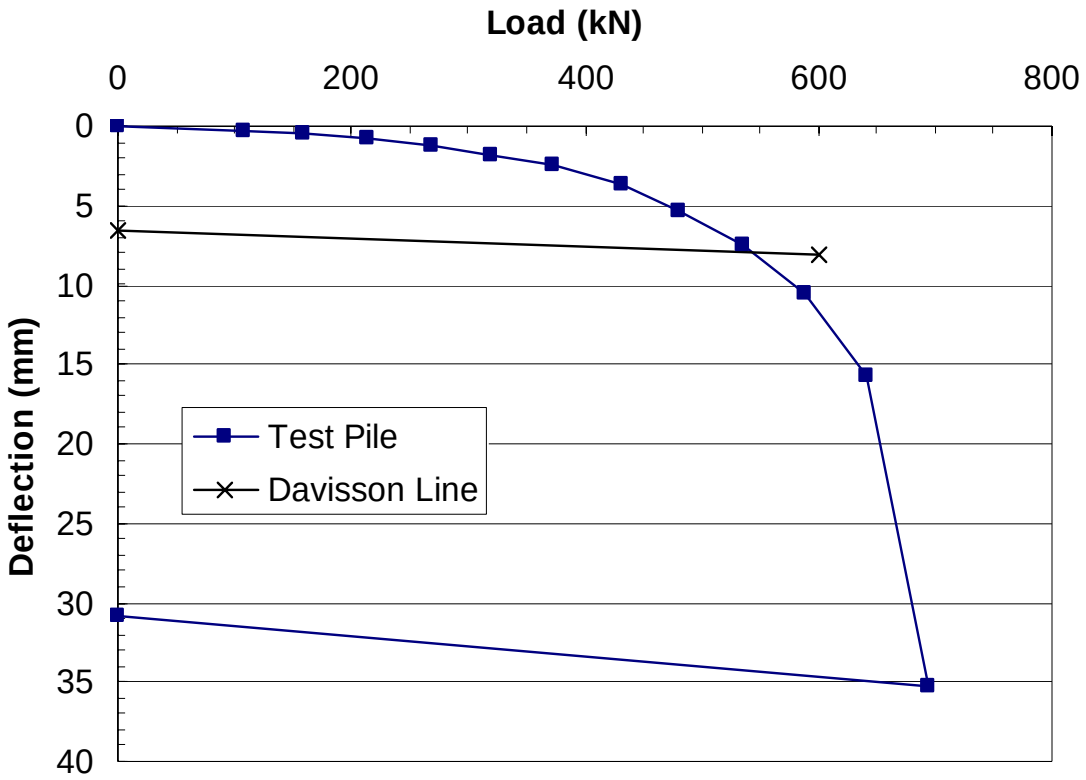

Figure 4.19 Load Versus Deflection (54 Minute Test)

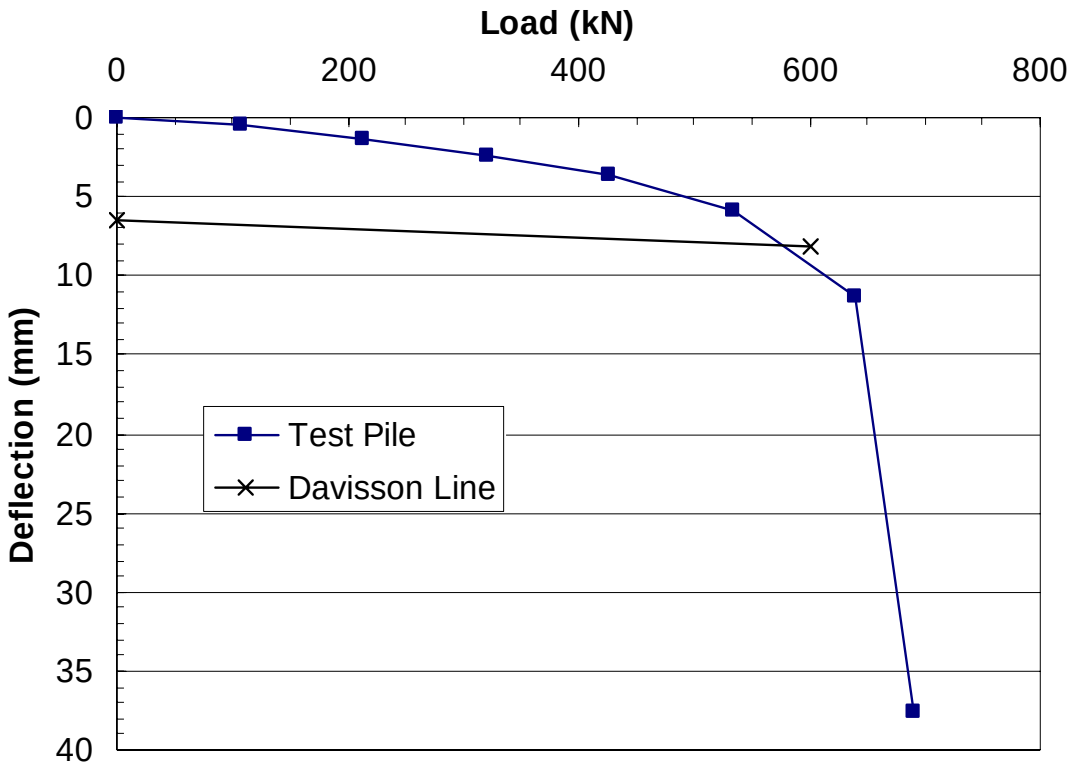

Figure 4.20 Load Versus Deflection (3 Minute Test)

Since the 3 minute test and the 25 second test were done shortly after the 54 minute test and on the same test pile, the failure loads produced by the 3 minute and 25 second tests cannot be directly compared to those of the other tests which were all done on previously untested piles. These data have however been included and would likely provide a lower bound estimate of the effect of the rate of loading because the unit side resistance on the pile-soil interface might have dropped to a residual value after the first load test.

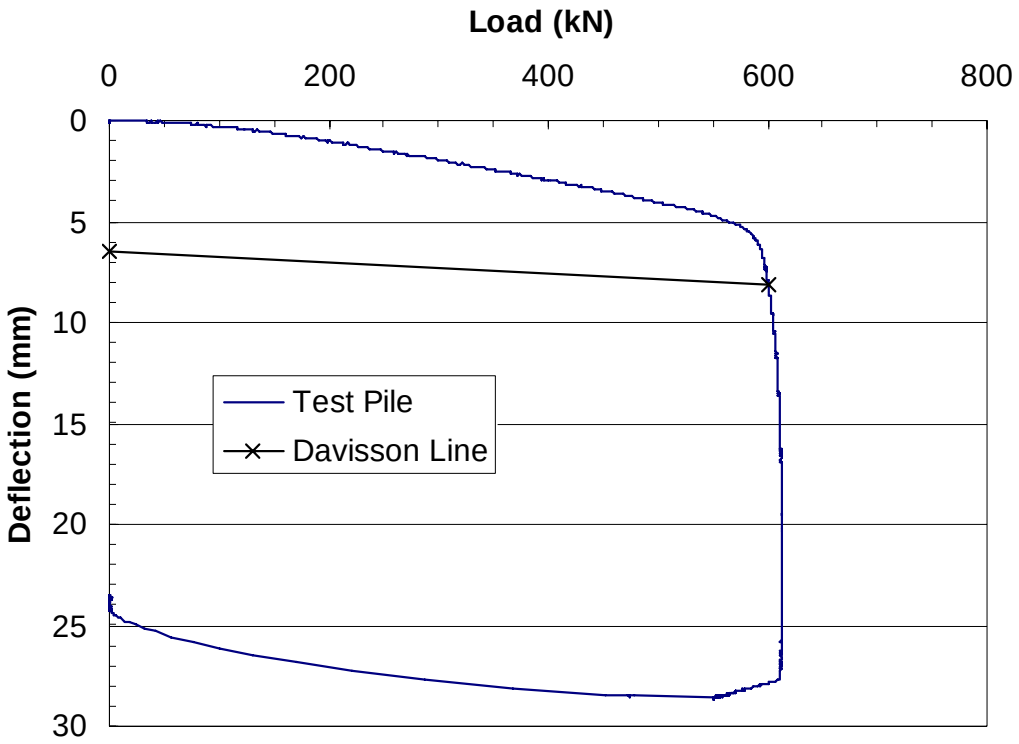

Figure 4.21 Load Versus Deflection (25 Second Test)

Figure 4.22 shows all of the static tests which produced failure. In this figure the loads at different rates can be compared. Two tests which do not fit the general pattern are the 3 minute and 25 minute tests. These tests were performed directly after the 54 minute test was performed, so therefore residual capacity of the soil remained after failure.

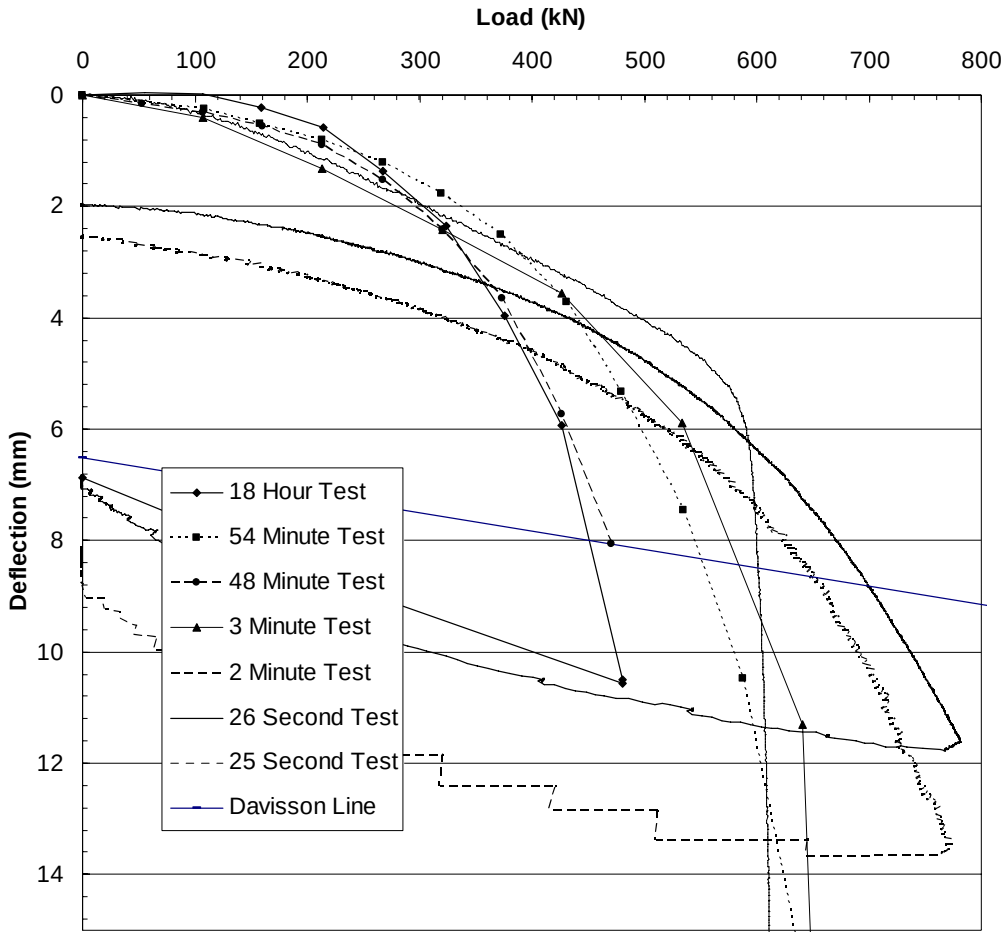

Figure 4.22 Combined Load Versus Deflection

4.2.7 Data Required for Load Determination at Various Depths

The load at the top of each test pile is measured directly by the load cell. Along the length of the pile, however, only strain, not stress, is measured. Nevertheless, the strain values from strain gages can be used to determine load at the depth of each strain gage located along the length of the pile. Equation 4.2 is used to obtain load values at each strain gage

$$P = EA\varepsilon \quad \textbf{(4.2)}$$

where:

P = Load
E = Modulus of elasticity of the pile (Young's Modulus)
A = Cross sectional area of the pile
ε = Strain of pile at depth

For each of the tests, a set of strain gages was placed in the pile above the surface of the ground where the load in the pile is equal to the load at the load cell since above the ground, no load is lost to soil friction. The cross sectional areas of the test piles were obtained, given their diameters as shown in Figure 4.2. Load and strain were obtained directly from the load cell and the strain gages, respectively. Once these values were known they were inserted into Equation 4.2 to solve for the modulus of elasticity of each test pile. Because each test pile had a uniform cross section down its full length, the assumption is made that the same composite modulus of elasticity can be used for the entire pile length. Figure 4.23 shows the equation for the load versus strain curve of the 54 minute test done in 2004. In this equation, the slope of the line (4,532,200 kN) is equal to load divided by strain, P/ε. Modifying Equation 4.2 gives:

$$\frac{P}{\varepsilon} = EA \quad \textbf{(4.3)}$$

Thus, the slope (4,532,200 kN) multiplied by the strain at any given depth gives us the axial load on the pile at that depth. Another proof of the accuracy of E is

that the R^2 value in Figure 4.23 is so close to one. This fact indicates that there is very little scatter in the data and that the E value remains relatively constant over the range of loads applied to the test pile.

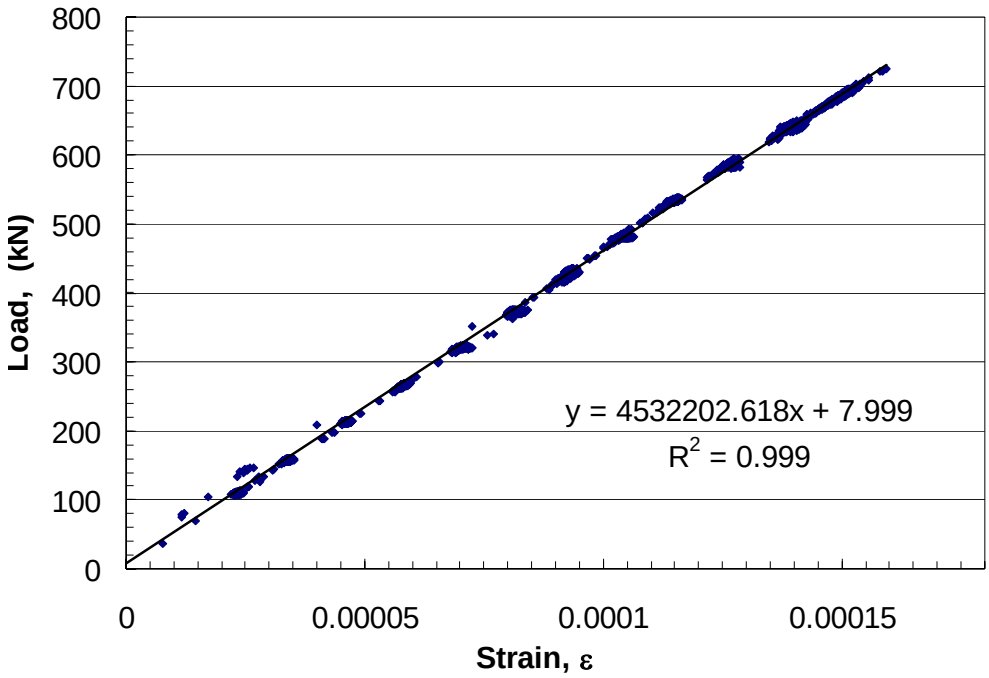

Figure 4.23 Load Versus Strain (54 Minute Test)

For each of the static test piles, the process shown in this section was carried out. The load versus strain graph and the associated values presented in this section are from the 54 minute test pile, but the other piles had very similar results. The 3 minute and 25 second tests were also performed on the test pile used for the 54 minute test, so these EA results were used for analysis of those tests as well. The EA values for the 2002 tests were slightly smaller than for those of the 2004 tests. This is a result

of a higher strength grout which was used for the 2004 tests, as discussed subsequently.

4.2.7.1 Determination of EA Based on Material Properties

The EA value for test pile 14 which was used in the 2004 static load tests was back-calculated using the measured load and strain as described previously. In addition, the EA value for this test pile was also determined using measured material properties and dimensions. This approach provides a separate check on the elastic modulus, E of test pile 14. When test pile 14 was filled with grout, test cylinders of the same grout were cast. Static load tests were performed on the pile on August 25, 2004. Two test cylinders were broken in the structures laboratory at BYU on August 29, 2004. The test cylinders were eight inches (20.3 cm) tall with a diameter of four inches (10.2 cm). The average, maximum compressive load, P_{max} of the two test cylinders was 42.6 kip (189 kN). The compressive strength of the concrete, f_c' in the test cylinders was therefore 3.39 ksi (2.33 kN/cm^2) from Equation 4.4.

$$f_c' = \frac{P_{max}}{Area} \tag{4.4}$$

The elastic modulus, E of concrete can be calculated directly from f_c' with Equation 4.5. The modulus is therefore estimated to be approximately 3,320 ksi (2,290 kN/cm^2).

$$E_{concrete} = 57{,}000\sqrt{f_c'} \quad \textbf{(4.5)}$$

The modulus of elasticity of steel is 29,000 ksi (20,000 kN/cm^2). Since steel and the grout in the pile have different values for modulus of elasticity, the modulus of the steel must be multiplied by the area of steel and added to the modulus of grout multiplied by the area of grout, in order to obtain a composite value EA for the pile cross section. These values are given in Table 4.2 below.

Table 4.2 Determination of Composite EA (54 Minute Test Pile)

	Area (in^2)	E (ksi)	EA (kip)	EA (kN)
(2) Angles	0.72	29,000	20,822	92,616
Pile	14.58	29,000	422,820	1,880,703
Inner Pipe	5.58	29,000	161,820	719,775
Grout	106.80	3,320	354,583	1,577,184
Total:	-	-	960,045	4,270,279

The total composite value of EA shown in Table 4.2 closely matches the value back-calculated from the load and strain data shown in Figure 4.23. The two values of EA deviate less than six percent from each other. The consistency in the EA values obtained using these two approaches suggests that the value is accurate and can be used with confidence to determine load from strain data at other locations along the pile length.

4.2.8 Load Versus Depth Curves for Various Load Increments

Figure 4.24 through Figure 4.27 show the axial load in the test pile as a function of depth for the 18 hour, 54 minute, 2 minute and 10 second tests, respectively. At some of the load increments, there was considerable scatter in the data, so trend lines are shown in addition to curved from point to point along the pile length.

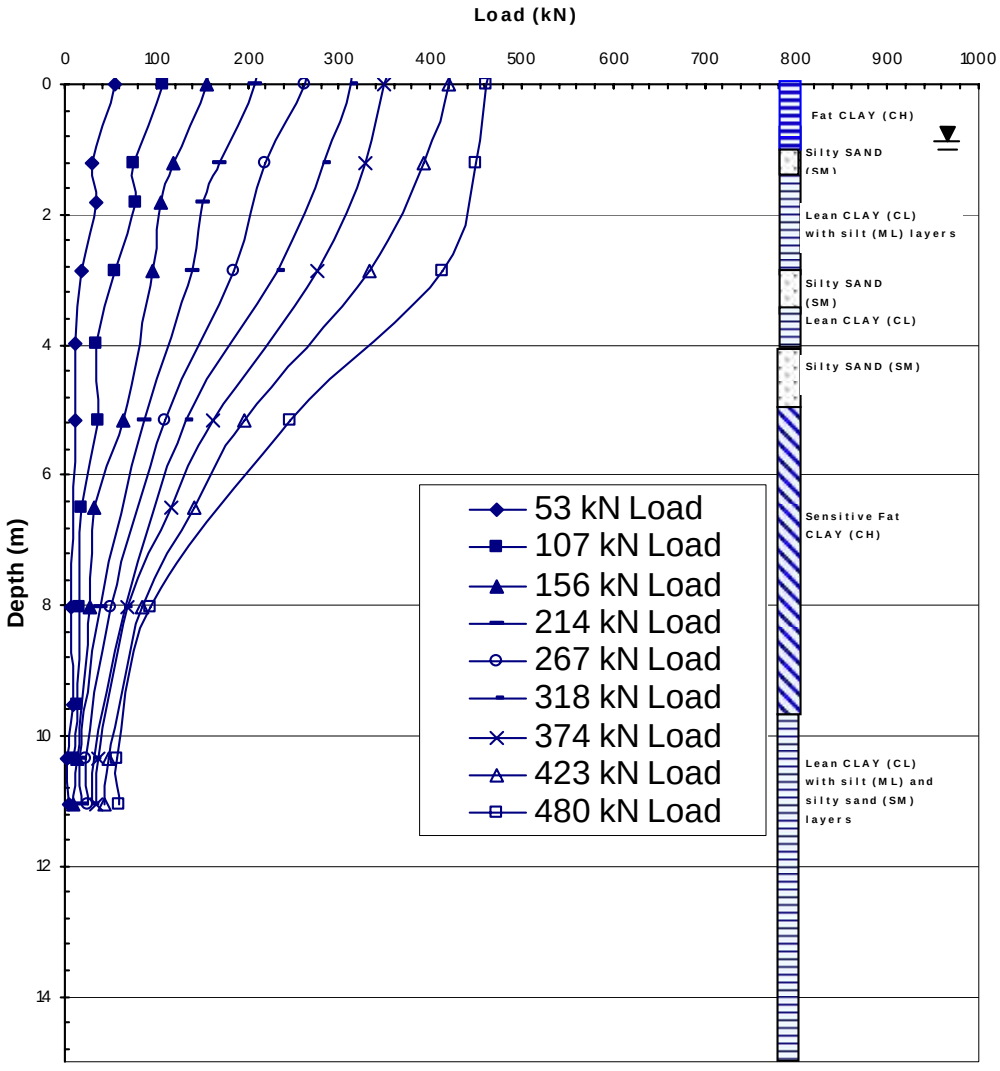

Figure 4.24 Load Versus Depth (18 Hour Test)

As explained previously, some problems occurred with the data acquisition of the strain gage data for the 48 minute test. Consequently, a load versus depth curve for that test is not available. Therefore, the test was repeated in 2004 with the 54 minute test. The 54 minute test was to failure, and accurate strain data was gathered along the length of the pile.

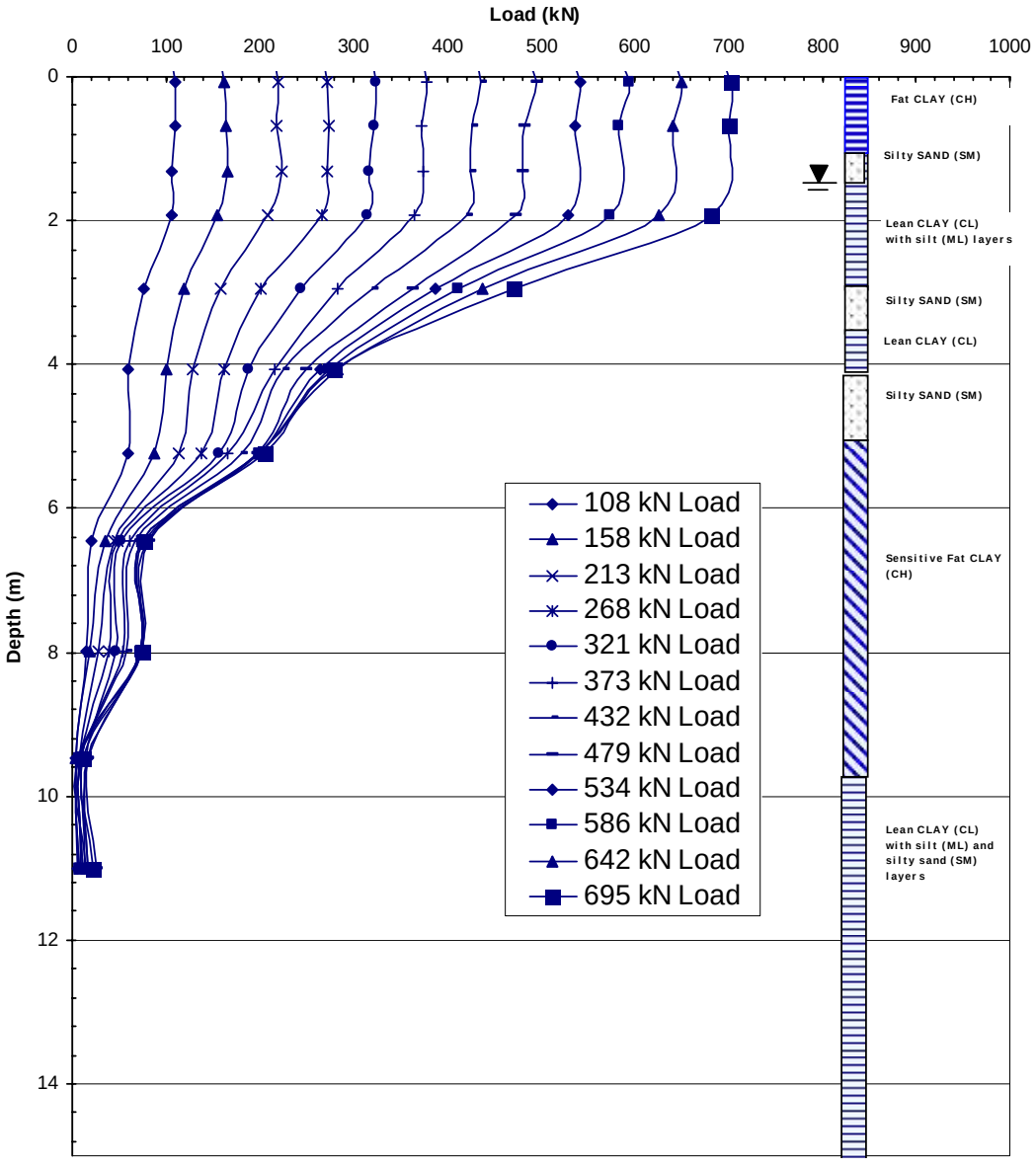

Figure 4.25 Load Versus Depth (54 Minute Test)

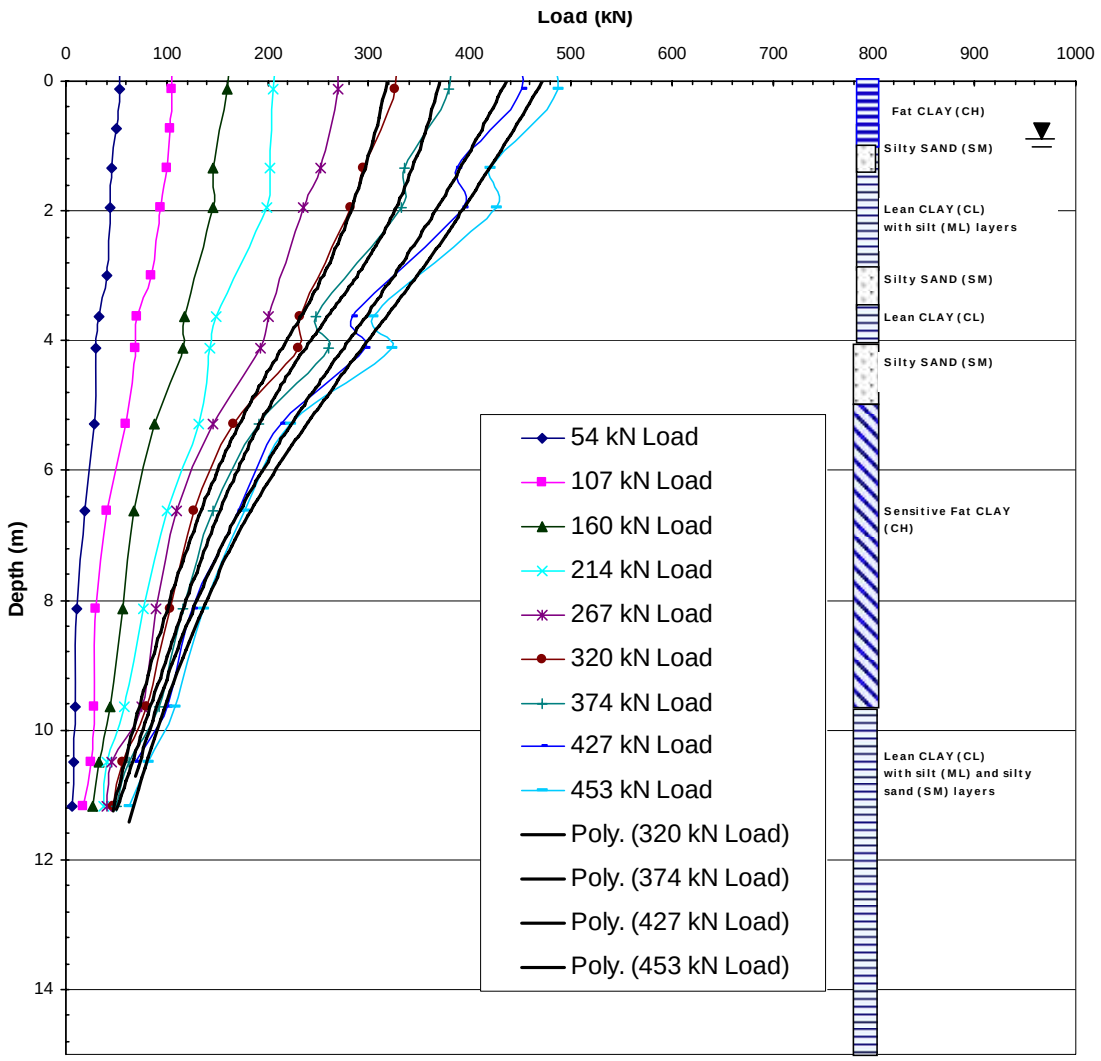

Figure 4.26 Load Versus Depth (2 Minute Test)

Included on Figure 4.26 are some trend lines. They are useful because considerable scatter is present in the measured data. The trend lines may better represent what the load is at each given depth. In all the plots the unit side resistance is relatively low in the upper 2 meters of the pile. As indicated previously, each of these test piles had been laterally loaded prior to the axial load tests. As a result, gaps had formed soil around the upper 2 meters of the pile which was subsequently filled in

by soil from the surface. This may explain the relatively low unit side resistance in this section of the piles.

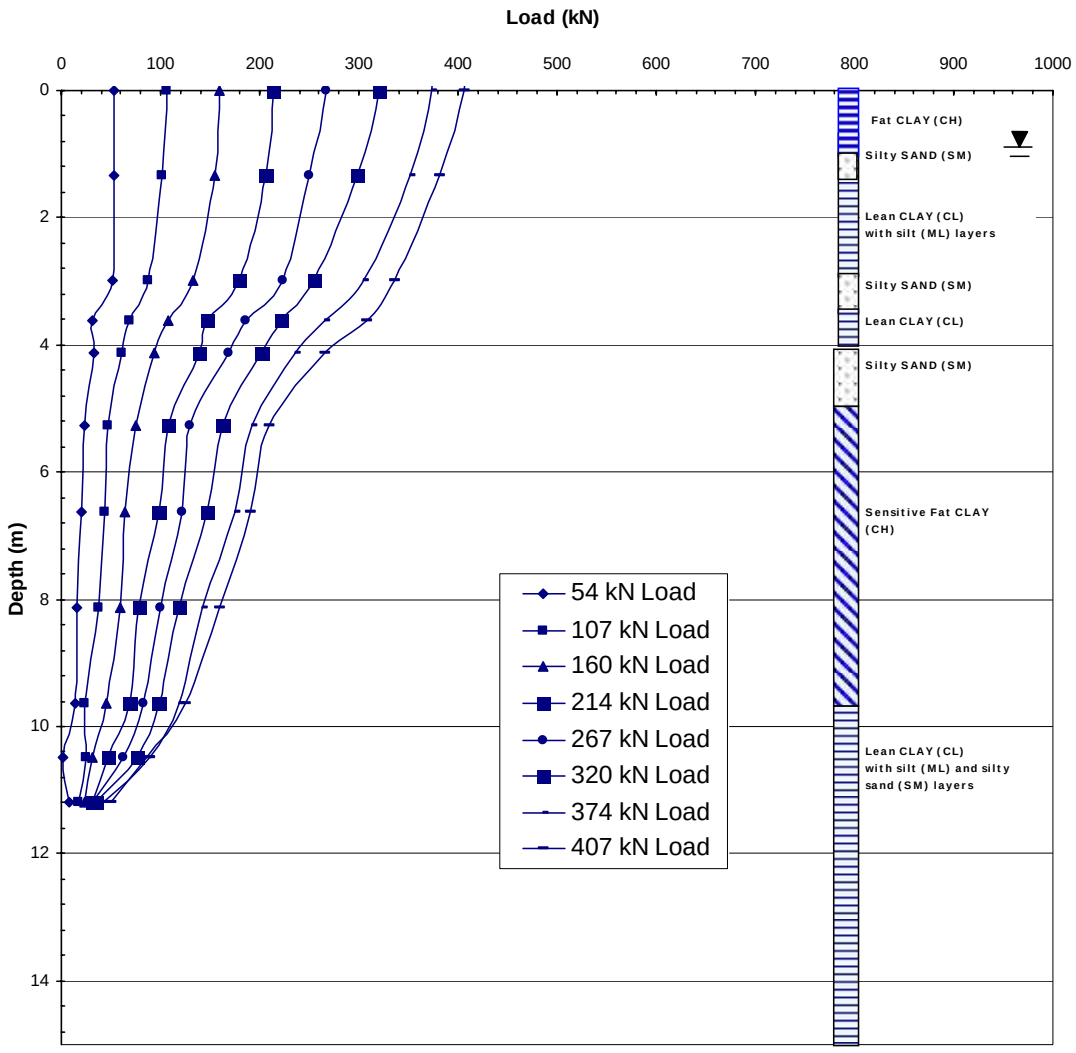

Figure 4.27 Load Versus Depth (10 Second Test)

4.3 Statnamic Load Test

Two Statnamic tests were performed on the one test pile (pile 27) on September 24, 2004. The test pile used for the Statnamic tests was driven in July of

2004. The first test did not produce failure using the Davisson method. The second test produced failure.

4.3.1 Test Pile Characteristics and Construction

The test pile for the Statnamic load test was identical to the piles in the static load tests. As noted previously, section 4.1 provides a detailed description of these test piles and their construction. The only difference is that the test piles were not loaded laterally prior to the Statnamic tests as were the test piles which were used for the static load test.

4.3.2 Description of Test Layout

An assembly including a piston (shown in Figure 4.28) and three accelerometers was placed on top of the test pile. Three reaction masses, with a hollow cylinder as part of their base, were lowered onto the piston containing the combustion chamber for the Statnamic fuel pellets. Section 2.2.4 contains a schematic drawing and an explanation of the Statnamic load test device. A steel frame was placed above the test pile and it also surrounded the reaction mass. This frame guided the reaction mass to move in a vertical direction. Hydraulic cylinders mounted to the frame were also used to catch the reaction mass and prevent it from dropping back onto the pile after each test was complete. Typically with Statnamic tests, the reaction mass rests on the test pile before the fuel is ignited. This induces a small static load on the pile before the Statnamic test. In these tests, however, the reaction mass was supported by the steel frame before ignition and thus, the test pile experienced no loading before the actual Statnamic test.

Figure 4.28 Statnamic Device

Figure 4.28 is a photo of the Statnamic frame in place over the test pile. In this figure the reaction mass is elevated above the loading piston.

Figure 4.29 is included to show the relative location of the Statnamic test frame and some existing pile caps and geopier caps. Some dimensions of the reference frame are given to show that its supports are located more than three pile diameters away from the test pile.

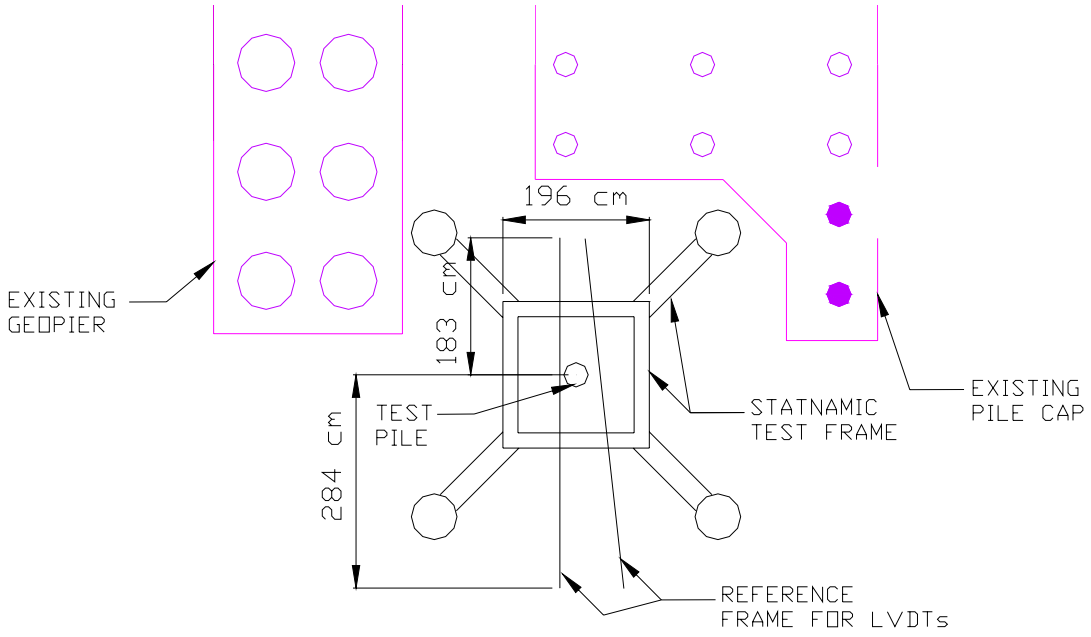

Figure 4.29 Statnamic Test Layout

4.3.3 Instrumentation

4.3.3.1 Load cell

A load cell was located at the base of the Statnamic load piston just above the test pile to measure the full axial force applied to the top of the pile.

4.3.3.2 Accelerometers

Three accelerometers were attached to the top of the pile. They monitor the acceleration of the pile throughout the test. They give results with units of g, where g is the acceleration of gravity or 9.8 m/s^2. Integration of the accelerometer time histories also makes it possible to determine time histories of velocity and displacement for the test pile.

4.3.3.3 LVDTs

Linear voltage displacement transformers or LVDTs are very similar to the string potentiometers which were used in the static load tests. They also measure the absolute movement of the pile. A small reference frame was built of wood around the pile. Its supports were at least three pile diameters away from the pile to minimize movement of the soil under the supports when the test was performed. The layout of this reference frame is shown in Figure 4.29. The LVDTs were clamped to the reference frame, and their telescoping ends were attached to the pile, in the same manner as the string potentiometers were attached to the statically loaded piles. LVDTs were used for the Statnamic tests instead of string potentiometers because they are better suited for high speed tests.

4.3.3.4 Laser

A laser was also used to monitor movement of the pile. It was positioned nine meters away from the test pile during the test, and was aimed at the test pile.

4.3.3.5 Strain Gauges

Strain gages were located at various depths along each test pile. For details on their precise locations, see section 4.3.8. Two strain gages were used at each indicated depth. The gages were placed at opposing sides of the pile. When data was collected, the average of the two strain gage values at each depth was used to account for any variation and eccentric loading of the pile. If no bending occurs, these values should be very similar since no bending occurs and thus strain and therefore stress are uniform for any given depth across the pile.

4.3.4 Statnamic Load Test Procedure

For each test, the reaction mass was lowered onto the pile. The explosive charge was then ignited, forcing the reaction mass to accelerate.

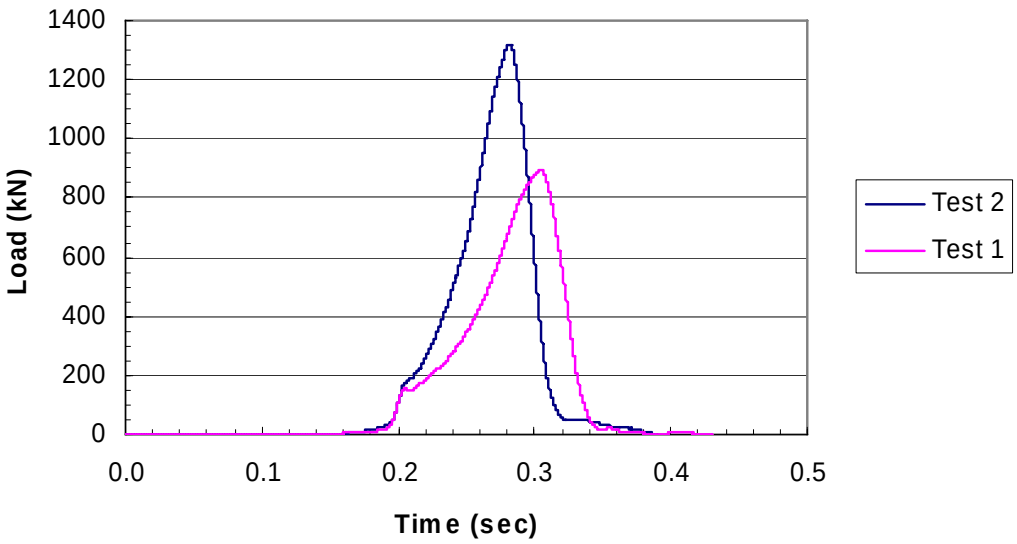

Figure 4.30 Load Versus Time (Tests 1 and 2)

Figure 4.30 shows the load versus time curves for the two Statnamic tests. The load readings were obtained from the load cell. The rise time (time from zero to peak load) was typically on the order of 0.1 second or less for each of the tests. This rise time is typical of Statnamic tests.

Plots of acceleration, velocity and deflection as a function of time are provided in Figure 4.31 and Figure 4.32 for tests 1 and 2, respectively. Pile head deflection is measured directly by the LVDTs, and pile head acceleration is measured directly by the accelerometers. The velocity values are from integration of the acceleration time histories from the accelerometers.

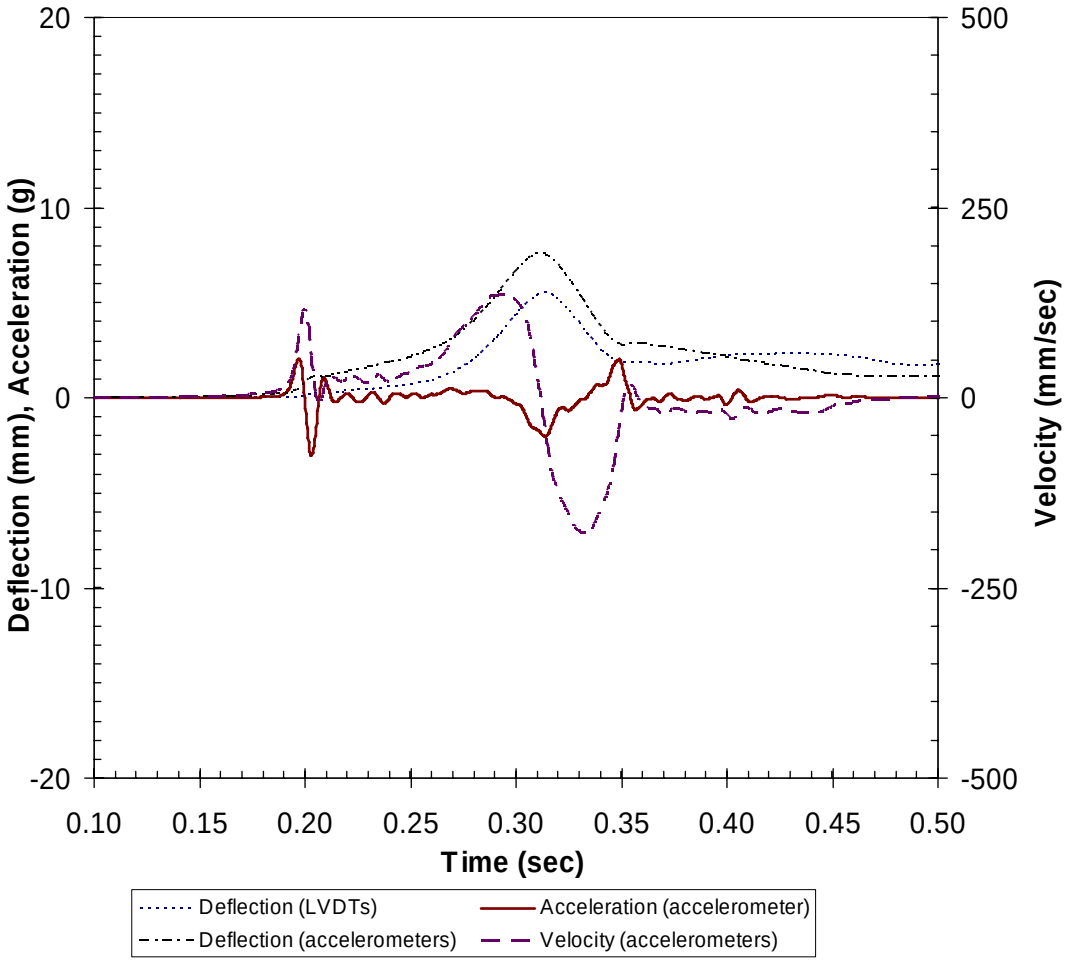

Figure 4.31 Acceleration, Velocity and Deflection Versus Time (Test 1)

Deflection is also calculated from the double integration of the acceleration time history data measured by the accelerometers. Deflection data measured directly by the LVDTs is used for analysis, but deflection data from the accelerometers is presented to show that the data from both types of instrumentation match closely, especially for test 2 which is the critical test, since failure was produced. No filtering of data was required and baseline correction was not done.

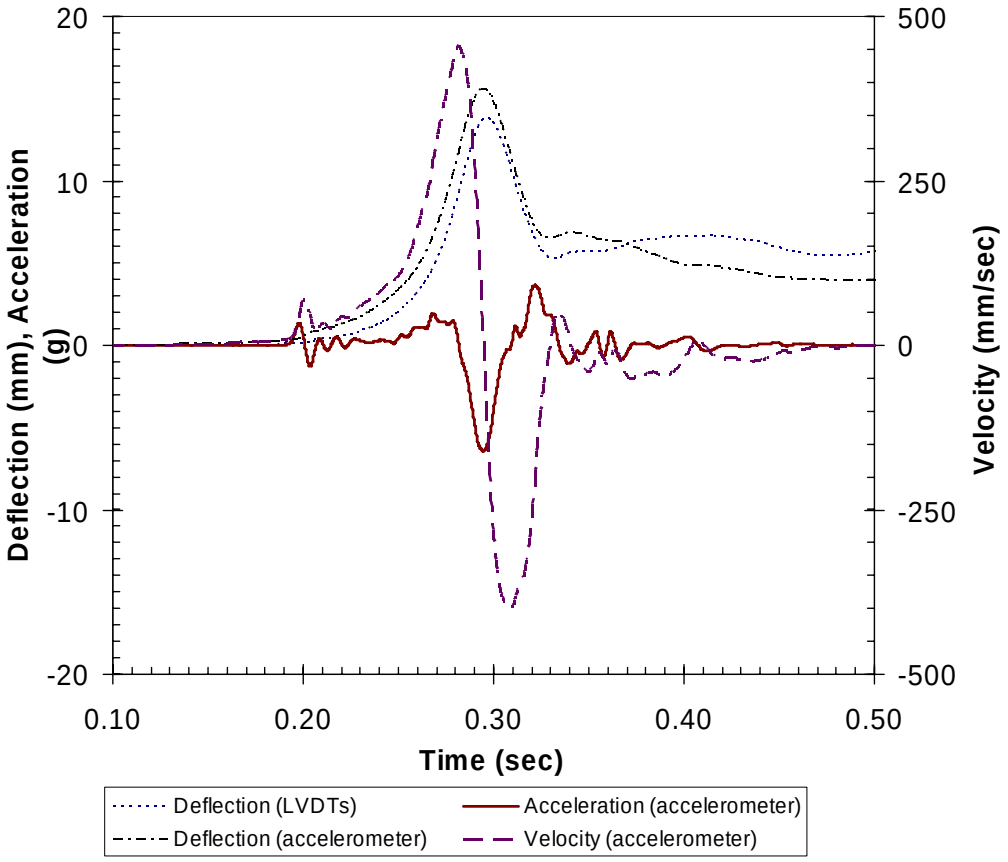

Figure 4.32 Acceleration, Velocity and Deflection Versus Time (Test 2)

4.3.5 Statnamic Load Versus Deflection Curves

Figure 4.33 shows the total pile head load versus deflection curves for both Statnamic tests together. The Statnamic load values were measured by the load cell and the displacement values came from the average of the LVDTs. After test 1 the pile was permanently displaced 1.93 mm. This is the displacement value at which test 2 begins. Since the Statnamic Load in Figure 4.33 is taken directly from the load cell, it is the full load applied to the pile by the Statnamic device.

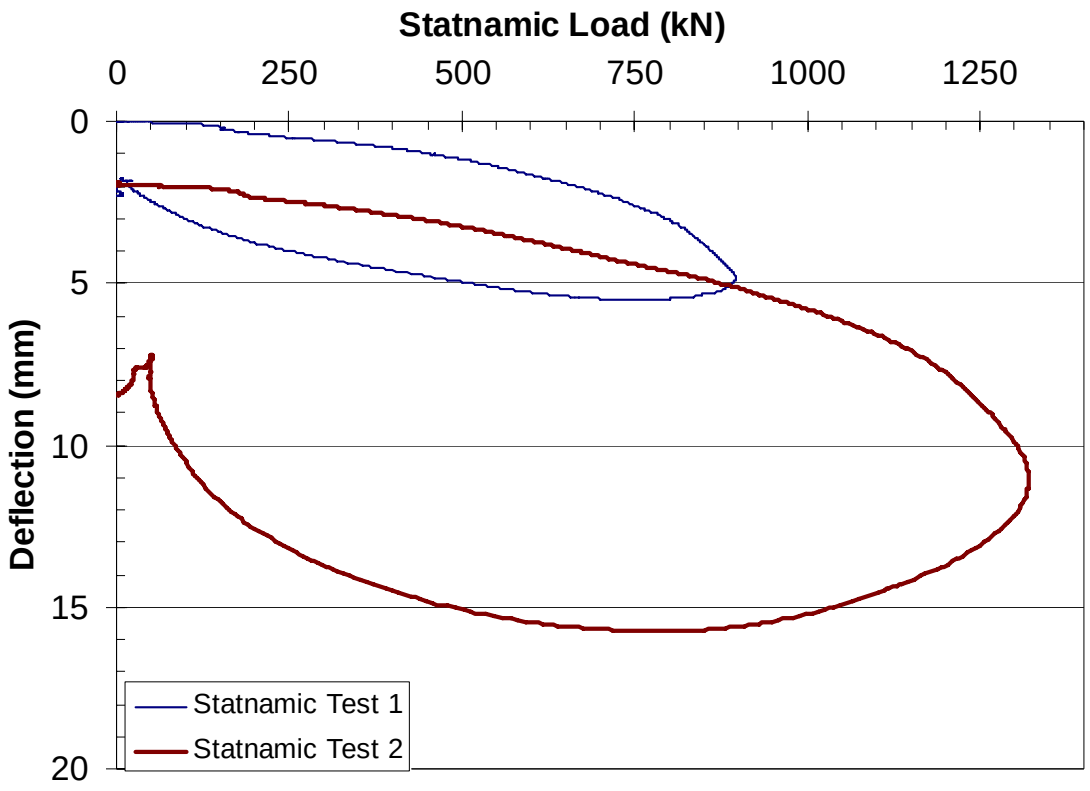

Figure 4.33 Statnamic Load Versus Deflection

The Statnamic load versus deflection curves in Figure 4.32 have not been corrected for dynamic effects, which means that they include inertia, damping and pore pressure effects; all of which would not be included in a traditional static load test. The Statnamic load is $F_{stn}(t)$ described in Equation 2.13.

4.3.6 Corrected Load Versus Deflection and Failure Load Determination

Since other tests in this study are static tests, it is desirable to convert the Statnamic load to a predicted static load, so that the two types of tests can be more directly compared. The predicted static load (corrected load) was obtained using the "Unloading Point Method" developed by Middendorp et al. (1992) and detailed in

section 2.2.4.1 of this document. The Unloading Point Method uses measured values of acceleration, velocity and deflection throughout the test. These values are shown in Figure 4.31 and Figure 4.32. The "Corrected Load" values, $F_u(t)$ come directly from the values shown in Figure 4.33 applied to Equation 2.16.

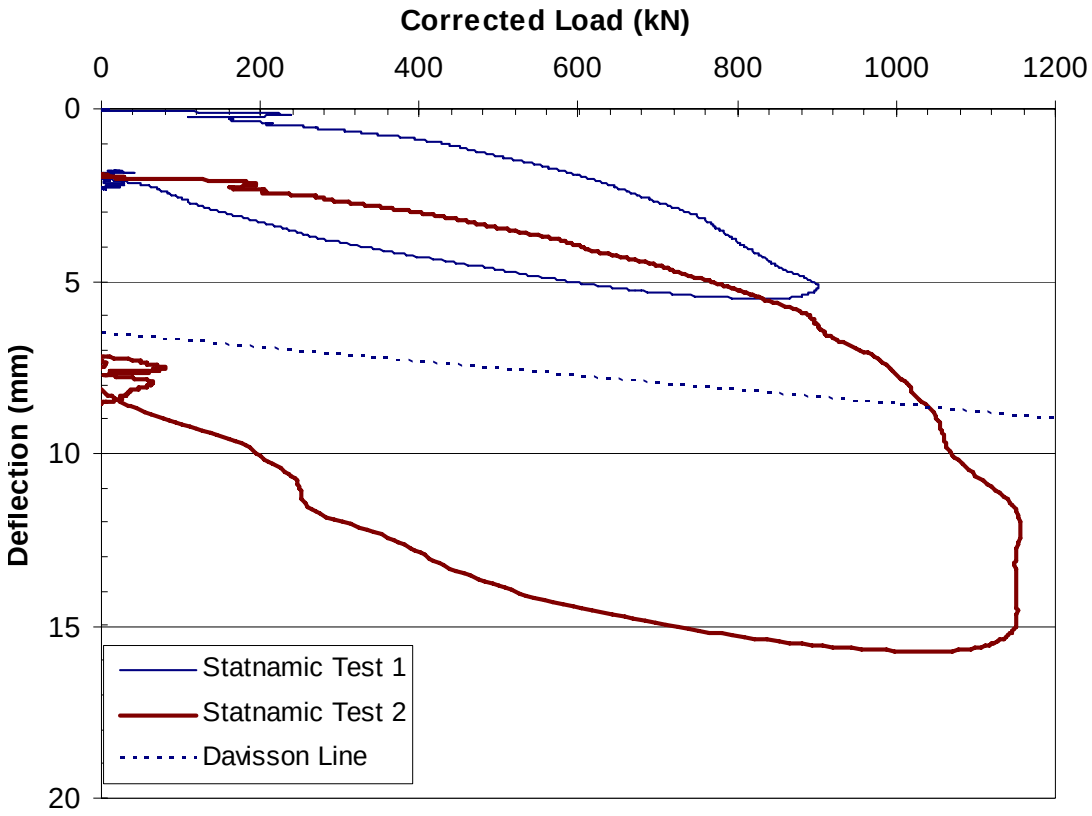

Figure 4.34 Corrected (Static) Load Versus Deflection (Statnamic Tests)

According to Section 2.2.4.1, piles must have certain characteristics in order for the Unloading Point method to produce accurate results. A wave number of 31 was obtained for the Statnamic test using Equation 2.12. The test pile used for Statnamic tests 1 and 2 consists of steel and concrete. To determine the wave number, a conservative value of value for the wave velocity, c of 4000 m/s, was used. With N_w

= 31, the Unloading Point Method is expected to be accurate in its prediction of static, axial capacity.

The corrected or interpreted static load versus deflection curves for both Statnamic tests are plotted in Figure 4.34 along with the Davisson failure line. The Davisson line gives a predicted static failure load of 1042 kN. The time at failure was 0.117 second and the displacement was 8.70 mm. The Statnamic (uncorrected) load at the time of failure was 1250.4 kN.

4.3.7 Data Required for Load Determination at Various Depths

As with the static load tests, load was measured directly, only at the top of the pile. Strain, ε recorded by strain gages, was multiplied by EA according to Equation 4.2 to obtain the load in the pile at various depths.

EA of the Statnamic test pile was obtained in the same way as with the static test piles. A set of strain gages was placed in the pile above the surface of the ground where the load in the pile was equal to the load at the load cell since above the ground, no load is lost to soil friction. Figure 4.35 shows the equation for the load versus strain curve for Statnamic load test 2. In the equation for the load versus strain curve, the slope of the line (6,173,444 kN) is equal to EA and the load divided by strain, P/ε. Thus, the slope (6,173,444 kN) was multiplied by strain to obtain values of load at various depths. Each of these strain values was acquired by the strain gages which were attached to the sides of the pile.

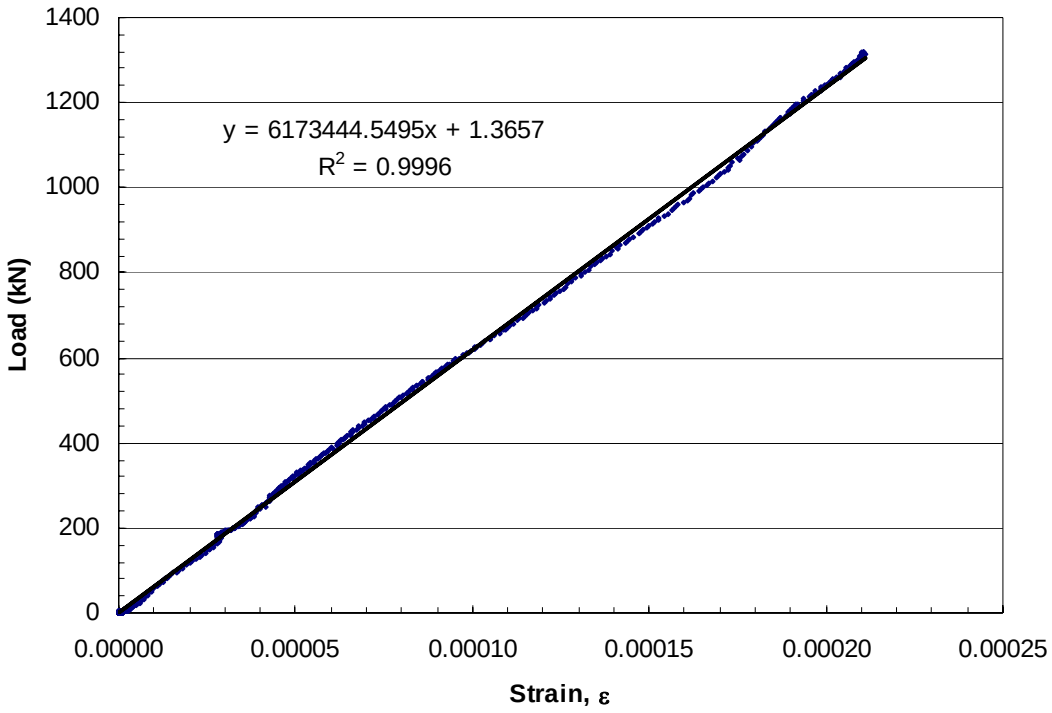

Figure 4.35 Load Versus Strain (Statnamic Load Test 2)

4.3.7.1 Determination of EA from Pile Properties

The EA value for the test pile used in the Statnamic testing was also computed based on the material properties and dimensions of the pile itself as a check on the back-calculated EA. Test cylinders of the grout that filled the Statnamic test pile were cast. Statnamic load tests were performed on the pile on September 24, 2004. Four test cylinders were broken in the structures laboratory at BYU on September 29, 2004. The test cylinders had the same dimensions as the cylinders tested for the static load tests. The average, maximum compressive load, P_{max} of the four test cylinders was 53.6 kip (238 kN). The compressive strength of the concrete, f_c' in the test cylinders as well as in the test pile is therefore 4.27 ksi (2.94 kN/cm^2) from Equation 4.4.

The elastic modulus, E of concrete can be calculated directly from f_c' with Equation 4.5. The modulus is therefore 3,725 ksi (2,570 kN/cm^2). EA values and the numbers in the calculation of EA are shown in Table 4.3.

Table 4.3 Determination of Composite EA for Statnamic Test Pile

	Area (in^2)	E (ksi)	EA (kip)	EA (kN)
(2) Angles	0.72	29,000	20,880	92,874
Pile	14.58	29,000	422,820	1,880,703
Inner Pipe	5.58	29,000	161,820	719,775
Grout	106.8	3,725	397,830	1,769,548
Total:	-	-	1,003,350	4,462,901

The theoretical value of EA found in Table 4.3 and the back-calculated value found in Figure 4.35 vary by 28%. It is assumed that the rate of strain has an effect on the EA of the pile, so the value which is used for calculations in this work is the one obtained by the load versus strain relationship in Figure 4.35. The R^2 value in this figure is nearly one which indicates that scatter in the data is minimal.

4.3.8 Load Versus Depth Curves at Failure

Statnamic load values of the test pile at failure are presented in Figure 4.36. These load values were obtained by multiplying EA, from Figure 4.35, and the strain values of each strain gage.

The inertial force of the pile during the Statnamic load of 1250.4 kN as calculated by the Unloading Point Method was 43.9 kN. Figure 4.37 shows the inertial force subtracted from the load values shown in the previous graph.

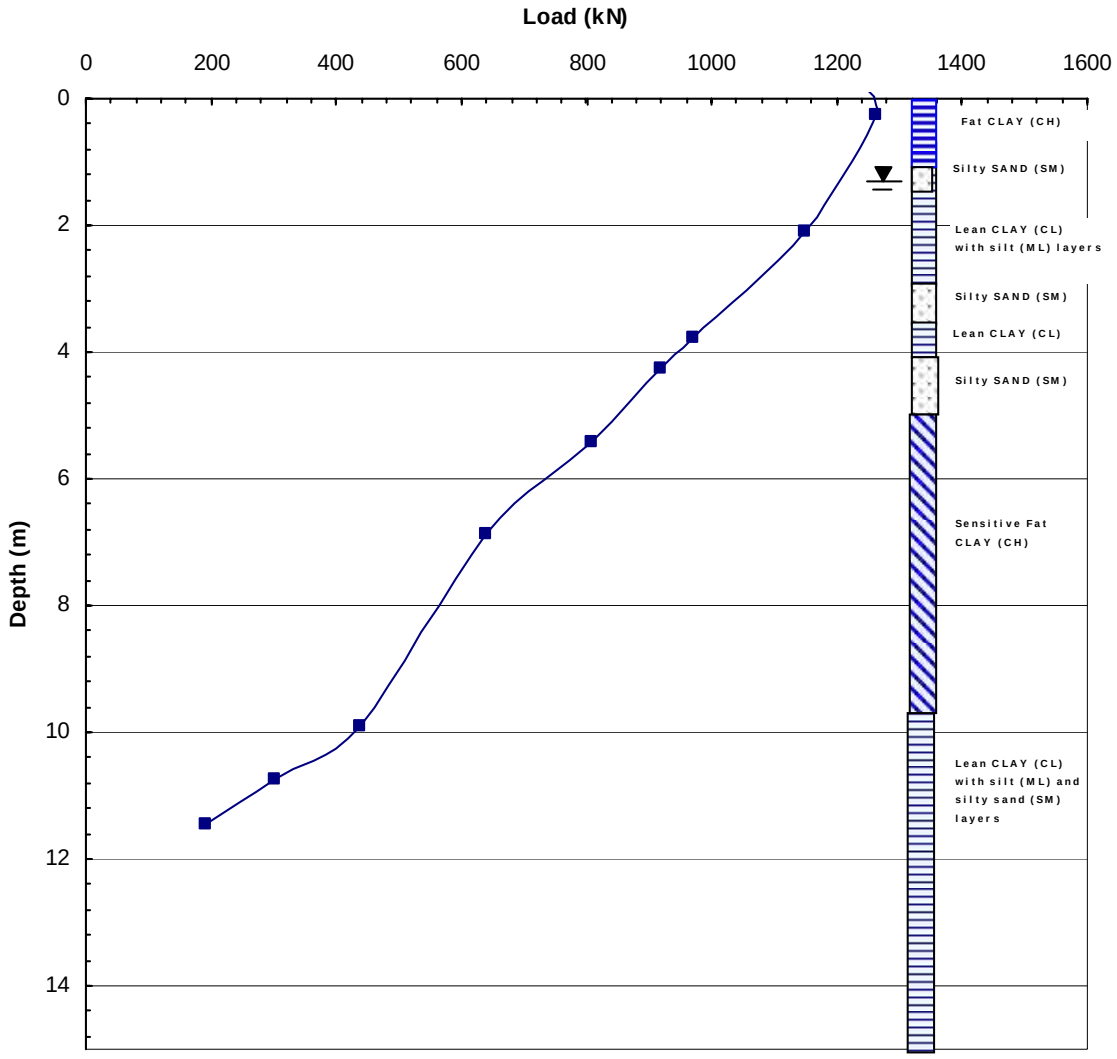

Figure 4.36 Statnamic Load Versus Depth, at Failure

At the top of the pile, the full 43.9 kN was subtracted, to more closely model the equivalent static force. Inertial force is a function of mass, so lower down on the pile, less force is required to overcome inertia than at the top of the pile, where the inertia of the entire pile mass is felt. The inertial force is reduced linearly down the pile, eventually becoming zero at the bottom of the pile. It can be seen therefore, that

load values near the top of the pile changed significantly from Figure 4.36 to Figure 4.37, while load values near the bottom of the pile changed very little.

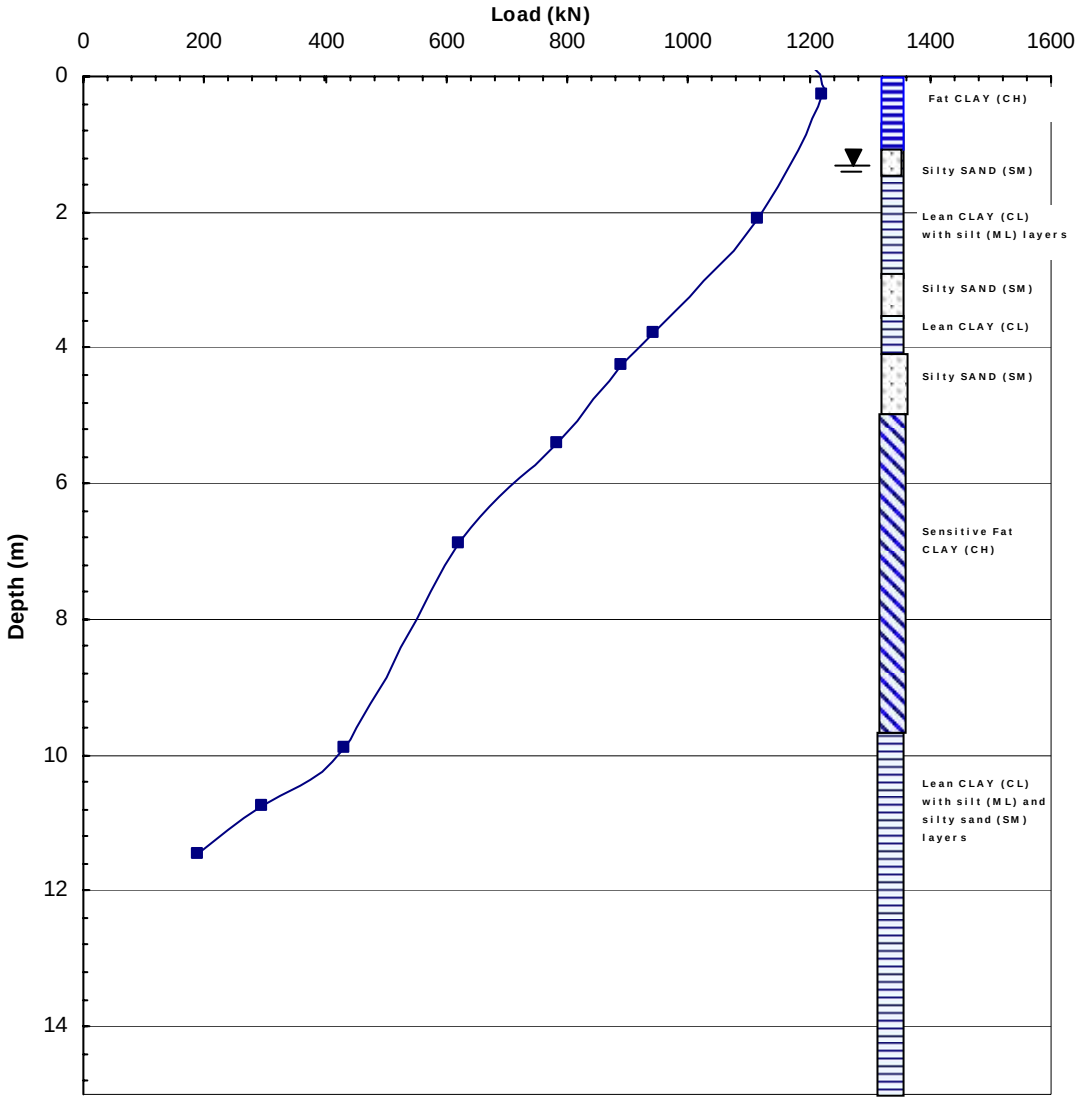

Figure 4.37 Statnamic Load Minus Inertia Versus Depth, at Failure

The damping of the pile during the Statnamic load of 1250.4 kN as calculated by the Unloading Point Method was 164.4 kN. Figure 4.38 shows the damping subtracted from the load values shown in the previous graph.

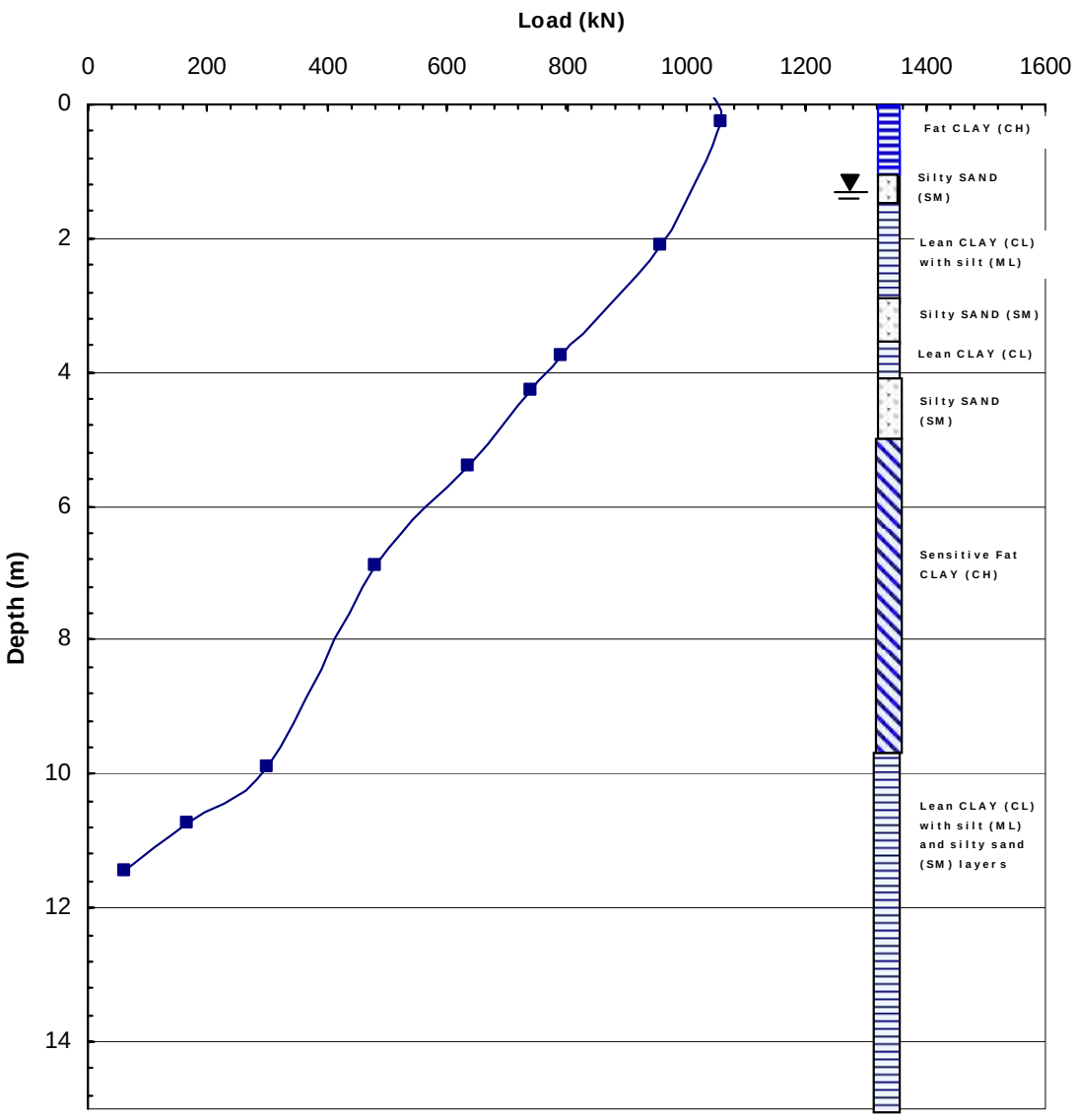

Figure 4.38 Corrected (Predicted Static) Load Versus Depth at Failure

The load values in this figure represent the predicted static loads at failure of the Statnamic test pile using the unloading point method. At the top of the pile, the full 164.4 kN of damping was subtracted, to more closely model the equivalent static force. Damping is treated differently from inertia in this work. Inertia was shown to be zero at the bottom of the pile, because no pile mass is accelerated below the pile tip.

According to Ishida et al. (2000), faster tests show an increase in strength at the tip of a driven pile. This phenomenon can be seen with the Statnamic load test in this work.

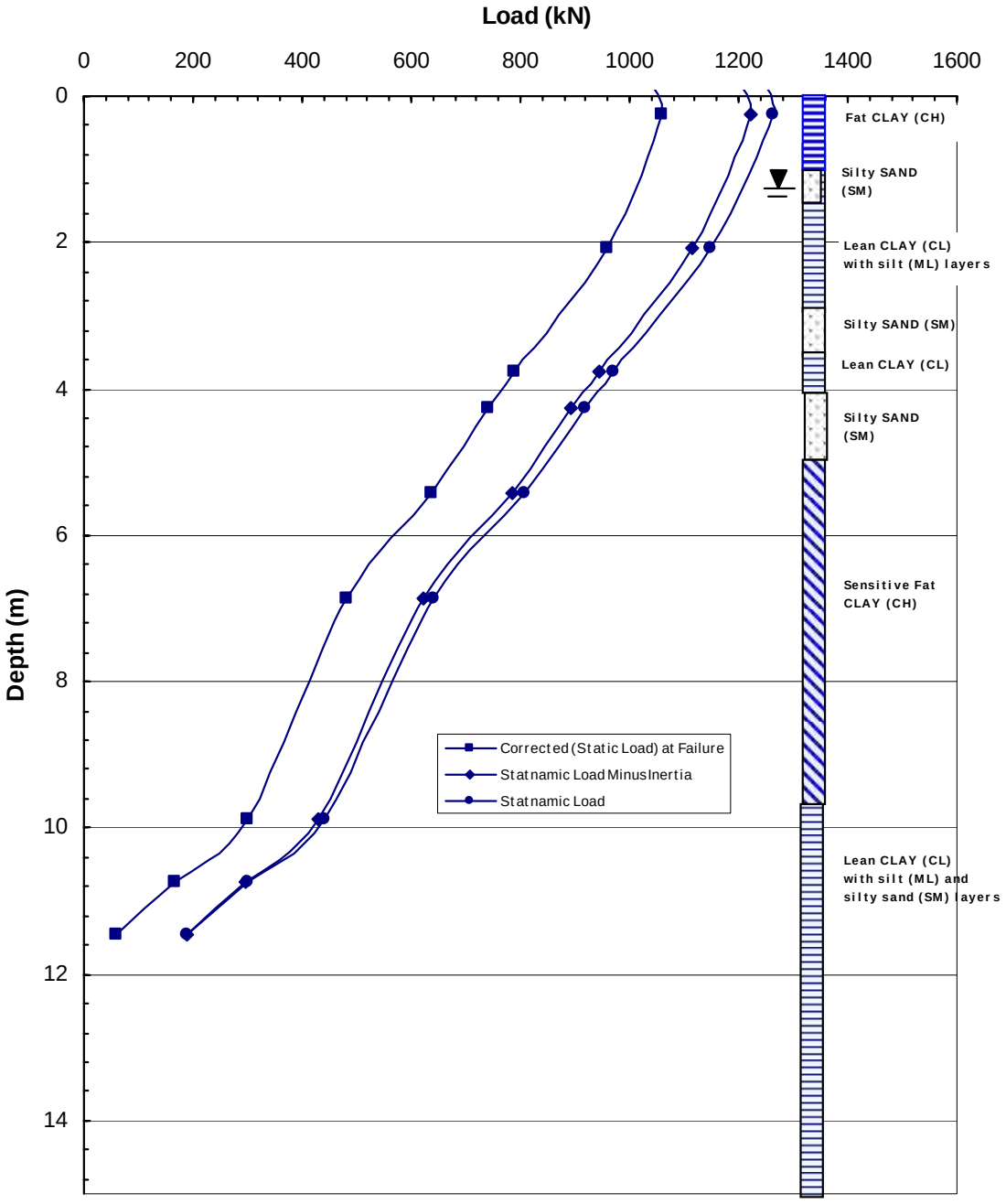

Figure 4.39 Load Versus Depth at Failure

The 18 hour test which is a true static test shows the load at the pile tip to be 60.5 kN at the time of failure, and the load at the tip during the Statnamic test was 190.6 kN.

The damping of the entire pile during the Statnamic test can be calculated using the Unloading Point Method, however the distribution of this damping force is not known exactly. If 76% of the damping occurs at the pile tip, then the load at the tip matches that of the static test. This force distribution is shown in Figure 4.38. The remaining 24% of the 164.4 kN of damping is evenly distributed along the length of the pile.

For perspective, the graphs in all three of the preceding figures are shown in Figure 4.39. In this figure it can be seen that the inertia is greater at the top of the pile, since the curve showing the Statnamic load minus inertial force deviates more from the Statnamic load at the top of the pile than at the bottom. The corrected (predicted static) curve is shifted away from the other curves along the whole depth because most of the damping actually takes place below the pile tip.

5 Analysis of Results

5.1 Comparison of Failure Loads from Pile Load Tests

The piles that were tested were all nearly identical in terms of cross-section and materials. In addition, they were driven into essentially the same soil profile. Therefore, the major difference in the tests was the rate at which load was applied to them. This makes it possible to compare the influence of the rate of loading on the measured failure load. The failure loads from the Davisson method for each pile test are plotted versus their respective times to failure in Figure 5.1. As load is applied at a faster rate, the strain rate and therefore the pile capacity also increase. The failure load for the Statnamic test is over two times larger than the failure load for the 18 hour test. Two best-fit lines through the data were obtained using linear regression techniques. The equations for the line are

$$Q_u = 889\left(T_f\right)^{-0.0624} \quad \textbf{(5.1)}$$

$$Q_u = -152\log\left(T_f\right) + 893 \quad \textbf{(5.2)}$$

where Q_u is the failure load and T_f is the time to failure in seconds. Equation 5.1 applies the idea that strength increase is linear and Equation 5.2 assumes that it is not.

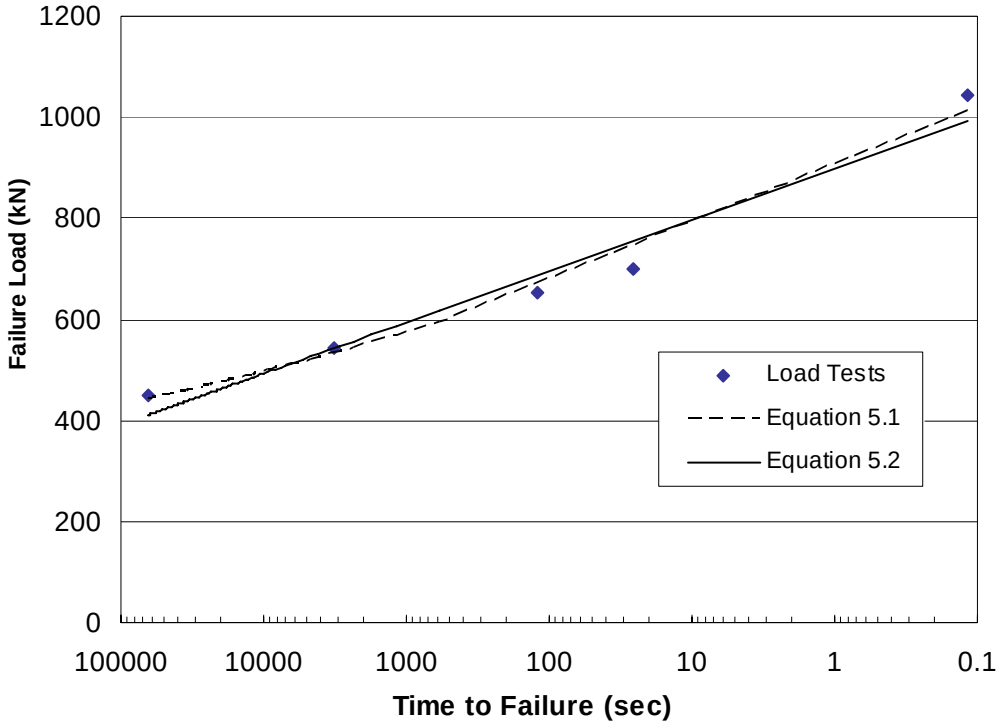

Figure 5.1 Failure Load Versus Time to Failure

A careful review of the data point suggests that the increase in failure load for the Statnamic load test is somewhat higher than what might be expected based on the rate of increase from the other static tests. The higher failure load for the Statnamic test could from a number of factors. First, it could simply mean that the rate of increase in failure load with rate of loading is non-linear as suggested by several investigators noted in the literature review. This phenomenon is accounted for in Equation 5.1. Secondly, the higher failure load could be due to difficulties in properly interpreting the static load from the Statnamic test. Finally, the increased failure load could be due to greater strength in the soil around the Statnamic test pile relative to the other test piles. In this regard, it should be noted that the Statnamic test pile was located about 50 meters southwest of the test piles used for the other static load tests.

5.1.1 Effect of Velocity of Pile on Axial Capacity Tests

Obviously, as the rate of load application increases, so does the overall velocity of the test pile. Displacement data at failure were divided by their respective times to failure to determine an overall velocity of the piles in each test.

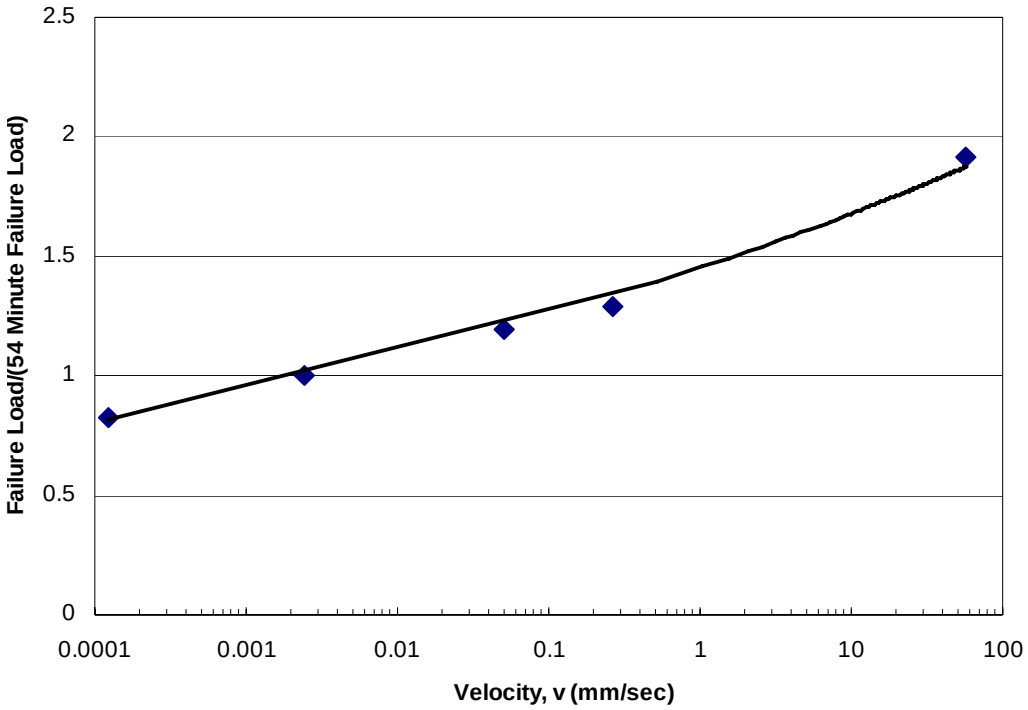

Figure 5.2 Normalized Failure Load Versus Velocity

In Figure 5.2, the failure loads were normalized by dividing each failure load by the failure load of the 54 minute test. These values were then plotted against the velocity of the piles in each test to obtain the graph shown in Figure 5.2. Velocity was obtained by dividing the deflection at failure by the time to failure. Based on the data points in Figure 5.2, a best-fit line was obtained by linear regression to define the failure load as a function of velocity. The equation for failure load, Q_u is given by

$$Q_u = 0.145\left(T_f\right)^{0.0631} \quad \textbf{(5.3)}$$

Figure 5.2 and Equation 5.3 show that the increase of failure load is linear through the static tests, but the increase in strength rises with increased velocity. The idea of a threshold strain rate is supported by this phenomenon. The R^2 value of Equation 5.3 is 0.99

It can be seen in Figure 5.2 that the slope is constant for all of the static tests. Figure 5.3 is the same graph without the results of the Statnamic test. Equation 5.4, which is the equation of the best fit line of Figure 5.3, indicates that for every ten fold increase in velocity of static tests, the test pile shows a 13.7% increase in capacity. The R^2 value for this equation is 1.00 which shows that there is nearly no scatter in the data.

$$Q_u = 0.137\log\left(T_f\right) + 1.36 \quad \textbf{(5.4)}$$

In chapter 2 it was established that the shear strength, s_u of clays typically increases by about 10% with every ten fold increase in strain rate. Since the shear strength of the soil is what gives these test piles their capacity, it is logical to assume that as the shear strength increases, so will the axial capacity. Thus, the comparison of the failure loads from pile tests yields results as expected. An increase of 13.7%, while somewhat higher than 10%, is still reasonable.

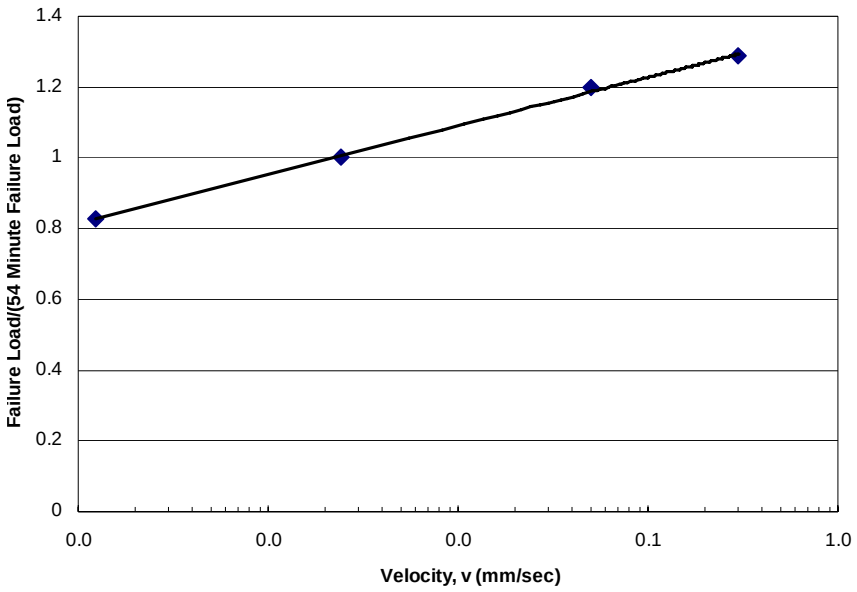

Figure 5.3 Normalized Failure Load Versus Velocity of Static Tests

Because an axial Statnamic test loads piles at a rate around six orders of magnitude faster than a conventional slow maintained load (SML) test, the results from this study suggest that the interpreted static capacity from a Statnamic load test in clay would be six times 13.7%, or 82.2%, higher than that obtained from the SML test. This would indicate that the interpreted static failure load from a Statnamic load test in clay would have to be multiplied by the factor 1/1.82 or 0.55 to obtain the failure load from an SML test. Alternatively, if the pile failure load to increased by 10% for each 10 fold increase in load rate as suggested by the undrained shear strength test data in Figure 2.1, then the Statnamic test would yield an interpreted static failure load about six times 10% or 60% higher than that obtained from the SML test. This would require a correction factor of 1/1.60 or 0.625 to obtain the failure load from an SML test. This correction factor is close to the 0.65 factor suggested by Mullins et al. (2002) to account for rate effects in Statnamic load tests.

5.2 Load Versus Depth Summary

The capacity of the test piles is dependent upon load rate. Figure 5.4 shows the load versus depth curve at failure for the static and Statnamic tests. With all of the data shown in Figure 5.4, it is difficult to see a pattern. Therefore, Figure 5.5 is included to more clearly show the results of three tests. These three tests are the most reliable. The tests that have been removed were either not to failure or were performed on a test pile shortly after a previous test.

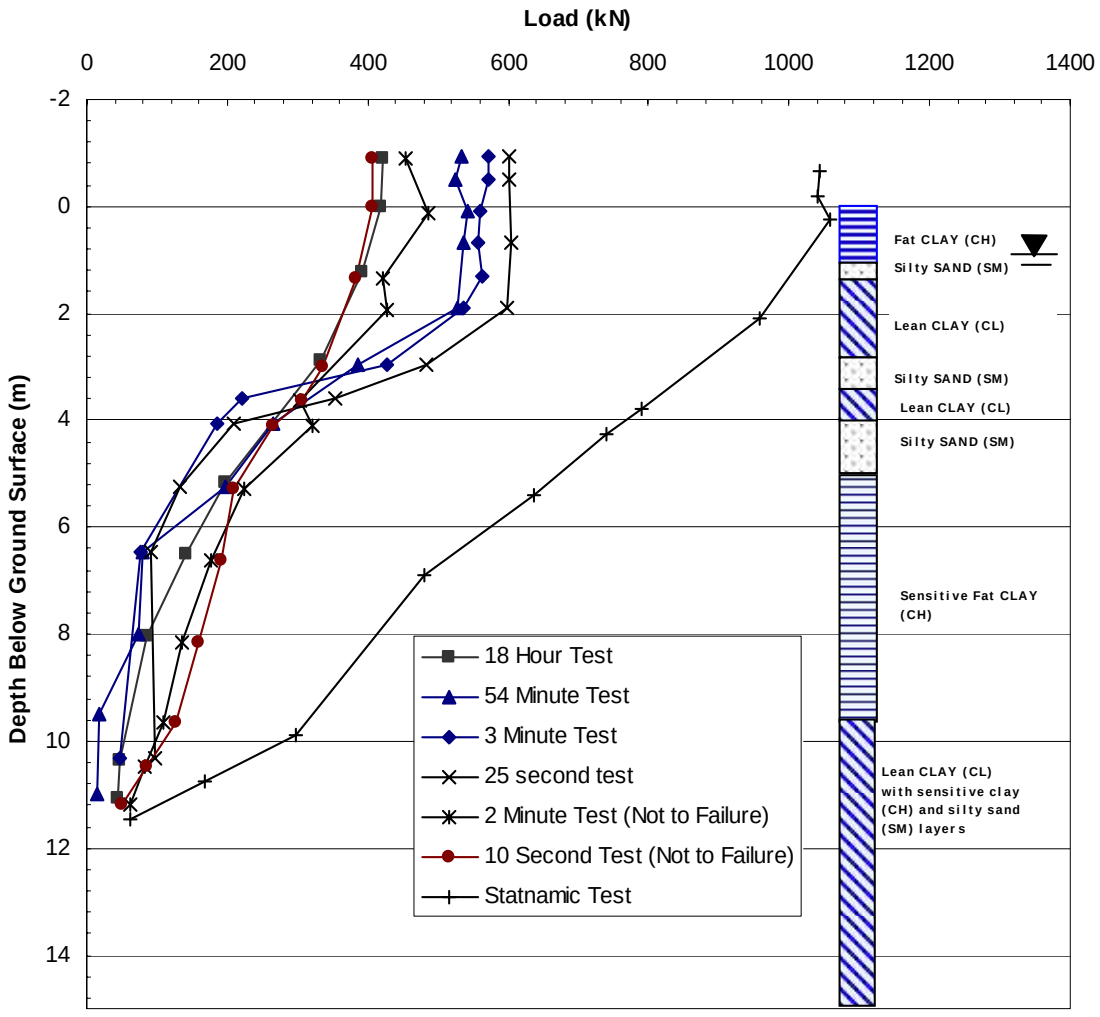

Figure 5.4 Load Versus Depth at Failure for Various Tests

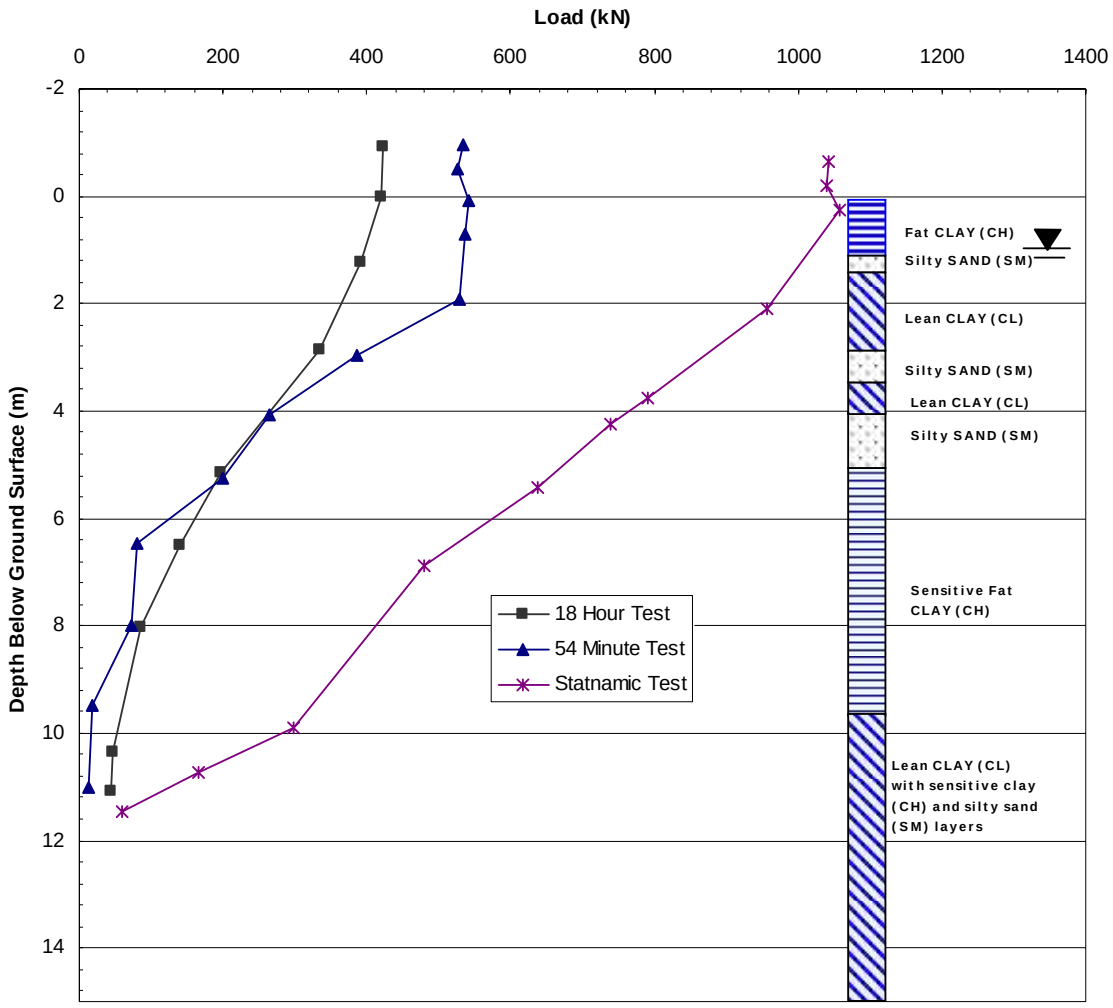

Figure 5.5 Load Versus Depth at Failure for Three Tests

5.3 Unit Side Friction Versus Depth

Three depth ranges were chosen to be compared; 0-3 meters, 3-5 meters and 5-11 meters. Graphs of the velocity versus shear strength at different depths are found in Figure 5.6, Figure 5.7 and Figure 5.8. Shear strength is obtained by dividing the difference in load in the depth described by the pile surface area along that same

depth. These graphs also include a theoretical shear value of the pile based on the soil properties.

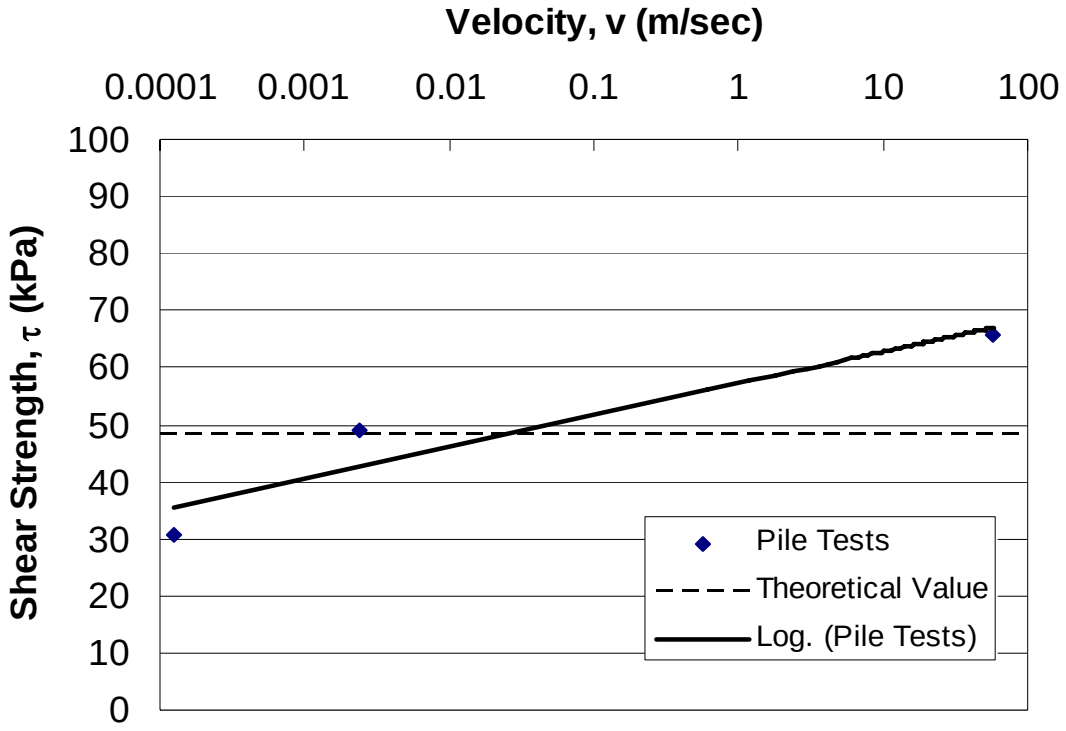

Figure 5.6 Velocity Versus Shear Strength (0-3 meters)

$$\tau = 5.56\log(v) + 57.2 \quad \textbf{(5.5)}$$

Equation 5.5 represents the data shown in Figure 5.6. Equation 5.5 has an R^2 value of 0.89 indicating that it is a reliable model of the represented data. Equation 5.6 represents the data presented in Figure 5.7. Equation 5.6 has an R^2 value of 0.77. This shows a little more scatter than the previous depth, but shows the trend is very similar.

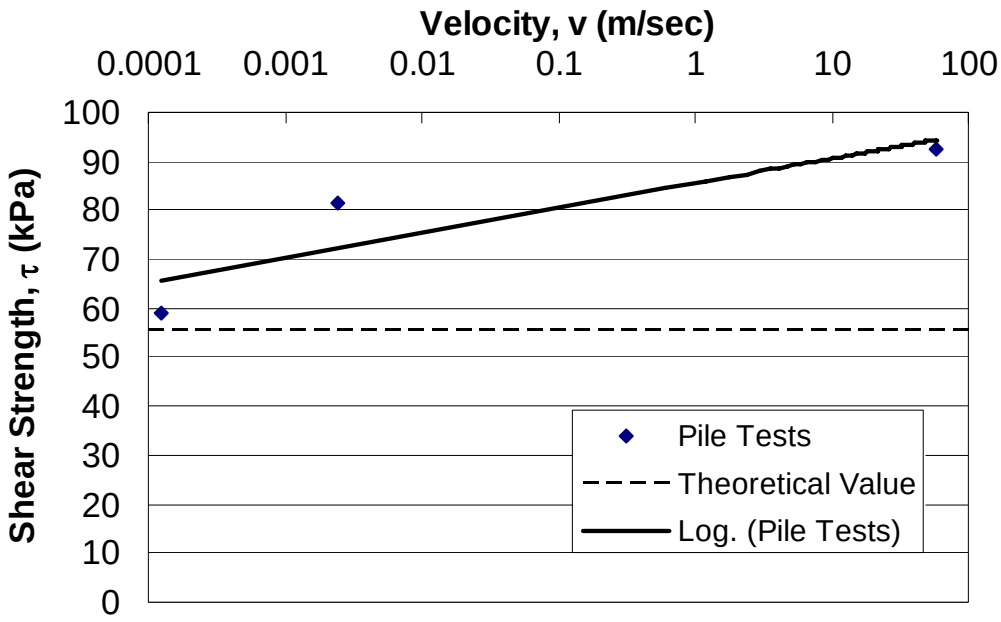

Figure 5.7 Velocity Versus Shear Strength 3-5 meters

$$\tau = 5.05\log(v) + 85.5 \qquad \textbf{(5.6)}$$

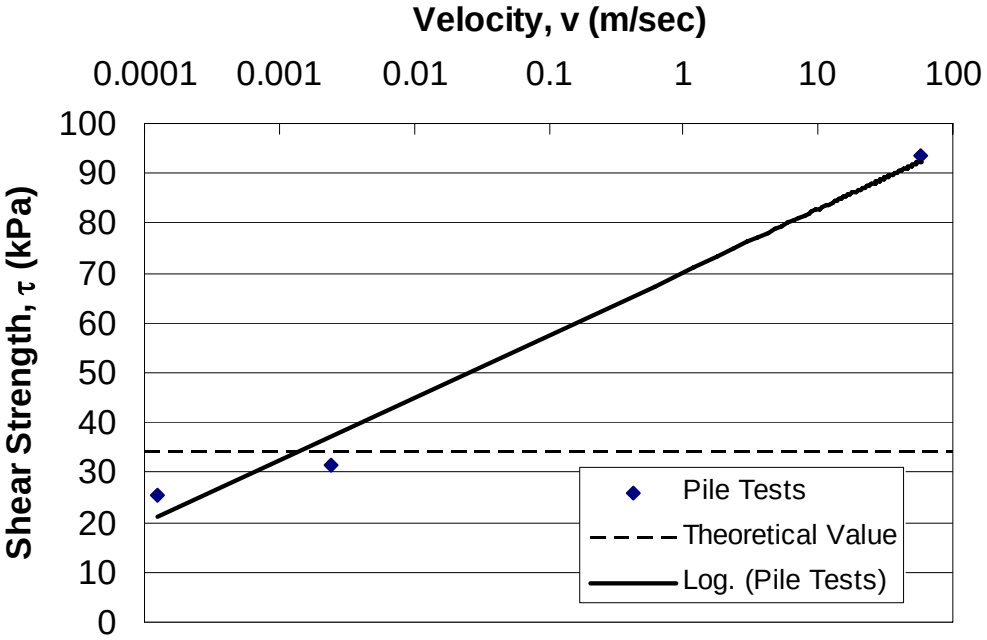

Figure 5.8 Velocity Versus Shear Strength 5-11 meters

The equation of the 5-11 meter data is

$$\tau = 12.6\log(v) + 70.2 \quad \textbf{(5.7)}$$

Figure 5.8 shows a steep best-fit line indicating a significant rate effect in the lower six meters of the piles.

Figure 5.9 shows the velocity versus average shear strength throughout the depth of the pile. The equation that represents these data is Equation 5.8. The R^2 value of Equation 5.8 is 1.0.

$$\tau = 8.93\log(v) + 69.1 \quad \textbf{(5.8)}$$

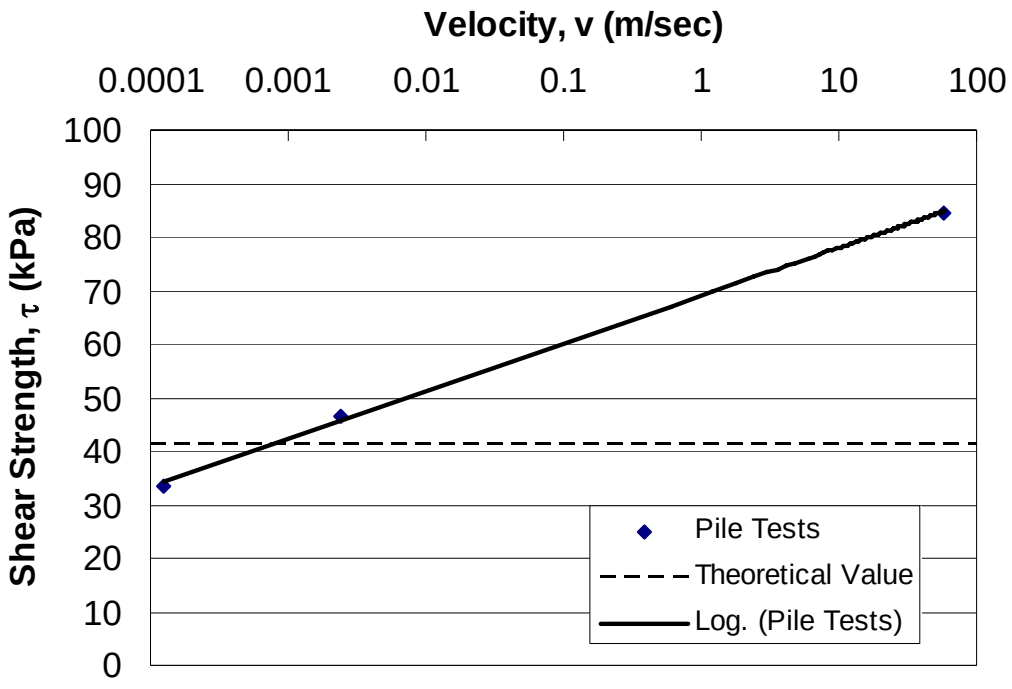

Figure 5.9 Velocity Versus Shear Strength (Average for Entire Depth)

5.4 Factors Influencing Rate Effects Versus Depth

Along the depth of the piles, the greatest rate effect occurred in the bottom six meters of the piles. The increased rate effect at the bottom of the pile may be attributed to two factors. First, the soil at the lowest 6 meters of the piles was all clay which has been shown to display more rate effect than larger grained soils. The top five meters consist of clay with layers of silty sand. Second, the upper five meters of soil showed higher O.C.R. than the bottom six meters of soil. The fact that rate effects decreased with increasing O.C.R. supports the findings of many researchers as noted in section 2.1.3.

5.5 Test Data Versus Equation 2.1

With the 18 hour test (static test) and Statnamic test (dynamic test) values inserted into Equation 2.1, the obtained value for n is 0.070. If n is calculated from the numbers attained in pile testing, Equation 2.2 gives n = 0.522, Equation 2.3 gives n = 0.06, Equation 2.4 gives n = 0.048, and Equation 2.1 gives n = 0.07. The recommendation is that the most conservative value for n be used. Results from Equation 2.2 seem quite high, especially since Briaud and Garland (1985) recommend using a value of n between 0.1 and 0.01. However, the back-calculated value of 0.070 is in line with their findings and is the most conservative assumed value, with the exception of the Equation 2.2 results.

5.6 Possible Reasons for Inaccuracies with Static Test Data

5.6.1 Tests Stress Controlled

The static tests done in load steps were stress controlled, not strain controlled. Therefore the velocity of each test is not necessarily constant. The more precise way to test would by controlling strain instead of stress. Stress controlled testing, the accepted standard test method, is a practical way to simulate a constant velocity.

5.6.2 Load History

Some lateral load tests were performed in July and August of 2000 and in August of 2002 on the piles used for static load tests in this thesis. A record of these lateral tests can be found in Cole (2003). It is possible that these lateral tests may have reduced the soil adhesion of the static test piles, particularly at the top few feet of the piles, where the deflection due to lateral tests was the greatest. As was stated in section 4.2.6, the three minute and 25 second tests were done within hours of the 54 minute test. This fact could have affected the strength of the soil-pile interaction of the three minute and 25 second tests.

5.6.3 Residual Loads

Fellenius (2002) explained that installation, subsequent reconsolidation and other time-dependent phenomena lock stress or residual load into a pile. Residual load develops in every pile, driven or bored. In order to determine the stresses induced by testing, residual loads must be subtracted from stress data acquired during pile testing. Residual load usually takes the form of negative shear forces in the upper portion of

the pile, positive shear forces in the lower portion of the pile and toe resistance. Typically, load versus depth curves develop a “squeezed-S” shape when the existence of residual load is neglected.

Residual load was neglected in the analysis of all of the pile tests in this work. Just as Fellenius (2002) suggested, the load versus depth curves for most tests in this work have the “squeezed-S” shape associated with analyses that neglect residual loads. Because residual loads have been neglected, loads induced by pile tests may be inaccurate. It is impossible to determine precisely how much residual load each of the test piles harbored before tests were performed. Therefore, the tests in this work do not show the accuracy that they would, if residual load had been measured. It is assumed in this work, that the effect of residual loads is minor.

5.6.4 Equipment

The strain gages for all of the tests were attached to the center pipes of the test piles in 2002. The pipes for the tests in 2004 were stored in the structures lab at Brigham Young University for two years. Many of the strain gages became detached in that time and were reinstalled before the 2004 tests. The strain gages could have lost part of their adhesion, aged or been damaged in two years’ time.

5.7 Possible Reasons for Inaccuracies with Statnamic Test Data

5.7.1 Residual Loads

Residual loads could be present in the Statnamic test pile just as in the static test piles. See section 5.6.3.

5.7.2 Inertia of Soil

Without doubt, during Statnamic tests there is some soil which adheres to the sides of the test pile. The amount of adhered soil is difficult to estimate, so in practice its inertia is neglected. The mass of any attached soil would increase the predicted static capacity of the Statnamic test. This may be a partial reason for the higher than expected capacity of the Statnamic tests. In addition to soil adhering to the sides of the pile, the displaced soil at the toe of the pile also will have an inertial component which is neglected. See section 2.2.4.2.

5.7.3 Effect of Creep

Load-settlement behavior may seem to be stiffer with a Statnamic test than a static test. The reason is that with a static test, time is allowed for soil creep. Therefore, in a static test, more settlement can be expected than with a Statnamic test (Ng and Justason, 1998).

5.7.4 Load History

Failure load was not reached on the first Statnamic test. Another test was done which did produce failure. The permanent displacement caused by the first Statnamic test was taken into account however in the failure load determination. Since the permenant displacement was taken into account, the failure load determination should be very accurate. The entire displacement had a break in the time which means that the rate of load was not consistent. When calculations for the velocity were made, the actual velocity during the failure test was used.

5.7.5 Equipment

The potential equipment issues are the same as presented in section 5.6.4.

6 Summary and Conclusions

6.1 Summary

A detailed review of published literature was done, and axial tests were performed on full-sized piles with failure times ranging from 0.1 seconds to 18 hours. Piles were identical and driven through the same profile. A detailed geotechnical investigation showed that the soil profile is extremely uniform, thus each pile can be considered identical.

6.2 Conclusions

1. The literature review clearly indicates the undrained shear strength for clay increases with strain rate due to soil viscosity; however, cohesionless soils appear to be much less affected. Nevertheless, some studies indicate that some increase in frictional resistance may occur as strain rate increases even in sands.
2. Based on the literature review and subsequent analysis the undrained shear strength of clay increases by 10% for every ten-fold increase in strain rate assuming a log-linear relationship.

3. Scatter in the data relating normalized strength gain and the log of strain rate increases at the higher strain rate levels. This fact has led some researchers to conclude that the rate of strength gain might be greater at higher strain levels rather than being log-linear. This fact also suggests that it may be relatively difficult to obtain correction factors for Statnamic load tests which will provide consistent results.
4. Literature review suggested that an increase in O.C.R. produces a small decrease on rate effects in clays; however, other factors such as plasticity index and shear strength had little effect on rate effects.
5. Plots of the failure load as a function of velocity of loading indicate that the test piles gained about 13.7% capacity for every ten-fold increase in loading rate assuming a log-linear relationship.
6. The pile test data also suggest that rate effects on shear strength may become more pronounced at higher loading rates or velocities as suggested by some laboratory investigations.
7. To obtain a failure load compatible with that from a slow maintained load (SML) test, the interpreted static load from a Statnamic test would need to be multiplied by factors of 0.55 and 0.625 assuming 13.7% and 10% increases in shear strength per log cycle of loading rate from field and laboratory testing, respectively. These adjustment factors are somewhat lower than the factor of 0.65 for clays proposed by Mullins et al. (2002) for use with Statnamic load tests.

6.3 Future Research Recommendations

Similar tests as were reported in this study should be repeated at other sites because of the scarcity of Statnamic test data in clay and the importance of the adjustment factors that are used in determining static load capacity from a Statnamic test. More research on the Statnamic testing method is required to increase its usefulness when testing in clay soils. Therefore, all available test data from companion static and Statnamic pile load tests should be collected and evaluated to provide improved confidence in the correction factors necessary to obtain equivalent static pile failure loads. In subsequent field tests, additional care should be taken to protect strain gages, and residual loads should be taken into account when analyzing unit side resistance and end-bearing by taking strain readings before and after the piles are driven.

References

Abe, A., Kubota, H., Kuwabara, F., Tamura, M. and Inoue, N. (1998). "Effect of Loading Duration on the Estimation of Vertical Bearing Capacity of Pile by Quick Loading Test", *Proceedings, Second International Statnamic Seminar*, Tokyo, Japan, pp. 373-380.

Akai, K., Adachi, Tl, and Ando, N. (1975). "Existence of a Unique Stress-Strain-Time Relation of Soils", *Soils and Foundations,* Vol. 15, No. 1, pp. 1-16.

Berre, T. and Bjerrum, L. (1973). "Shear Strength of Normally Consolidated Clays", *Proceedings, 8th International Conference on Soil Mechanics and Foundation Engineering*, Vol. 1, pp. 39-49.

Bjerrum, L. (1973). "Problems of Soil Mechanics and Construction on Soft Clays and Structurally Unstable Soils (Collapsible, Expensive and Others)", *General Report, 8th International Conference on Soil Mechanics and Foundation Engineering*, Vol. 3, pp. 111-159.

Brand, E., (1984). "Discussion of 'Time Effects on the Stress-Strain Behavior of Natural Soft Clays'", *Geotechnique*, Vol. 34, No. 3, pp. 435-438.

Briaud, J. and Garland, E. (1985). "Loading Rate Method for Pile Response in Clay", *Journal of Geotechnical and Engineering*, Vol. 111, No. 3, pp. 319-335.

Briaud, J., Ballouz, M. and Nasr, G. (2000). "Static Capacity Prediction by Dynamic Methods for Three Bored Piles", *Journal of Geotechnical and Geoenvironmental Engineering*, July 2002, pp. 640-649.

Brown, D.A. (1994). "Evaluation of Static Capacity of Deep Foundations from Statnamic Testing", *Geotechnical Testing Journal*, Vol. 17, No. 4, pp. 403-414.

Casagrande, A and Wilson, S. (1951). "Effect of Rate of Loading on the Strength of Clays and Shales at Constant Water Content", *Geotechnique,* Vol. 2, pp. 251-263.

Coduto, D.P. (2001). Foundation Design, 2nd Edition, Prentice-Hall, New Jersey.

Cole, R. (2003). "Full-Scale Effects of Passive Earth Pressure on the Lateral Resistance of Pile Caps", PHD Dissertation, Dept. of Civil and Environmental Engineering, Brigham Young University, Provo, UT.

Crawford, C. (1959). "The Influence of Rate of Strain on Effective Stresses in Sensitive Clay", *Papers on Soils (STP 254),* ASTM, Philadelphia, pp. 36-48.

Eide, O. and Holmberg, S. (1972). "Test Fills to Failure on Soft Bangkok Clay", *Proceedings, ASCE Specialty Conference on Performance of Earth and Earth-Supported Structures,* Vol. 1, West Lafayette, pp. 159-180.

Fellenius, B. (2002). "Determining the True Distributions of Load in Instrumented Piles", *International Deep Foundation Congress "Down to Earth Technology",* Orlando, Florida.

Goble, G., Rausche, F. and Likins, G. (1995). "Discussion on 'Evaluation of Static Capacity of Deep Foundations from Statnamic Testing' by Dan Brown", *Geotechnical Testing Journal*, GTJODJ, Vol 18, No.4, pp. 493-498.

Hajduk, E., Paikowsky, S., Mullins, G., Lewis, C., Ealy, C. and Hourani, N. (1998). "The Behavior of Piles in Clay during Statnamic and Different Load Testing Proceedures", *Proceedings, Second International Statnamic Seminar,* Tokyo, Japan, pp. 59-73.

Hanzawa, H. and Tanaka, H. (1992). "Normalized Undrained Strength of Clay in the Normally Consolidated State and in the Field", *Soils and Foundations,* Vol. 32, No. 1, pp. 132-148.

Hyde, A., Anderson, W. and Robinson, S. (1998). "Vertical Load Tests in Different Loading Speeds on Model Piles", *Proceedings, Second International Statnamic Seminar,* Tokyo, Japan, pp. 365-371.

Ishida, M., Akita, N., Toshigami, T. and Nishimura, S. (1998). "Vertical Load Tests in Different Loading Speeds on Model Piles", *Proceedings, Second International Statnamic Seminar,* Tokyo, Japan, pp. 365-371.

Katti, D., Tang, J. and Yazdani, S. (2003). "Undrained Response of Clays to Varying Strain Rate", *Journal of Geotechnical and Geoenvironmental Engineering,* November, pp. 278-282.

Kulhawy, F. and Mayne, P. (1996). "Manual of Estimating Soil Properties for Foundation Design", *Geotechnical Engineering Group,* Cornell University, Ithica.

Kutter, B. and Sathialingam (1992). "Elastic-Viscoplastic Modeling of the Rate-Dependent Behaviour of Clays", *Geotechnique,* Vol. 42, No. 3, pp. 427-441.

Lefebvre, G. and LeBoeuf, D (1987). "Rate Effects and Cyclic Loading of Sensitive Clays", *Journal of Geotechnical Engineering,* ASCE, Vol. 113, No. 5, pp. 476-489.

Leroueil, S. and Marques, M. (1996). "Importance of Strain Rate and Temperature Effects in Geotechnical Engineering", *Geotechnical Special Publication,* No. 61, pp. 1-60.

Middendorp, P., Bermingham, P., and Kuiper, B. (1992). "Statnamic Load Testing of Foundation Piles", *Proceedings, Fourth International Conference on Application of Stress-Wave Theory of Piles,* The Hague, Netherlands, pp. 581-588.

Middendorp, P. and Bielefeld, M. (1995). "Statnamic Load Testing and the Influence of Stress Wave Phenomena", *Proceedings, First International Statnamic Seminar,* British Columbia, Canada, pp. 207-221.

Mullins, G., Lewis, C., Justason, M. (2002). "Advancements in Statnamic Data Regression Techniques", *Geotechnical Special Publication,* No. 116 II, pp. 915-930.

Murakami, S., Yasuhara, K. and Bessho, K. (1996). "Prediction of Time-Dependent Behaviour of Remolded Soft Marine Clay in Axi-Symmetric Conditions", *Geotechnical Special Publication,* No. 61, pp. 181-194.

Nakase, A and Kamei, T. (1986). "Influence of Strain Rate on Undrained Shear Characteristics of K_0-Consolidated Cohesive Soils", *Soils and Foundations,* Vol. 26, No. 1, pp. 85-95.

Ng, J. and Justason, M. (1998). "Comparison of Statnamic and Static Tests of End Bearing Piles on Shale", *Proceedings, Second International Statnamic Seminar,* Tokyo, Japan, pp. 179-187.

Nishimura, S. and Matsumoto, T. (1995). "Wave Propagation Analysis During Statnamic Loading of a Steel Pipe Pile", *Proceedings, First International Statnamic Seminar,* British Columbia, Canada, pp. 23-34.

Penumadu, D. and Chameau, J. (1997). "Strain Rate Effects in Model Pressuremeter Testing", *Journal of Geotechnical and Geoenvironmental Engineering,* Vol. 123, pp. 1051-1059.

Penumadu, D., Skandarajah, A. and Chameau, J. (1998). "Strain Rate Effects in Pressuremeter Testing Using a Cuboidal Shear Device: Experiments and Modeling", *Can. Geotech. J.,* Vol. 35, pp. 27-42.

Perzyna, P. (1966). "Fundamental Problems in Viscoplasticity", *Adv. Appl. Math.,* 9, pp. 243-377.

Poulos, H. (1998). "Pile Testing – From the Designer's Viewpoint", *Proceedings, Second International Statnamic Seminar,* Tokyo, Japan, pp. 3-21.

Richardson, A. and Whitman, R. (1963). "Effect of Strain-Rate Upon Undrained Shear Resistance of a Saturated Remoulded Fat Clay", *Geotechnique,* 13, pp. 310-324.

Sheahan, T., Ladd, C. and Germaine, J. (1996). "Rate-Dependent Undrained Shear Behavior of Saturated Clay", *Journal of Geotechnical Engineering,* pp. 99-108.

Smith, E. (1960). "Pile Driving Analysis by the Wave Equation", *Journal of the Soil Mechanics and Foundation Engineering Division,* ASCE, Vol. 86, pp. 35-61.

Vaid, Y. and Campanella, R. (1977). "Time-Dependent Behavior of Undisturbed Clay", *Journal of Geotechnical Engineering Div.,* ASCE, Vol. 103, pp. 693-709.

Vaid, Y., Robertson, P. and Campanella, R. (1979). "Strain Rate Behavior of Saint Jean Vianney Clay", *Canadian Geotechnical Journal,* Vol. 16, No. 1, pp. 34-42.